ATP - EMTP Modeling of Distance Relays to Simulate Single Line to Ground Fault Performance in Transmission Network

Master of Science Thesis

A.R. Hakim
[Student Number: 4335317]

August 2015

Department of Electrical Sustainable Energy
Faculty of Electrical Engineering, Mathematics and Computer Science
Electrical Sustainable Energy
Delft University of
Technology

ATP - EMTP Modeling of Distance Relays to Simulate Single Line to Ground Fault Performance in Transmission network

A. R. Hakim

Thesis Committee:

Dr. ir. Marjan Popov
Dr. ir. J.L. Rueda Torres
Dr. J.L.A. Dubbeldam

Department of Electrical Sustainable Energy
Faculty of Electrical Engineering, Mathematics and Computer Science
Electrical Power Systems
Delft University of Technology

Abstract

The thesis deals with the modeling and simulation of distance relays in ATP - EMTP. Transmission line which is 125.6 miles long operates at 60 Hz and 115 kV line voltages are simulated in ATP - EMTP. The first part of the thesis discusses the implementation and simulation of the ATP - EMTP model for microprocessor based mho distance relay using angle comparator method in the network. The model includes the modeling of input filter, sample and Fourier fundamental frequency detector, which process the input for mho distance relay model. A number of simulations of single line to ground faults (SLGF) with different fault locations were carried out to verify the correct operation of the relay based on the developed protection scheme. The results of the simulation show the operation of the relay based on its protection scheme and its response time related to the fault locations. The study is also extended to the double line to ground fault for the same purpose. The second part of the thesis discusses the model for an electromechanical mho distance relay, which includes the modeling of current transformer (CT) and capacitive voltage transformer (CVT). A validated ninth-order mathematical model of the electromechanical Mho distance relay is constructed in ATP - EMTP to observe the dynamic behavior of the relay during a critical fault. For that purpose, SLGF were tested in critical locations which is very close to the relay. The results show how CT saturation and CVT transient influence the relay operation. The applied procedure can be used for testing of distance protection performance against single phase fault currents.

Keyword: ATP - EMTP, microprocessor based mho distance relay, electromechanical mho distance relay, current transformer (CT), capacitive voltage transformer (CVT).

Acknowledgements

Foremost, I praise Allah, the almighty, for everything I have accomplished would never be possible without his permission. I would like to thank Dr. Ir. Marjan Popov as my supervisor for giving me the opportunity to work with him and for guiding me during my Thesis. Dr. ir. Marjan Popov is very helpful during the discussion and provided a lot of significant information regarding the ATP – EMTP software and the distance protection which is very important to the success of the project.

The opportunity of pursuing master degree in TU Delft was a great experience for me. I would like to express my gratitude to PT. Pelabuhan Indonesia III (persero) for giving me this wonderful opportunity to study and pursue my master degree here in TU Delft. To all my classmates and friends, thank you for all the helps, guidance and most importantly the great supports. I will miss all great moments I spent with all of you. Special thanks to Hariadi Aji for being the dearest colleague during my study in Delft.

Thank you to Keluarga muslim delft (KMD) for becoming my new family in Delft. I would also like to thank Pelindo III family in Delft (Wahyu Cahyo and family, Ali Afandi and family, Arendra, Yudi) for always supporting each-other to accomplish our goals.

Finally I would like to thank my beloved wife Rifa Aghina Arif. Her support, prayer, encouragement, patient and relentless love are my greatest motivation in life. Thank you for my mother, Masdhuha, I believe you always mention my name during your prayers, thank you for giving me your faith in pursuing my dream. Thanks for all my family members for all the support.

August 28th, 2015

Arif Rohman Hakim

Table of Contents

List of Figures

List of Tables

Abbreviations

ATP - EMTP	*: Alternative transient program – Electromagnetic Transient Program*
CT	*: Current transformer*
CVT	*: Capacitive voltage transformer*
LCC	*: Line/cable constant*
POW	*: Point-on-wave*
PT	*: Potential transformer*
SLGF	*: Single line to ground fault*

---This page is intentionally left blank---

1. Introduction

1.1. Power Systems, Transmission Lines, Single Line to Ground Fault and Protection

Electric power systems are made up of facilities and equipment that generate, transmit and distribute electrical energy with the purpose to provide energy for human in a secure, reliable and economic manner. It is one of the biggest and most complex systems have ever been built by mankind. The importance of the services carried out by power systems together with the huge investment for its facilities and equipment make the sustainable operation of power system is very critical to the society. To maintain sustainability of power systems against faults that normally occur in the power systems, an additional protection system that is able to take corrective actions against such faults have to be applied. This system consists of transformer, relays and circuit breakers. The purpose of the protection system is to disconnect the faulted element in the power system and re-establish its services.

As mentioned earlier, one of the power system's tasks is to transmit power from the generating stations to the load by transmission systems. At present, the transmission system are predominantly using overhead lines which is prone to disturbances caused by lightning that either directly strikes the lines or indirectly strikes the branches of tree in the vicinity of the lines. Statistics shows that 5-10% of lightning-caused faults are thought to cause permanent damage to equipment [1].

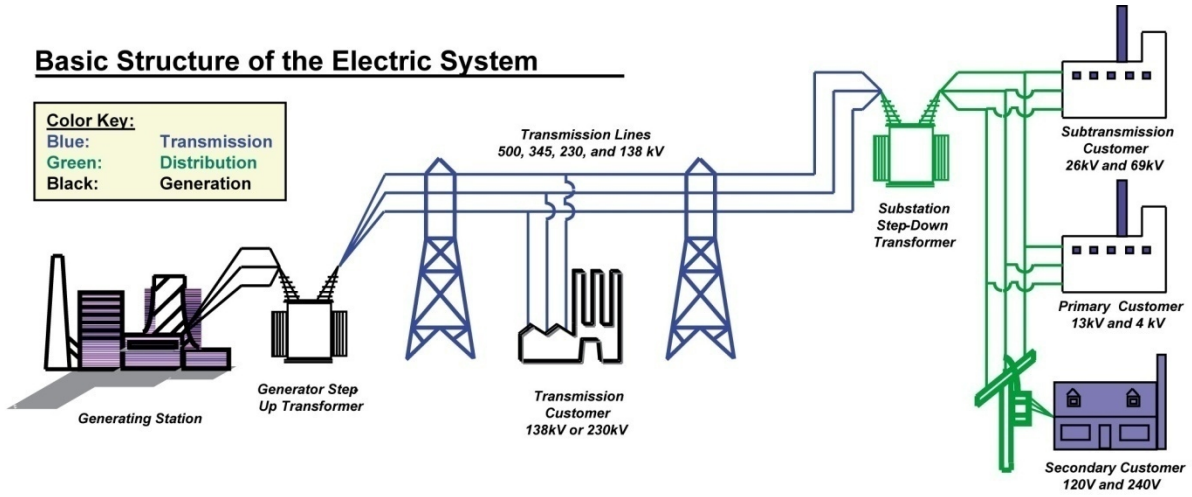

Figure 1-1. Basic structure of electric power system

Great amount of energy involved in a fault represents a serious threat to the power system equipment. Thus it is very important for the protection systems to promptly correct the faults. It can be seen from Figure 1-1, electrical power systems operate in several different states. Consequently, different fault scenarios may occur. The installed protection systems are required to be able to detect and react to all of these possible scenarios.

The high requirement of protection systems is a big challenge for the protection engineers. To comply with the requirement, a thorough test in high-voltage laboratory has to be conducted. However, not all

utility companies have sufficient high-voltage equipments needed to do such tests to the protection equipments, especially when it is related with the transient response of the equipment such as transformer. Furthermore, laboratory testing costs are very expensive albeit the ultimate accuracy it has to offer.

Measuring transient behavior of protection system is very important to ensure its successful operation during the faults. The main problem is that transient tests are always expensive and occasionally damage the equipment involved in the test. Also, if protection equipment fails in services, an improved design has to be developed rather than using simple trial error method. Modeling is the potential solution for these problems.

Modeling for transient studies has been successfully developed in majority of the components that constitute to modern electrical power systems. One exception to this rule is protective relays. The reason is because the previous generation relays, electromechanical relays, are less sensitive to system transient effects [2]. Modeling and testing of relays for transient response has become a critical issue since the introduction of electronic and microprocessor-based relays. Furthermore, precise modeling of the relays will allow a thorough analysis to be conducted for the purpose of evaluating the relay overall performance.

This thesis focuses on ATP – EMTP (Automatic Transient Program – Electromagnetic Transient Program) modeling and simulation of electromechanical and microprocessor-based mho distance protections relay. A transmission line of 125.6 miles operating at 60Hz and 115 kV is used as the test case. [3] provides general guidelines for the modeling of electrical power system protections in electrical transient simulation programs. The microprocessor based relay model in this work is based on the relay model developed by [4], using separate sub-model for low-pass anti-aliasing filter, sampling, a Fourier detector, and a quadrature-voltage polarized mho measuring unit. While the electromechanical relay model is developed using dynamic state space model derived and by [5].

1.2. Research Objectives

The objectives of this study are:

- Detailed model of the transmission line configuration consisting of the power source and line electrical characteristic of the line derived from the geometrical parameter of the overhead line.

- Detailed model of CT and CVT that is used in the distance protection scheme.

- Detailed model of the signal conditioning consists of low pass filter, sampling and Fourier detector.

- Detailed model of microprocessor-based mho distance relay, the developed algorithm should describe the relay's operating logic under normal and faulty conditions, by taking into account certain simplifications.

- Detailed model of electromechanical mho distance relay using verified state space model. The model is focused on the torque developed by the relay especially under very critical fault (fault very close to the relay location).

1.3. Thesis Layout

A brief description of the chapters' content is presented below:

- *Chapter* 2: Deals with the description of the various models implemented in ATP – EMTP. The models' description of the power sources, the overhead transmission lines, the high voltage overhead cable and the series reactors, which form the configuration between two substations.

- *Chapter 3:* Thoroughly describes the operation and the main characteristics of the CT and CVT. Moreover, it focuses on the saturation of the current transformer and the transient response of the capacitive voltage transformers.

- *Chapter 4:* Presents the basic principles of the distance protection. Together with the relay model built in ATP – EMTP. The signal conditioning model blocks which consist of Filtering, Sampling and Fourier detector are also discussed in this chapter.

- *Chapter 5:* Presents the results obtained by the various simulations of fault conditions. Single line to ground fault with different locations are simulated. The chapter also discusses the simulation of double line fault in microprocessor-based mho relay.

- *Chapter 6:* Discusses the conclusions reached by the obtained results and some recommendations for further research.

---This page is intentionally left blank---

2. Modeling of the Transmission Network in ATP - EMTP

2.1. Transmission Lines Model

The basic differential equation that describes the drop voltage at certain distance along the overhead line for the single phase can be given as [6]:

$$-\frac{\partial v}{\partial x} = R^{'} i + L^{'} \frac{\partial i}{\partial t} \qquad \textbf{Eq. 2-1}$$

$R^{'}$ and $L^{'}$ parameters are however not constant but rather functions of frequency. Thus the voltage drops must be expressed in the form of phasor equations at a specific frequency. For the three conductor lines, the vector equation can be represented as:

$$-\begin{bmatrix} \frac{dV_1}{dx} \\ \frac{dV_2}{dx} \\ \frac{dV_3}{dx} \end{bmatrix} = \begin{bmatrix} Z^{'}_{11} & Z^{'}_{12} & Z^{'}_{13} \\ Z^{'}_{21} & Z^{'}_{22} & Z^{'}_{23} \\ Z^{'}_{31} & Z^{'}_{32} & Z^{'}_{33} \end{bmatrix} \cdot \begin{bmatrix} I_1 \\ I_2 \\ I_3 \end{bmatrix} \qquad \textbf{Eq. 2-2}$$

In general this equation may also be expressed as:

$$-\left[\frac{dV}{dx}\right] = [Z'] \cdot [I] \qquad \textbf{Eq. 2-3}$$

Where:
[V] : vector of phasor voltages (conductor to ground)
[I] : vector of phasor currents in the conductors.

$[Z'] = [R'(\omega)] + j\omega[L'(\omega)]$ is the series impedance matrix which is complex and symmetric. The diagonal element $Z'_{ii} = R'_{ii} + j\omega L'_{ii}$ is the series self impedance per unit length form by conductor i and ground return. The off-diagonal element $Z'_{ki} = R'_{ki} + j\omega L'_{ki}$ is the series mutual impedance per unit length form by conductor *i* and conductor *k* which determines the longitudinally induced voltage in conductor *k* if a current flows in conductor *i*, or vice versa. Carson's formulas [7] for calculating Z_{ii} and Z_{ik} are used for LINE CONSTANTS and CABLE CONSTANTS supporting routine which is provided by EMTP.

Correct representation of transmission line as the key component of power system is very critical to study the steady state or transient behavior of power system. Equivalent PI lumped element section model which assumes constant parameters (e.g. at 60 Hz) is often used for short transmission line, where the travelling time is less than the simulation time step [8].

This model however cannot adequately simulate the response of the line over the wide range of frequencies which are present during the transient situations. For the transmission line with a fair length, that is a transmission line with traveling time longer than the simulation time-step, frequency dependent model is used. This model provides an accurate representation of the distributed nature of all line parameters, as well as their frequency dependence. Therefore, the line parameters for this model are not constant but functions of frequency [9]. It has been long recognized that one of the most important aspects in the modeling of transmission lines for electromagnetic transient studies is to account for the frequency dependences of the parameters and for the distributed nature of the losses [10].

Generally, EMTPs provides two major categories of transmission line models [9]:

1. Constant parameter model
2. Frequency-dependent model

EMTPs provide five types of model (as can be seen in Figure 2-1) for the frequency dependent category: PI, Bergeon, JMarti, Semlyen and Noda. Which are calculated by means of Line and Cable Constant (LCC) supporting routine in ATP – EMTP.

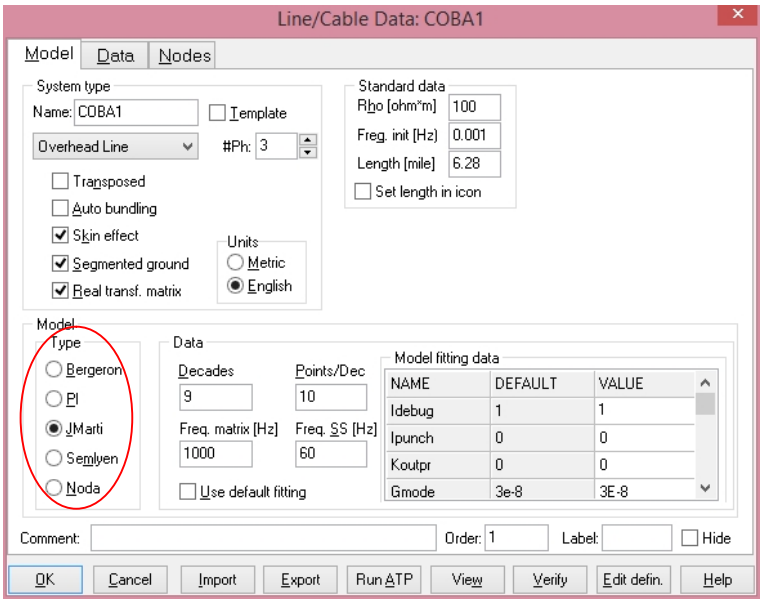

Figure 2-1. LCC model selection

For the adequate modeling of the transmission line using LCC routine, exact geometrical characteristics of the HV towers including DC resistance of the wires, inner and outer radius of the wires, distance between wires, tower height and also height of each wires must be specified [11]. The physical geometry of the line is given in the Figure 2-2. Jmarti model is chosen to perform the transmission line electrical parameter calculation based on the given geometry parameters.

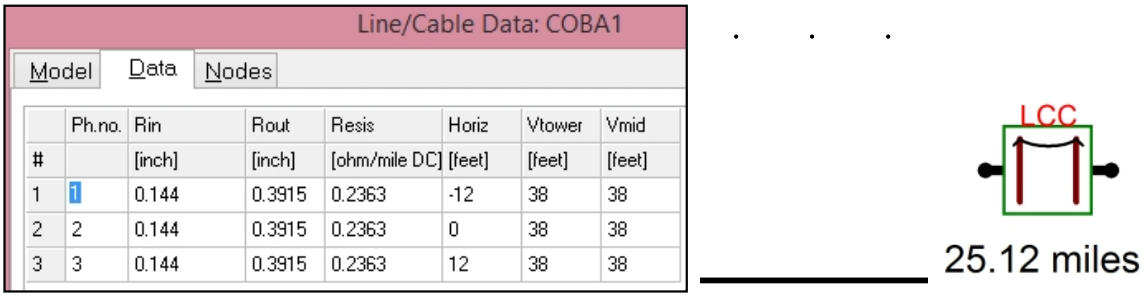

Figure 2-2. LCC Geometry

The comparison between Jmarti calculation results with the PI model is shown in the Figure 2-3(a) for the zero sequence impedance and Figure 2-3(b) for the positive sequence impedance. Figure 2-3(c) shows the impedance calculation based on the 60 Hz power frequency.

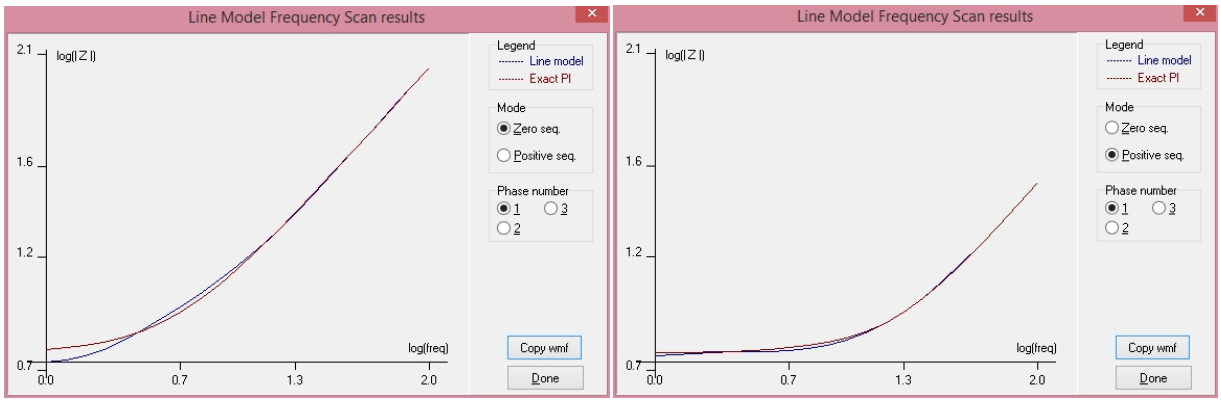

(a) Zero sequence impedance (b) Positive sequence impedance

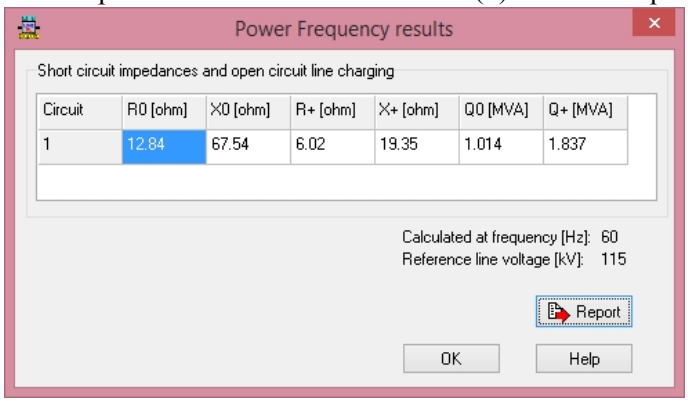

(c) Impedance verification

Figure 2-3. Jmarti calculation results compared to PI-model

The calculation result in the Figure 2-3(c) shows the impedance calculation for 25.12 miles transmission line. The total impedance of the transmission lines with the total length of 125.6 miles can then be calculated by:

- Positive sequence impedance:

$$Z_1 = \frac{125.6}{25.12} \cdot \sqrt{R_1^2 + X_1^2} \angle \tan^{-1}\left(\frac{X_1}{R_1}\right)$$

$$Z_1 = 101\Omega \angle 73$$

- Zero sequence impedance:

$$Z_0 = \frac{125.6}{25.12} \cdot \sqrt{R_0^2 + X_0^2} \angle \tan^{-1}\left(\frac{X_0}{R_0}\right)$$

$$Z_0 = 342\Omega \angle 79$$

2.2. Power Source Model

An ideal three-phase voltage source in series with sub-transient model for the positive and zero sequence resistance and inductance are used for the model of power source in ATP – EMTP. More specifically, Symmetric RL coupled line - *LINESY_3* provided by ATP - EMTP is used as the sub-transient impedance model. This component requires the values of R_0, L_0, R_1 and L_1 as the input parameter for the model. The equivalent circuit of the power source model used in this simulation is given in the Figure 2-4.

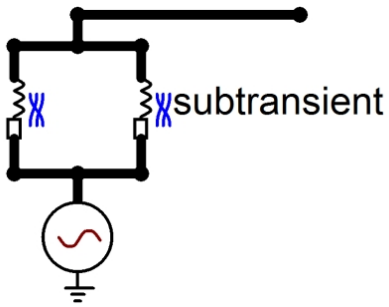

Figure 2-4. Power source model in ATP - EMTP

Further, this thesis discusses the condition where the transmission line is using double in-feed with load transfer, which requires a phase shift between two power sources. Figure 2-5 shows a three phase circuit containing transmission line between two buses. A single line to ground fault occurs at fault location F at *p* percentage of the transmission line measured from bus **S**. Considering the relay is at **S** location, part of the fault current which is supplied by bus **R** will not be detected by the relay in **S** location. Consequently, the relay may over-reach/under-reach depending upon the direction of power flow and the fault resistance magnitude.

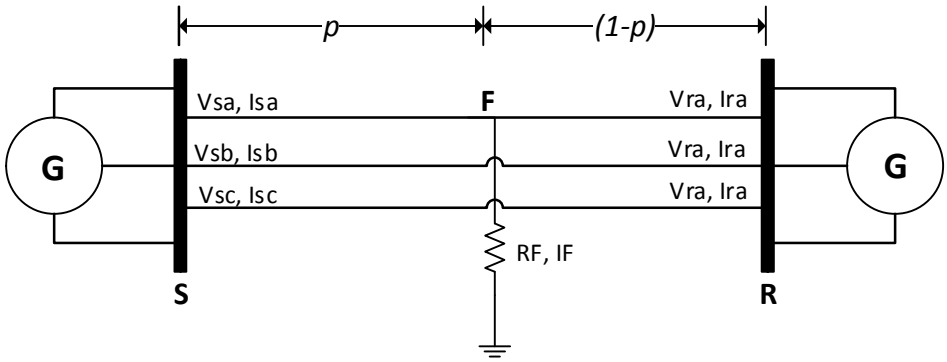

Figure 2-5. Double in-feed transmission lines

Input parameter for two power sources used in the simulation is given in the Figure 2-6. The figure shows the **S** power source leads the **R** power source by 10 degrees. The power transfer in the transmission line is described as:

$$P = \frac{U_s . U_R}{X_L} . \sin \delta_L \qquad \textbf{Eq. 2-4}$$

Where:

P : Real power transfer

U_s-U_R : Terminal **S** and **R** voltage

X_L : Reactance of transmission line

δ_L : Phase shift between voltage S and R

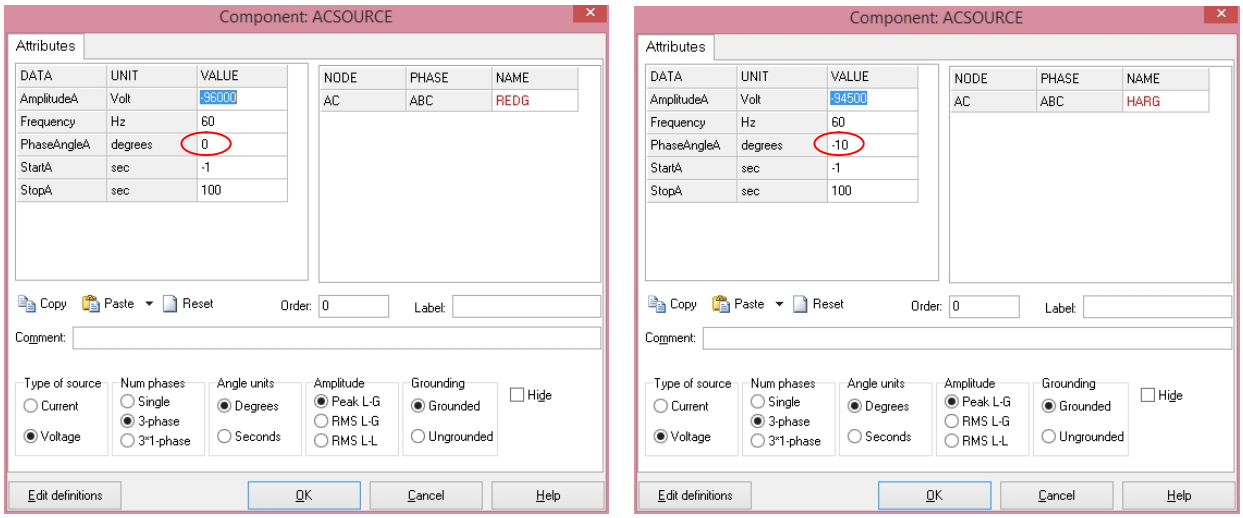

(a) **S** substation (b) **R** substation

Figure 2-6. Parameter input for the power source

Since I_R and I_S are not in phase in this particular case, the fault resistance R_F will contribute an error to the apparent impedance measured by the distance relay. Based on the direction of the power flow, the apparent impedance may be over-reach or under-reach of the protection scheme as can be seen in Figure 2-7. The apparent impedance is given by [12]:

$$Z_{app} = p.ZL_1 + Z_F \qquad \textbf{Eq. 2-5}$$

Where:

$$Z_F = \frac{I_F \cdot R_F}{I_{SA} + k_0 \cdot I_{S0}} \qquad \textbf{Eq. 2-6}$$

k_0 = zero compensation factor.

The phasor diagram of the shifting apparent impedance due to the power flow is given in the Figure 2-7.

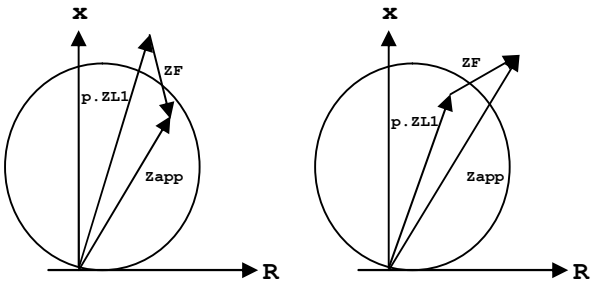

(a) Power flow from S to R (b) Power flow from R to S

Figure 2-7. Effect of the power flow to the measured apparent impedance

It is very clear from the given equation that under low resistance fault, the distance relay will still be able to provide satisfactory results. However, in the case of high resistance fault, particularly for some cases in single line to ground fault due to indirect lightning strike, protection from the distance relay may no longer be adequate.

3. CT and CVT Model in ATP - EMTP

3.1. CT (Current Transformer)

3.1.1. Introduction

The role of current transformer (CT) is very important for an accurate operation of relay protection. Along with potential transformer (PT), or in some cases capacitive voltage transformer (CVT), CT delivers the substantial data needed by the relay for its operation. Only when the data given by CT and PT (in form of current and voltage) from its secondary terminal properly represents the current and voltage at the primary side then the correct operation of relay protection can be achieved.

3.1.2. Basic Principle

Current Transformers are primarily used to provide isolation between the main high voltage primary circuit and the secondary control and metering devices. This isolation is achieved by magnetically couples the two circuits. Current transformers consist of a magnetic circuit in toroid form. The primary is made up of *n* turns or simply a single conductor crossing the toroid ($n_1 = 1$). The secondary is wound in *n* regular turns around this toroid [13].
Ampere's theorem states that the sum of the ampere-turns is equal to the circulation of the magnetic field vector.

$$n_1.i_1 + n_2.i_2 = \oint \overline{H}.\overline{n}.dl \qquad \textbf{Eq. 3-1}$$

Where:
H = Magnetic field strength
n = tangential unit vector

Transformer is said to be ideal if $\oint \overline{H}.\overline{n}.dl = 0$. In the practice with real transformer, this ideal condition cannot be fulfilled. In this case, the term refers to error introduced by magnetic circuit due to an excitation current i_e.

$$\oint \overline{H}.\overline{n}.dl = n_2.i_e \qquad \textbf{Eq. 3-2}$$

The equation then can then be rewritten as:

$$n_1.i_1 + n_2.i_2 = n_2.i_e \qquad \textbf{Eq. 3-3}$$

Thus the transformer can be represented as having two parallel elements:

1. Perfect transformer with ratio $n = \frac{n_2}{n_1}$ delivers current $\frac{i_1}{n}$ at secondary circuit.
2. An impedance which consumes i_e.

Figure 3-1 below shows the equivalent circuit of CT. where R_1 and R_2 are the winding resistance which will slightly reduce the voltage and introduce the voltage drop, l_1 *and* l_2 are the leakage inductances. $i_e = i_m + i_a$ is the exciting current which is divided into:

- i_m the magnetizing current which transfers power from one winding to the other by creation of a magneto-motive force (MMF) which induces the flux Φ and
- i_a which represents losses in CT due to hysteresis and eddy currents.

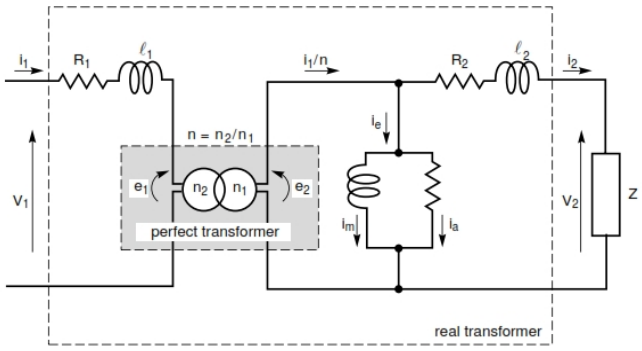

Figure 3-1. CT equivalent circuit

Further, the excitation current i_e will introduce a displacement angle δ between the primary current i_1 and the secondary current i_2. This can be explained graphically in Figure 3-2 below.

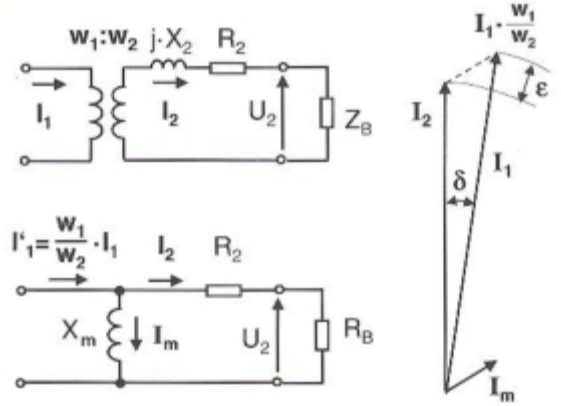

Figure 3-2. Error introduced by excitation current i_e

It can be seen from the figure that larger excitation current i_e, primarily from the magnetization current i_m part will lead to larger displacement angle δ, and thus larger error ε.

3.1.3. Specification for Protection CT

In general, CTs are divided into two major categories based on their functionality: instrument CTs and protection CTs. The measurement or instrument type of CTs are intended for use with indicating or integrating devices while the protection CTs are intended for use with protection devices. The main distinction between the two is that the operating currents of the instrument type of CTs are lower than the ones of the protection types [14].

As discussed in the previous section, there is always some difference in expected value and actual output value of CT which is mainly due to the magnetization currents. Accordingly, limiting factor is introduced as the guidance for selecting the CTs. In the protection CTs, this limiting factor is known as

accuracy limit factor (ALF). ALF is given as a multiplication factor of the primary currents below which the protection CTs able to provide currents to secondary winding with the given accuracy stated in the accuracy class. Thus the rated accuracy limit current is indicated by:

$$I_{a1} = ALF \cdot I_N \qquad \textbf{Eq. 3-4}$$

ALF is given by assuming that the CT is connected with the rated burden. If the connected burden is different than the rated one, the ALF has to be re-calculated. This means that the internal MMF related with the saturation voltage of the CT has the same value for both cases. The voltages at the secondary terminals of the CT correspond to the voltage drop across the connected burden $U_2 = I_2 \cdot R_B$. The power supplied by CT, assuming that the burden is purely resistive, is equal to:

$$P_2 = U_2 . I_2 = I_2^2 . R_B \qquad \textbf{Eq. 3-5}$$

The induction in the CT under nominal operating condition is proportional to the internal MMF:

$$E_2 = I_2 (R_{CT} + R_B) \qquad \textbf{Eq. 3-6}$$

The internal MMF that arises when the rated accuracy limit currents $I_{2,al}$ is flowing through secondary winding corresponds to the saturation voltage of the CT.

$$E_{al} = ALF . I_{2N} (R_{CT} + R_{BN}) \qquad \textbf{Eq. 3-7}$$

When different burden is connected to the CT, the internal MMF value will still be the same. The ALF then has to be re-calculated:

$$E_{al} = ALF' . I_{2N} (R_{CT} + R_{B,connected}) \qquad \textbf{Eq. 3-8}$$

From Eq. 3-7 and 3-8, the change in ALF due to the change of the burden connected to the secondary winding of CT can be re-calculated as:

$$ALF' = ALF . \frac{R_{CT} + R_{BN}}{R_{CT} + R_{B,connected}} \qquad \textbf{Eq. 3-9}$$

Eq. 3-9 implies that smaller connected burden resistance results in an increase of the ALF.

The basic specification of current transformer as a whole can be represented in the table 3-1 below:

Rated transformation ratio	Ratio of nominal primary to nominal secondary current I_{PN}/I_{SN}, e.g. 600/5 or 1200/5
Rated power P_N	Rated power provided at the secondary side of CT under rated current and rated burden, e.g: 25 VA for 5A secondary winding current at B-01 burden designation.
Accuracy limit factor	ALF, multiplication factor of the rated current (without DC component) which determines the maximum current that can be transformed into the secondary with the defined accuracy class if the connected burden equals the rated burden, e.g: 10 or 20.
Accuracy class	Composite error, ε_c, at ALF times rated current, e.g: 5P or 10P.
Secondary internal resistance	R_{CT} in ohm, nominal resistance of the secondary given by the CT manufacturer.

Table 3-1. Basic data of a protection CT

3.1.4. CT saturation

Figure 3-3 below shows the typical magnetization curve for multi-ratio C-class current transformer [15].

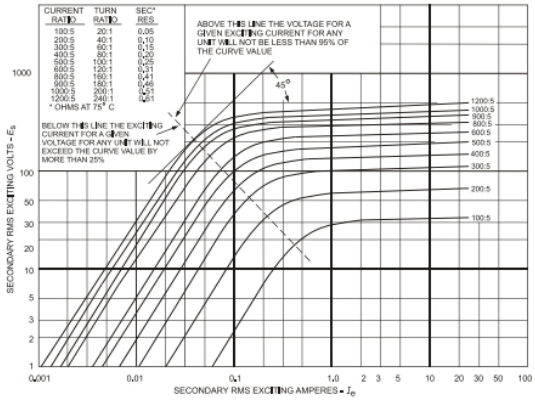

Figure 3-3. Typical magnetization curve for multi-ratio C-class CT

As can be seen from the figure, the CT operation is characterized by magnetization curve which consists of linear and saturated part. When CT operates in its linear magnetizing curve, the total error in the secondary side is very small and negligible. However, when the CT is driven into saturation because the magnetizing branch draws more currents and the magnetic induction exceeds the *knee point*, the large error current will arise. The knee point itself is defined by *IEEE* as the point where the tangent is at 45° to the abscissa of the magnetization curve. This large error further will threaten the correct operation of the protection relay.

CT may be driven into saturation due to pure AC fault current that exceeds the accuracy limit current ($ALF < I_F/I_N$) or due to fault current that consist of DC component.

- CT saturation due to pure AC fault current

This type of saturation occurs when the currents in primary winding exceeds the accuracy limit of the CT.

$$I_1 > ALF' \cdot I_N$$

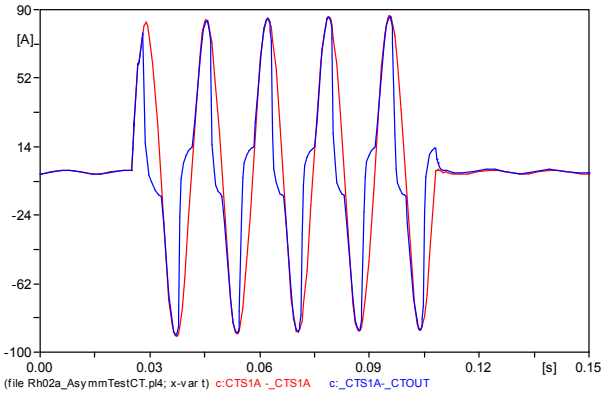

Figure 3-4. Steady state saturation on CT with AC currents

The red line in the figure above shows the ideal output currents while the line shown by the blue color is the distorted currents output in the secondary winding due to saturation.

- CT saturation due to fault current with DC component

The DC offset will significantly increase the core flux. This is more likely the cause for the saturation on CT because in this case more inductions are occur as explained in Figure 3.5 [16] below.

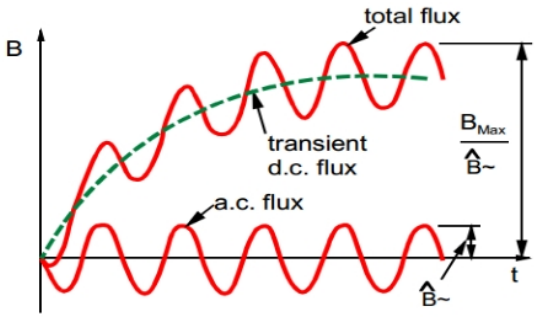

Figure 3-5. CT induction due to DC offset

Graphical representation of the saturation due to DC offset on the secondary winding of CT is given in the Figure 3-6 below. Green line on the graph shows the saturated currents in the secondary winding of CT:

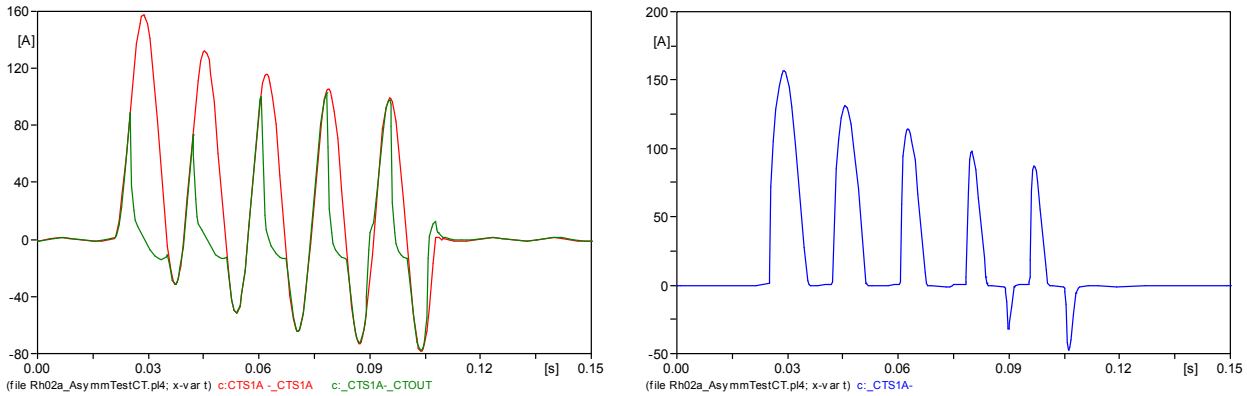

(a) saturated current (b) magnetizing current

Figure 3-6. Saturation with DC offset current

3.1.5. CT Transient Performance (TP) Classes

Apart from the basic technical specification, CTs are also specified with regards to their transient responses. IEC 60044-6 standard differentiates protection CTs into four classes based on the construction of CT core:

1. Class TPS : closed iron with very low leakage inductance

   The transformation response is defined by the magnetization curve and the secondary winding resistance. Thus the residual flux is not limited.

2. Class TPX : closed iron core without limitation of the remanence

   AC and DC components transient current within the defined range are transformed with high accuracy. However, the remanence is very high (may reach 80%).

3. Class TPY : CT with anti-remance air gap (Remanence $B_r \leq 10\%$)

   Considerably limits the residual flux (up to only 10%) due to small air gaps (in the range of some millimeters) in the magnetic core.

4. Class TPZ : CT with linear core (Remanence negligible)

   The air gap in this case is centimeters sized. Thus the residual flux is extremely limited that it can be neglected.

   The typical magnetization curve of TPX, TPY and TPZ class can be shown in the Figure 3-7 below.

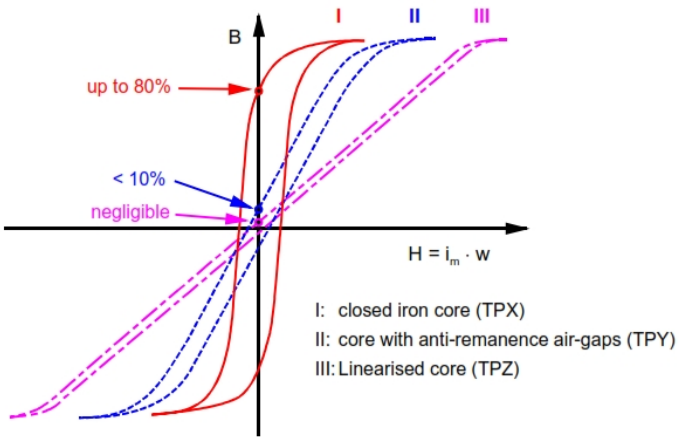

Figure 3-7. Magnetizing curve and point of remanence of different TP class

3.1.6. CT Modeling

[17] explains the step-by-step construction of CT model in ATP – EMTP. The CT model is built using TRAFO_S – saturable transformer single phase, while modeling of the magnetization curve is done by using NLIND96 – Pseudo-nonlinear hysteretic inductor TYPE 96.

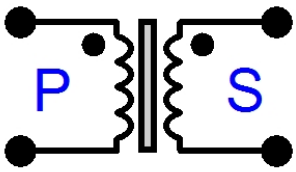

Figure 3-8. TRAFO_S component in ATP – EMTP

Figure 3-9. NLIND96 in ATP – EMTP

Modeling of CT saturation using Type-96 has been validated by [18, 19] confirming the performance of the CT under transient. The saturation curve is entered with the $(I_{e,rms}, V_{2,rms})$ value depicted from CT 600:5A saturation curve. Satura subroutine provided by ATP – EMTP is used to convert RMS saturation curve data into peak data of excitation current and flux linkage ($I_{e,peak}, \lambda_{peak}$) with the hysteresis loop being ignored. The simplified per phase equivalent of the CT model including the magnetization curve as modeled in ATP – EMTP can be given in the Figure 3-10 below. Table 3-2 represents $I_{e,peak}, \lambda_{peak}$ pairs of the CT magnetization curve. The magnetization curve is also represented in graph in the Figure 3-11.

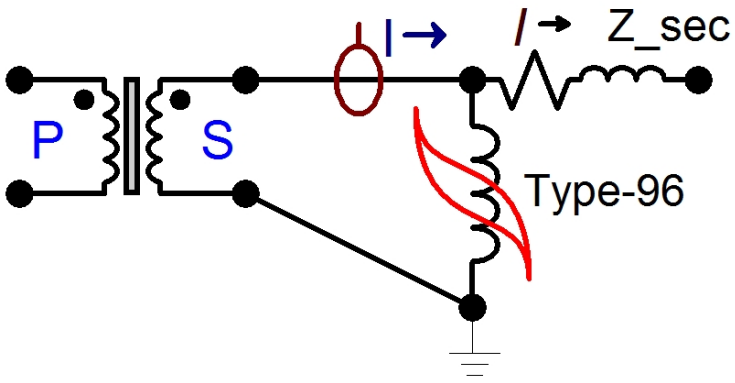

Figure 3-10. CT model

$I_{e,peak}$ (A)	λ_{peak} (Wb-T)
-2.186547	-1.524134
-1.457698	-1.514952
-0.6559641	-1.482817
-0.2915396	-1.450682
-0.1093274	-1.423137
0.03644245	-1.368048
0.1275486	-1.303777
0.2113662	-1.193599
0.2550971	-1.009968
0.2915396	-0.7345224
0.3644245	0.4912118

0.4008669	0.6794332
0.5101943	0.9181529
0.6559641	1.101784
0.7944454	1.193599
1.03861	1.285414
1.421256	1.368048
1.949671	1.432319
2.550971	1.478226
3.644245	1.524134
5.830792	1.56086
8.017339	1.570042

Table 3-2. pairs of $I_{e,peak}, \lambda_{peak}$ of the magnetization curve

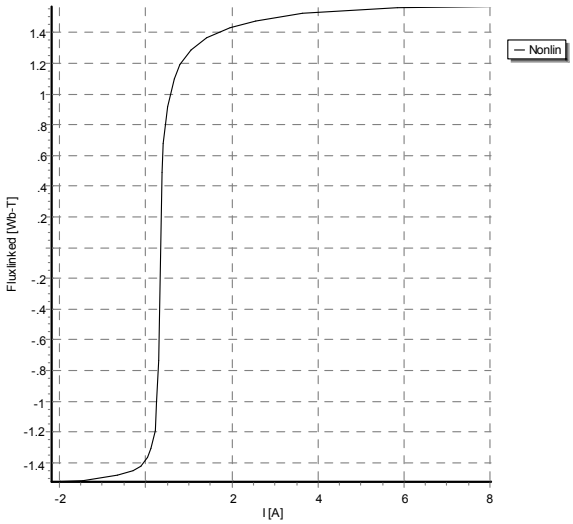

Figure 3-11. Graph representation of magnetization curve

3.2. CVT (Capacitive Voltage Transformer)

3.2.1. Introduction

Conventional voltage transformer with the usual electromagnetic type is very costly to be implemented in high-voltage systems. Thus the application of the capacitive type voltage transformer which later known as capacitive voltage transformer (CVT) became widely used in the field as this type of voltage transformer offers considerable savings compared to the conventional one. More specifically, it is suggested that CVT possesses considerable economical advantages over the conventional type in systems of 66 kV and above [20]. CVT transforms the line voltage to low voltage through a sequence of capacitive potential dividers and an electromagnetic voltage transformer. A schematic of simplified circuit of CVT is depicted in Figure 3-12.

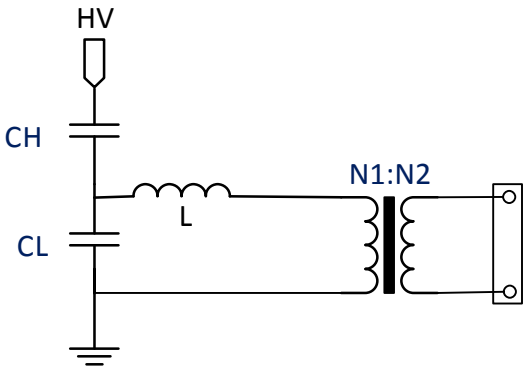

Figure 3-12. Simplified CVT connection

Basic CVT circuit mainly consists of the following components:

1. Coupling capacitors (CH and CL)
2. Compensating reactor (L)
3. Step-down transformer
4. Ferroresonance-suppression circuit

The coupling capacitor C_H and C_L functions as the voltage divider which steps down the high voltage of the line to intermediate level (5 to 15kV). However, these coupling capacitors also introduce reactance which later creates an undesirable phase shift between primary and secondary voltage. Hence the compensating reactor L is used to cancel this reactance at power frequency. Further, the step down transformer reduces the intermediate voltage to typical relaying voltage.

The compensating reactor and step-down transformer have iron cores which besides introduce copper and core losses they also produce ferroresonance due to the nonlinearity nature of the iron cores. Thus the manufacturers include the ferroresonance suppression circuit to avoid dangerous and destructive overvoltage that can be caused by ferroresonance [21].

When a fault occurs and suddenly reduces the line voltage, the CVT secondary output cannot instantaneously represent the primary voltage because the energy storage elements, such as coupling capacitors and the compensating reactor, cannot instantaneously change the charge or flux. These energy storage elements introduce transient in the CVT secondary output. CVT transients differ depending on the fault point-on-wave (POW) initiation. The CVT transients for faults occurring at voltage peaks and voltage zeros are quite distinctive and different [22].

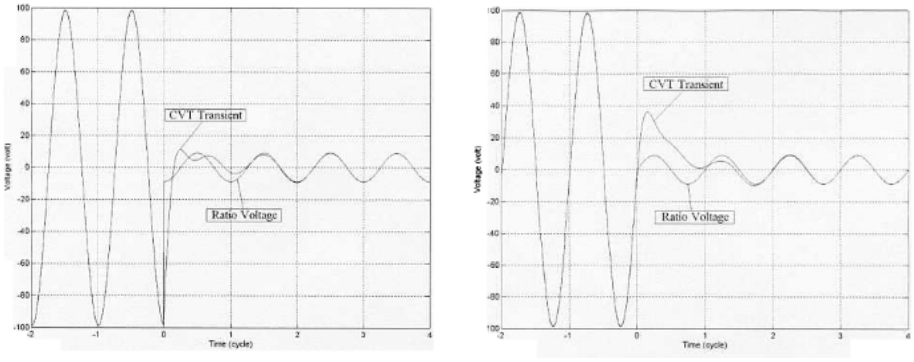

(a) fault at voltage peak (b) fault at voltage zero

Figure 3-13. CVT transient under faults

3.2.2. CVT Modeling

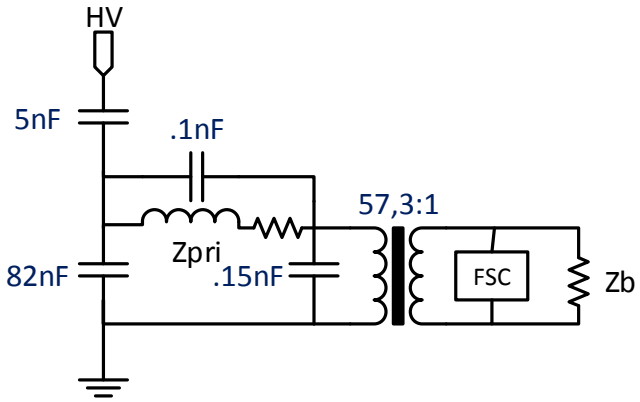

Figure 3-14. CVT Model

Sum of the coupling capacitors C_L + C_H is normally set at approximately 100nF. Higher capacitance selection can decrease the transient but at the same time it will increase the cost. In this model, C_L is set at 82nF while C_H is set at 5nF. Thus the voltage enters the step down transformer is given as:

$$V_L = \frac{C_H}{C_H + C_L} \cdot V_H = \frac{5nF}{5nF + 82nF} \cdot 115kV = 6.6kV$$

The turn ratio $N_p : N_s$ is 6.6kV:115V. Thus the final step down ratio can be calculated by:

$$V_s = \frac{N_s}{N_p} \cdot V_L = \frac{115}{6.6kV} \cdot 6.6kV = 115V$$

4. Mho Distance Relay and Signal Conditioning Model

4.1. Mho Distance Relay

Distance protection is a universal short-circuit protection which the mode of operation is based on the short-circuit impedance, which in the classic case is proportional to the distance to the fault. The distance protection relay measures the line voltage and line current at the relay location and evaluates the ratio between these quantities. This ratio represents the apparent impedance from the fault to the relay location. Consider the relay at sub-station A in Figure 4-1 below.

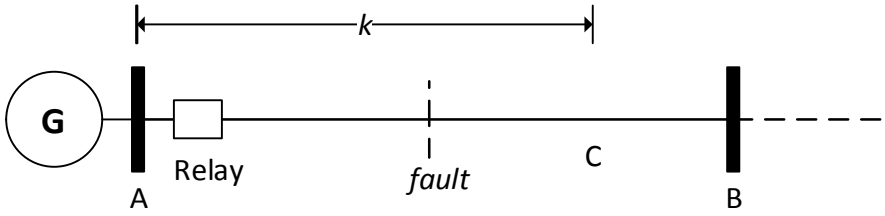

Figure 4-1. Fault occurrence in power system

When a fault occurs on the protected line, the fault current I_F and voltage V_F is fed into the relay. The relay then calculates the apparent impedance Z_{app} as the ratio of fault voltage V_F and fault current I_F, $Z_{app} = \frac{V_F}{I_F}$. The relay should trip if the fault occurs within the fractional distance *k*, which is called "the reach setting" of the distance relay, of the total distances between buses A and B. the reach given is thus considered as the tripping threshold. Assuming the point C in the Figure 4-1 as the threshold point, the voltage drop along the line when the fault occurs at point C is equal to:

$$U_f = k.Z_L.I_F \qquad \textbf{Eq. 4-1}$$

Where:
Z_L : Total Impedance of the line.

While the setting impedance can be calculated as:

$$Z_{setting} = k.Z_L \qquad \textbf{Eq. 4-2}$$

If the apparent impedance Z_{app} calculated by the relay during the fault is smaller than $Z_{setting}$, which means that the fault occurs within the fraction *k* of the line measured from the relay location, then the relay will trip.

$$\text{Re}lay\_Trip\begin{cases} Yes, & Z_{app} \le Z_{setting} \\ No, & Z_{app} > Z_{setting} \end{cases} \qquad \textbf{Eq. 4-3}$$

During normal operation, the impedance seen by the relay is approximately equal to the load impedance Z_{load}, which is normally much higher than the line impedance.

$$Z_{load} >> Z_L \qquad \textbf{Eq. 4-4}$$

4.1.1. Setting of the Distance Zones

Line impedances which are proportional to the line length are used as the main parameter to determine the distance from the relay location to the fault. However, the relay is fed by the current and voltage transformer which converts the signal measured in the primary side connected to the transmission line to the secondary terminal based on the winding ratio of the transformer. Therefore, the relay setting for the impedance is based on the secondary value obtained from the following expression [23]:

$$Z_{\text{sec}} = \frac{I_{\text{Pr}i} / I_{Sec}}{U_{\text{Pr}i} / U_{Sec}} . Z_{\text{Pr}i} \qquad \textbf{Eq. 4-5}$$

Where I_{pri} / I_{sec} and U_{pri} / U_{sec} are the transformation ratios of the current and voltage transformers, respectively.

For the electromechanical relay in this study, the 600:5 transformation ratio of the CT is chosen, while for the ratio of CVT is 115kV:115. Thus the setting impedance can be calculated as:

$$Z_{\text{sec}} = \frac{600/5}{115kV/115} . Z_{\text{Pr}i}$$

$$Z_{\text{sec}} = 0.12 \cdot Z_{\text{Pr}i}$$

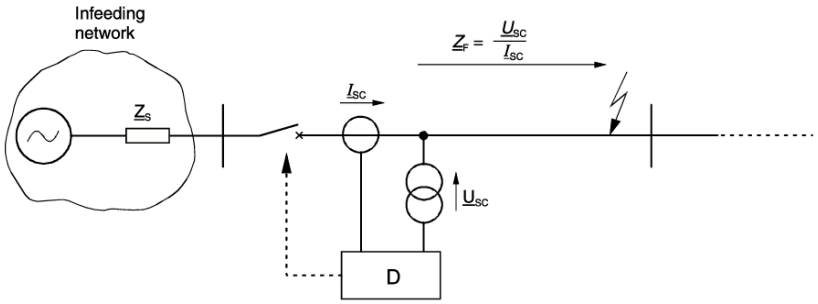

Figure 4-2. Distance Protection measurement of fault impedance

The distance protection is set to cover a section of the transmission lines and to provide a back-up protection for adjoining parts of the network, such as bus-bars, transformers and further feeders. The performance of distance relay near its zone boundaries is not very predictable due to various types of errors introduced by the inaccuracies of instruments involved as well as fault resistance or even the inaccuracy of line impedance which is usually based on a calculation rather than a measurement [24]. The concept of stepped distance protection scheme based on the protection reach is applied to accommodate the operation of distance relay. The protection is usually divided into two to three zones:

- Zone 1: this is set to protect between 80-85% of the line length AB and operates without any time delay.

- Zone 2: this is set to protect 100% of the line length AB plus 20% of the adjacent line BC and operates with time delay t_2.
- Zone 3: this is set to protect 100% of the line length AB + BC plus 25% of the third line CD and operates with time delay t_3

The protection schemes of distance relays can be explained graphically in the Figure 4-3. Due to the earlier mentioned inaccuracies, protection reach setting of 100% of the line length with a distance protection is not possible in practice. A security margin (10-15%) from the remote end of the line must be selected for the so called under-reaching stage (1st zone) to ensure secure protection selection between internal and external faults [23].

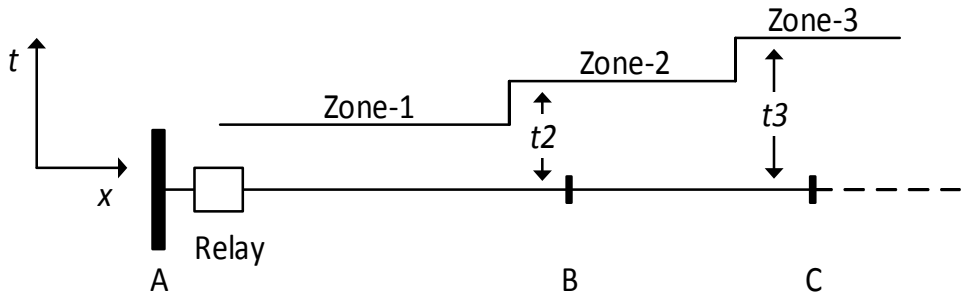

Figure 4-3. Distance Relay Protection Scheme

4.1.2. Phasor Diagrams and R-X Diagrams

The relay characteristic is given in the R-X plane which is generally known as R-X diagrams. It is very useful diagram to determine the response of distance relays for different types of system conditions including faults, load changes, and power swings. The distance relay responses in R-X plane is derived from the phasor diagrams representing the current and voltage as the inputs for the distance relay.

$$Z_{app} = R + jX = \frac{E}{I} \qquad \textbf{Eq. 4-6}$$

Figure 4-4 illustrates of the variations in current magnitude and phase angle effects on the R-X diagram. In the condition when the current is lagging to the voltage, the resulting apparent impedance will fall in the first quadrant which represents the active and reactive power flowing from the bus into the line. Right half of the plane corresponds to the real power flowing into the line, while the left half corresponds to the real power flowing into the bus. Similarly for the upper half of the plane corresponds to the reactive power flowing into the line, while the lower half corresponds to the reactive power flowing into the bus. When the fault occurs, the voltage magnitude decreases and at the same time the current magnitude will increase. This condition brings the apparent impedance closer to the origin of the R-X diagram. This is the main principle of the R-X diagram used as the characteristic of distance relay.

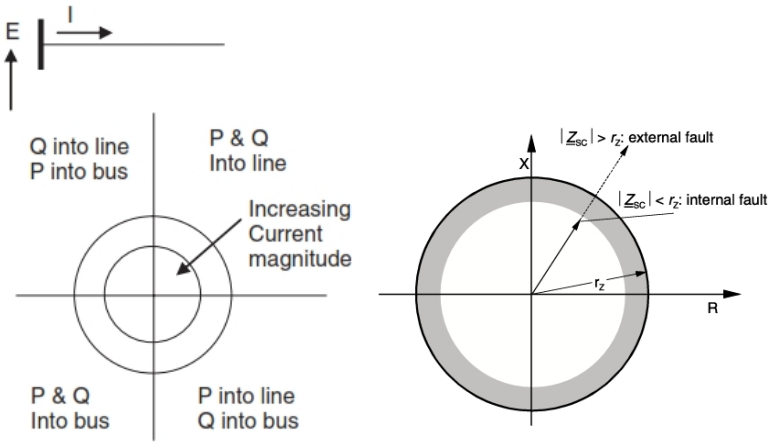

(a) Apparent impedance behavior (b) Impedance circle

Figure 4-4. Distance relay characteristic in R-X diagram

Throughout years of implementation, the shape of the distance relay operation zones has been developed to meet the adequate protection required. Originally, the operating characteristic was a circle shaped with the center located in the origin of R-X coordinates as depicted in Figure 4-4. However, this type of relay is non-directional and sensitive to power swings and load encroachment due to large impedance circle. Therefore, the circle diameter was reduced with the center of the circle passed through the origin of R-X coordinates resulting in mho-relay.

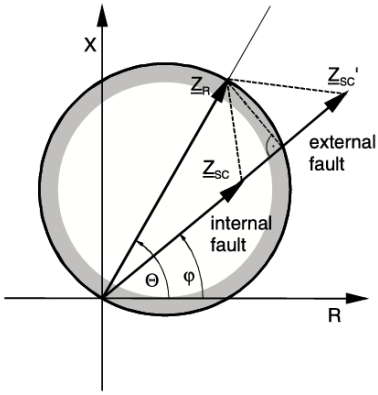

Figure 4-5. Mho relay characteristic

4.1.3. Polarized Mho Relay

Apparent impedance measured by calculating the ratio of the voltage and current of a particular phase is the line impedance from the relay location to the fault if it is a three-phase fault. However, this is not the case for different types of fault. Different voltage and current combinations are used for different types of fault in order to obtain consistent measurements.

Listed below are the voltage and current combinations for detecting single line to ground faults (table 4-1) and line to line faults (table 4-2) respectively. The constant *k* in table 4-1 is explained in more details in chapter 4.1.5.

Voltage applied	Current applied	Faults
Va	Ia+*k*3I0	Phase A to ground
Vb	Ib+*k*3I0	Phase B to ground
Vc	Ic+*k*3I0	Phase C to ground

Table 4-1. Voltage and current combination for detecting single line to ground faults

Voltage applied	Current applied	Faults
Va-Vb	Ia - Ib	Phase A to Phase B Phase A to Phase B to ground
Vb-Vc	Ib - Ic	Phase B to Phase C Phase B to Phase C to ground
Vc-Va	Ic - Ia	Phase C to Phase A Phase C to Phase A to ground

Table 4-2. Voltage and current combination for detecting single line to ground faults

This study will further discuss the microprocessor based mho distance relay model developed by using phase angle comparator function. The phase angle comparator mho function has two inputs for its operation: operating signal ($\mathbf{IZ_R - V}$) and polarizing signal ($\mathbf{V_{Pol}}$). These voltage signals (operating signal and polarizing signal) are derived from the system voltage and current supplied to relay. In an analog relay, the relay current is converted to a voltage in the relay, typically by a transactor. Transactor is an iron core reactor with an air gap. The transactor produces a voltage proportional to the input current. Simple one line diagram of analog distance relay system can be seen in the Figure 4-6 below.

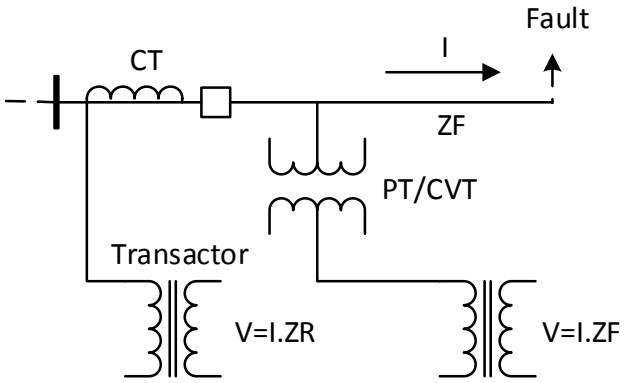

Figure 4-6. Simple analog relay

As mentioned earlier, the phase angle comparator function requires polarizing signal as one of its input beside the operating signal as the other input. This polarizing signal is used to provide a reliable angle reference for directional discrimination. During the fault, this angle reference should be stable and lasted long enough to ensure that the protection element consistently picks up until the fault is cleared. Following are the basic requirements need to be satisfied by the polarizing signal of angle comparator function of mho distance relay:

1. Provide reliable operation for all in-zone faults.
2. Be secure for all external faults.
3. Provide stable operation during single-pole open conditions.
4. Tolerate fault resistance.

A number of polarizing quantities have been used in developing phase and ground mho distance functions. Following are some of the more commonly used [25]:

- Self-polarized (V_a for Phase A function, V_{ab} for the Phase AB function, etc.)
- Positive Sequence Voltage (V_{a1} for Phase A function, V_{ab1} for Phase AB function, etc.)
- Quadrature Voltage (V_{bc} shifted leading 90 for Phase A function)
- Median (midpoint of V_{bc} to V_a for Phase A function)
- Leading phase (V_c shifted leading 240 for Phase A function)

Mho function that uses other than self-polarization are often addressed as cross polarized. Self polarization, as explained above, uses the faulted phase voltage as the polarizing quantities. The resulting mho characteristic remains constant regarding the changes in power system and fault conditions. Thus the mho characteristic often referred as static mho. The drawback of this type of polarization is that during a close-in fault, where the faulted phase voltage falls to zero, the relay may not be able to work properly. It is very desirable for the polarizing voltage to be able to provide sufficient magnitude even during such fault.

Cross polarization voltage uses un-faulted healthy phase voltage as the polarizing quantity. The mho characteristic produced changes to different power system and fault conditions. Thus it is difficult to show this type of mho characteristic on an impedance diagram. This type of mho is referred as dynamic mho. Most of the modern mho distance relay uses this un-faulted phase voltages in the polarizing signal. Thus the actual mho characteristics of the relay do not have an invariant plot on the R-X impedance diagram. The characteristics vary based on power system conditions and fault type. The eminence of this polarization compared to the self-polarization is that during the close-in fault, this polarization is still able to provide sufficient magnitude of polarizing voltage.

The effect of polarizing voltage selection during the single line to ground fault and line to line fault will be studied in this project. Self polarization and cross polarization will be simulated to both faults.

1) Phase A to ground fault
   - Self polarization using phase-A voltage.
     In phasor form:
     $$V_a = \mathrm{Re}(V_a) + j\,\mathrm{Im}(V_a)$$
     The angle of polarizing voltage can be given by:
     $$Polarizing\_angle = \tan^{-1}\left[\frac{\mathrm{Im}(V_a)}{\mathrm{Re}(V_a)}\right]$$
   - Cross polarization using Vbc shifted by 90 degrees
     $$V_{bc} = V_b - V_c$$
     In phasor form:
     $$V_{bc} = \mathrm{Re}(V_b - V_c) + j\,\mathrm{Im}(V_b - V_c)$$
     The angle of polarizing voltage can be given by:
     $$Polarizing\_angle = \tan^{-1}\left[\frac{\mathrm{Im}(V_{bc})}{\mathrm{Re}(V_{bc})}\right] + 90^0$$

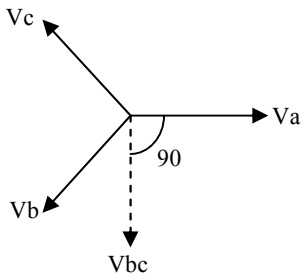

Figure 4-7. V_{bc} shifted 90 degrees as the polarizing signal for phase A fault

2) Line A to line B fault
   - Self polarization using Vab

     $V_{ab} = V_a - V_b$

     In phasor form:

     $V_{ab} = \mathrm{Re}(V_a - V_b) + j\,\mathrm{Im}(V_a - V_b)$

     The angle of polarizing voltage can be given by:

     $$Polarizing\_angle = \tan^{-1}\left[\frac{\mathrm{Im}(V_{ab})}{\mathrm{Re}(V_{ab})}\right]$$

   - Cross polarization using Vc shifted by -90 degrees

     In phasor form:

     $V_c = \mathrm{Re}(V_c) + j\,\mathrm{Im}(V_c)$

     The angle of polarizing voltage can be given by:

     $$Polarizing\_angle = \tan^{-1}\left[\frac{\mathrm{Im}(V_c)}{\mathrm{Re}(V_c)}\right]$$

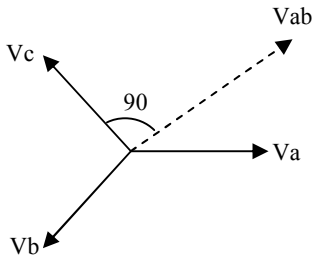

Figure 4-8. V_c shifted -90 degrees as the polarizing signal for line A to line B fault

The polarization by using 90 degrees phase shifting is also known as quadrature polarization.

4.1.4. IR-IX Diagram

Because mho characteristic uses the angle between voltage phasors, voltage diagram is chosen to plot the characteristic rather than the ***R-X*** diagram shown in Figure 4-5. This voltage diagram is obtained from the ***R-X*** diagram by multiplying each point with fault current. This can be shown in the Figure 4-9 below:

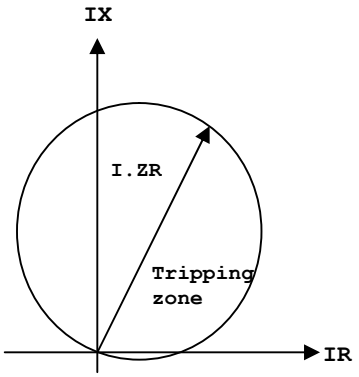

Figure 4-9. IR-IX Voltage diagram

Based on the location of the fault, the fault current will have different value. Thus resulting in the contracting and expanding of the $I.Z_R$ phasor and hence the voltage diagram. However, the voltage phasors will have the same phase angle and magnitude relationship as the impedance vectors on the ***R-X*** diagram.
Classical mho characteristic can be seen in the ***IR-IX*** diagram as shown in Figure 4-10 below:

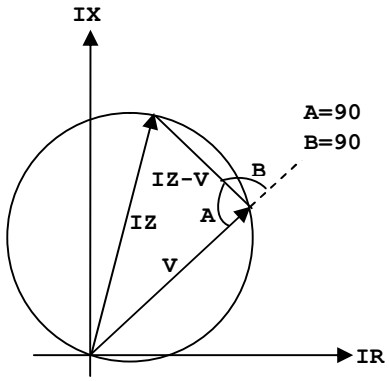

Figure 4-10. Classical mho characteristic

I.Z phasor shown above determines the diameter of the circle where it originates from the point of origin. Usually this diameter is referred as "angle of maximum reach" or in other term "angle of maximum torque".

Above characteristic shows the V_{pol} plot in the balance point. Looking back to the simple analog relay in Figure 4-6, voltage V_{pol} realized by the relay is equal to $I.Z_F$ where Z_F is the impedance from the relay location to the fault. The position of phasor V is along the impedance to the fault Z_F. In the condition depicted from Figure 4-10 above, we can see the $I.Z_R$-V leads V_{pol} by 90 degree. This condition can be shown in Figure 4-11 below:

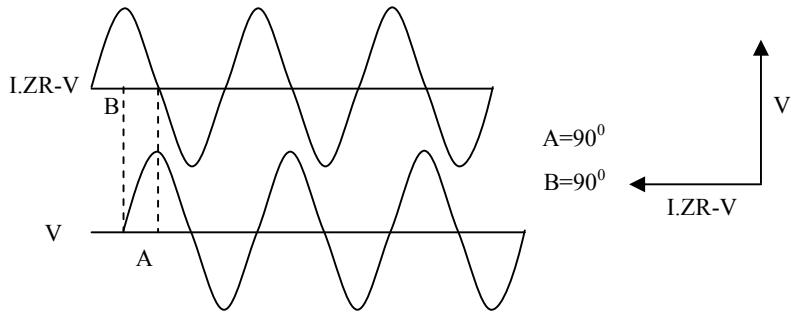

Figure 4-11. The operating voltage leading the polarization voltage by 90 degrees

If the fault is moved closer to relay, the magnitude of V will decrease relative to the magnitude of $I \cdot Z_R$ as it is shown in Figure 4-12. For this condition, the angle A is greater than 90 degrees while the angle B is less than 90 degrees. For this condition, $\boldsymbol{I \cdot Z_R - V}$ leads $\boldsymbol{V_{pol}}$ by less than 90 degrees.

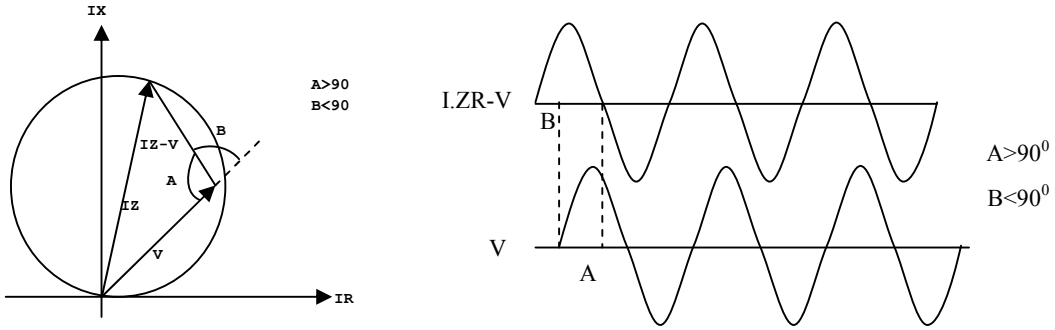

Figure 4-12. The operating voltage leading the polarization voltage by less than 90 degrees

The characteristic of the range of protection angle can be drawn as:

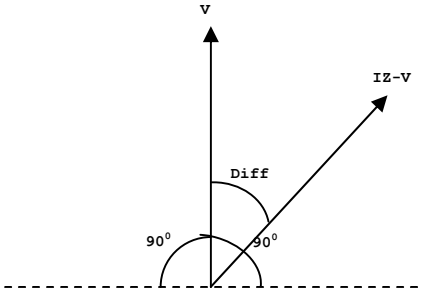

Figure 4-13. Protection angle of mho relay

The figure shows that the relay will trip when the angle difference between $\boldsymbol{I.Z - V}$ and $\boldsymbol{V_{pol}}$ is between -90 to 90 degree.

$$\text{Re}lay = \begin{cases} trip, & -90 < diff < 90 \\ no \quad trip, & others \end{cases} \qquad \textbf{Eq. 4-7}$$

Further, ground distance relays are originally developed based on the positive sequence impedance from the relay location to the fault location for the single line to ground fault. The impedance sensed by relay is a combination of positive, negative and zero sequence impedances of the system. While the positive and negative sequence impedances are generally equal to each other in magnitude and angle, the zero sequence impedance may have both a different magnitude and angle. "Zero sequence current compensation" is then applied to adjust the measured impedance to reflect the actual system impedances.

4.1.5. Single Line to Ground Fault with Zero Sequence Compensation

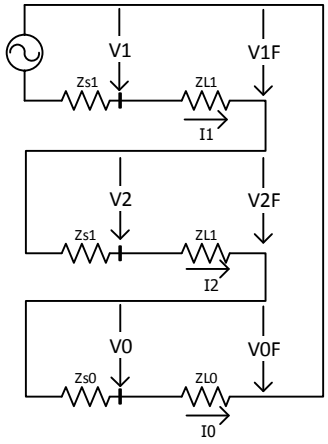

Figure 4-14. Sequence Network Connection for SLG Fault

From the sequence network in Figure 4-14, the voltage realized in relay location can be derived as:

$$V_a = V_1 + V_2 + V_0 \qquad \textbf{Eq. 4-8}$$

Where:

$$V_1 = I_1.ZL_1 + V_1F$$

$$V_1 = I_2.ZL_1 + V_2F$$

$$V_1 = I_0.ZL_0 + V_0F$$

$$V_a = I_0.ZL_0 + I_1.ZL_1 + I_2.ZL_1 + V_0F + V_1F + V_2F$$

With $(V_0F + V_1F + V_2F) = 0$

$$V_a = I_0.ZL_0 + (I_1 + I_2)ZL_1 \qquad \textbf{Eq. 4-9}$$

With $I_a = I_1 + I_2 + I_0$

If only positive sequence impedance is considered, and $\boldsymbol{Z_R}$ is assumed to be equal to $\boldsymbol{ZL_1}$ then the value of $\boldsymbol{I.Z_R}$ will be:

$$I.Z_R = I_a.ZL_1$$

$$I.Z_R = (I_1 + I_2)ZL_1 + I_0.ZL_1 \qquad \textbf{Eq. 4-10}$$

It can be noted from Eq.4-9 and Eq.4-10 that V_a and $I.Z_R$ value is not equal due to the difference between positive and zero sequence impedance. Zero sequence compensation is then introduced to deal with the problem by multiplying zero sequence current $I_0$with the ratio between positive and zero sequence impedance $(k_0 = \frac{ZL_0}{ZL_1})$. Thus the new $I.Z_R$ value can be derived:

$$I_{ac} = I_1 + I_2 + k_0.I_0 \qquad \textbf{Eq. 4-11}$$

$$I.Z_R = I_{ac}.ZL_1 \qquad \textbf{Eq. 4-12}$$

$$I.Z_R = (I_1 + I_2).ZL_1 + k_0.I_0.ZL_1$$

$$I.Z_R = (I_1 + I_2).ZL_1 + \left(\frac{ZL_0}{ZL_1}\right).I_0.ZL_1$$

$$I.Z_R = (I_1 + I_2).ZL_1 + I_0.ZL_0 \qquad \textbf{Eq. 4-13}$$

With the new $I.Z_R$, the ratio of voltage V_a to I_{ac} can be calculated as:

$$\frac{V_a}{I_{ac}} = \frac{I_0.ZL_0 + (I_1 + I_2).ZL_1}{I_1 + I_2 + k_0.I_0}$$

$$\frac{V_a}{I_{ac}} = \frac{(k_0.I_0 + I_1 + I_2).ZL_1}{I_1 + I_2 + k_0.I_0}$$

$$\frac{V_a}{I_{ac}} = ZL_1 \qquad \textbf{Eq. 4-14}$$

It can be concluded that by applying the zero sequence compensation, the function can be set by using the positive sequence impedance of the line.

Depending on the relay, the compensation factor k_0 can also be defined as:

$$k_0 = \frac{ZL_0 - ZL_1}{k.ZL_1} \qquad \textbf{Eq. 4-15}$$

The value of constant **k** can be 1 or 3 as determined by the relay design. In this particular case, the constant ***k = 3*** is chosen.

$$k_0 = \frac{ZL_0 - ZL_1}{3.ZL_1} \qquad \textbf{Eq. 4-16}$$

Operating signal can then be derived:

$$I.Z_R - V = (I_1 + I_2).ZL_1 + \left(\frac{ZL_0 - ZL_1}{3.ZL_1}\right).I_0.ZL_1 - V_a \qquad \textbf{Eq. 4-17}$$

However, above equation only true if the mutual impedance is not taken into the calculation. Looking back into the voltage equation:

$$\begin{bmatrix} V_a \\ V_b \\ V_c \end{bmatrix} = \begin{bmatrix} Z_s & Z_m & Z_m \\ Z_m & Z_s & Z_m \\ Z_m & Z_m & Z_s \end{bmatrix} . \begin{bmatrix} I_a \\ I_b \\ I_c \end{bmatrix}$$

Thus for the voltage in phase A:

$$V_a = Z_s.I_a + Z_m.(I_b + I_c) \qquad \textbf{Eq. 4-18}$$

Calculating $Z = \frac{V_a}{I_a} = Z_s + \frac{Z_m}{I_a}(I_b + I_c)$

Where

$$Z_s - Z_m = Z_1 \qquad \textbf{Eq. 4-19}$$

and

$$Z_s + 2.Z_m = Z_0 \qquad \textbf{Eq. 4-20}$$

$$Z_R = Z_1 + Z_m + \frac{Z_m}{I_a}(I_b + I_c)$$

$$Z_R = Z_1 + \frac{Z_m}{I_a}(I_a + I_b + I_c)$$

Because: $I_a + I_b + I_c = 3I_0$

The equation can then be rewritten as:

$$Z_R = Z_1 + Z_m.\frac{3I_0}{I_a}$$

with:

$$Z_m = \frac{Z_0 - Z_1}{3}$$

Thus:

$$Z_R = Z_1 + \left(\frac{Z_0 - Z_1}{3}\right).\frac{3I_0}{I_a}, \text{ or}$$

$$Z_R = Z_1 + (Z_0 - Z_1).\frac{I_0}{I_a} \qquad \textbf{Eq. 4-21}$$

The operating signal can then be derived as:

$$I_a.Z_R - V_a = I_a.ZL_1 + (ZL_0 - ZL_1)I_0 - V_a \qquad \textbf{Eq. 4-22}$$

In other reference, this operating signal may also be given in the different form:

$$I_a \cdot Z_R - V_a = I_a \cdot ZL_1 + \left(\frac{ZL_0 - ZL_1}{3 \cdot ZL_1}\right) I_0 \cdot ZL_1 - V_a \qquad \textbf{Eq. 4-23}$$

With $\left(\frac{ZL_0 - ZL_1}{3 \cdot ZL_1}\right) = k_0 (Zero \quad sequence \quad compensator)$

$$I_a \cdot Z_R - V_a = I_a \cdot ZL_1 + k_0 . I_0 \cdot ZL_1 - V_a \qquad \textbf{Eq. 4-24}$$

Obtaining the ***I.Z-V*** signal, the angle of the operating signal can be derived from tangent function:

$$Operating\_angle = \tan^{-1}\left[\frac{\mathrm{Im}(I.Z_R - V)}{\mathrm{Re}(I.Z_R - V)}\right] \qquad \textbf{Eq. 4-25}$$

As explained in chapter 4.1.3, three types of polarizing signals will be simulated in the microprocessor based mho relay for single line-A to ground fault:

1. Self polarization using Va
2. Cross-polarization using Vbc shifted by 90 degrees

4.1.6. Line-to-Line Fault

Based on Nordic grid Report-2013, line-to-line fault is the second mostly occurring fault in transmission line after single line to ground fault.

Type of fault	Nature	Percentage occurrence
Single line to ground fault	unbalanced	85%
Line to line	unbalanced	8%
Double line to ground	unbalanced	5%
Triple line	balanced	2%

Table 4-3. Statistics of fault type in transmission lines

Hypothetical connection of line-to-line connection is given in the Figure 4-15. While the sequence network connection of line-to-line fault is given in the Figure 4-16.

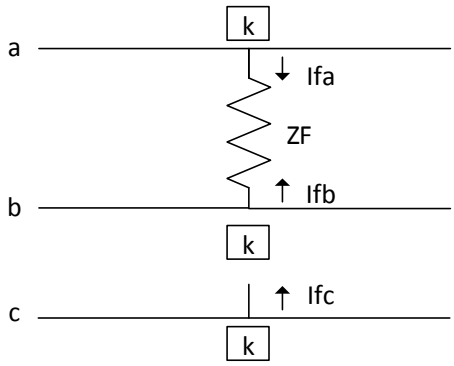

Figure 4-15. Connection of the hypothetical stubs for a line-to-line fault

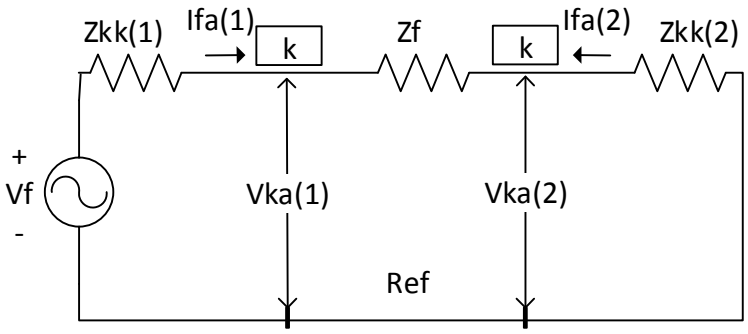

Figure 4-16. Sequence network connection for line-to-line fault

From Figure 4-15, following relations must be satisfied:

$$I_{fa} = -I_{fb} \qquad \textbf{Eq. 4-26}$$

$$I_{fc} = 0 \qquad \textbf{Eq. 4-27}$$

$$V_{ka} - V_{kb} = I_{fa} \cdot Z_F \qquad \textbf{Eq. 4-28}$$

The symmetrical components of the current can be calculated by:

$$\begin{bmatrix} I_{fa}^0 \\ I_{fa}^1 \\ I_{fa}^2 \end{bmatrix} = \frac{1}{3}\begin{bmatrix} 1 & 1 & 1 \\ 1 & a & a^2 \\ 1 & a^2 & a \end{bmatrix}\begin{bmatrix} 0 \\ I_{fa} \\ -I_{fa} \end{bmatrix}$$

Thus the results of the calculation are:

$$I_{fa}^0 = 0 \qquad \textbf{Eq. 4-29}$$

$$I_{fa}^1 = -I_{fa}^2 \qquad \textbf{Eq. 4-30}$$

It is clear from the Eq. 4-29 that zero sequence components is inactive and does not play any roles in the calculation for line-to-line fault. The equation for the positive current in line-to-fault can be determined from Figure 4-16 such that:

$$I_{fa}^1 = \frac{V_f}{Z_{kk}^1 + Z_{kk}^2 + Z_f} \qquad \textbf{Eq. 4-31}$$

For the bolted line $Z_f = 0$, thus the equation becomes:

$$I_{fa}^1 = \frac{V_f}{Z_{kk}^1 + Z_{kk}^2}$$

$$I_a - I_b = \frac{V_a - V_b}{ZL_1} \qquad \textbf{Eq. 4-32}$$

From the Eq. 4-32, the mho distance relay's operating and polarizing signal can be derived:

- Operating signal:

  $I.Z - V = (I_a - I_b) \cdot ZL_1 - V_{ab}$

- Two types of Polarizing signal will be simulated in the double line V_{ab} fault, as explained in chapter 4.1.3, namely:
  1. Self polarization using V_{ab}
  2. Cross polarization using healthy phase V_c shifted by -90 degrees

The mho characteristic for line to line fault compared to single line to ground fault is presented in the Figure 4-17 below.

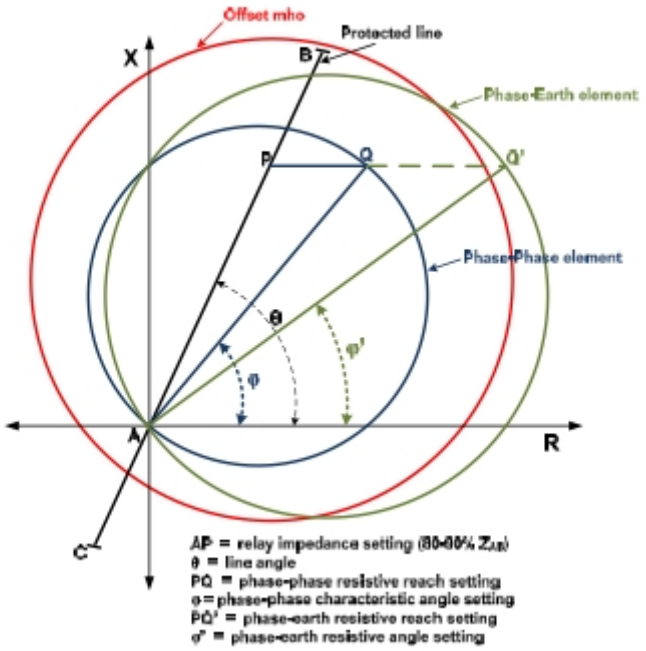

Figure 4-17. Mho characteristic in phase-to-phase and single line to ground fault

4.2. Signal Conditioning

Distance relay model consists of various block models, forming signal conditioning and data acquisition before reaching the analysis and logic block where tripping commands are generated. These blocks are responsible for filtering the analog signal, sampling the signals and converting the instantaneous signals from analog to digital signals. Figure 4-18 below shows the structure of the block models used in the project.

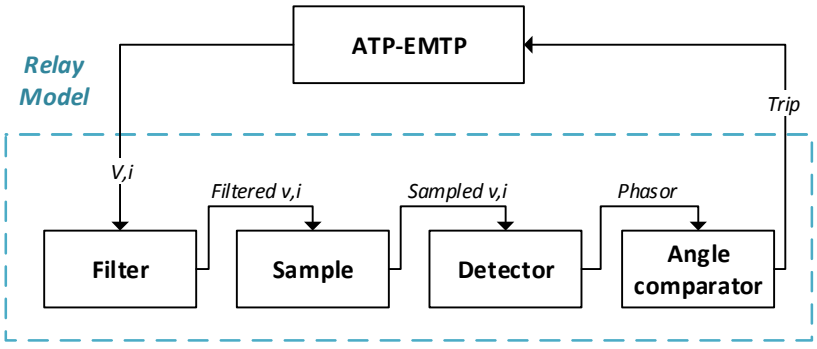

Figure 4-18. Modeling structure of Distance Relay

Following is a brief of each block function and responsibility related with the distance protection relay model used in the project.

- Filter: This block is responsible for removing the high frequency components. By using s-domain model of second order Butterworth low pass filter. The polynomial was also derived manually based on standard reference [26]. The gain input is set for unity output-to-input ratio at a low frequency.

- Sampling: This block is responsible for selecting and storing samples of instantaneous measured value with a specific sampling rate. Most relay applications apply sampling at a fixed rate that is multiple of the nominal power system frequency.

- Detector: This block is responsible for estimating the fundamental frequency's value from the samples to the phasor terms consisting cosine and sine values. These values can be translated to magnitude and angle value which further can be implemented in the relay algorithm calculation.

- SLG: This is the main block of the model. This block is responsible for analyzing the phasor diagram derived from the Fourier detector in order to generate the trip command to the relay.

4.2.1. Filtering

Filtering is an integral part and a very critical requirement for distance relay because the relay must be able to estimate quickly and precisely the distance to the fault, which further used for the tripping decision, based on highly distorted electrical input signals. The input signals to protective relays are contaminated with much noise from various sources such as: dc offset in current waveform due to resistance-inductance behavior of power system, high frequency damped oscillations due to shunt capacitance of longer transmission lines and harmonics due to nonlinearities of power system element and instrument transformer.

The requirement for filter arose especially since the introduction of electronic and microprocessor-based distance relay. The previous generation type of relay, electromechanical relay, designed to be optimized for one system frequency only (usually 50 or 60 Hz). Any other frequency will be less efficient for this type of relay. Consequently, this relay is less sensitive to any frequency distortions in current or voltage signals input [26].

This chapter will only give a brief explanation about the filter used in this application as it is not the main topic of the project. Details given only related with the equation for the transfer function of the filter and the gain function.

4.2.1.1. Implementation

Butterworth low pass filter is chosen for this application as this is considered to be the most commonly used type of filter. Given below is the equation for the transfer function of the particular filter:

$$H_{but\_low}(s) = \frac{\omega_c^n}{s^n + a_1\omega_c^n s^{n-1} + \ldots + a_{n-1}\omega_c^{n-1} + \omega_c^n} \qquad \textbf{Eq. 4-33}$$

Where:

$n = order\ of\ the\ system$

$\omega_c = cut-off\ frequency$

Further, the table consists of the coefficients for Butterworth low pass filter is given below.

n (order)	a_0	a_1	a_2	a_3	a_4
2	1.0	1.4142136	-	-	-
3	1.0	2.000000	2.0000000	-	-
4	1.0	2.6131259	3.4142136	2.6131259	-
5	1.0	3.2360680	5. 2360680	5. 2360680	5. 2360680

Table 4-4. Coefficient of the Butterworth polynomial

Second order is considered to be adequate for this application. The main advantage of this filter is higher attenuation rate of -40dB/decade compared to -20dB/decade of the first order. This is very important feature especially if the noise frequency is very close to the cut-off frequency.

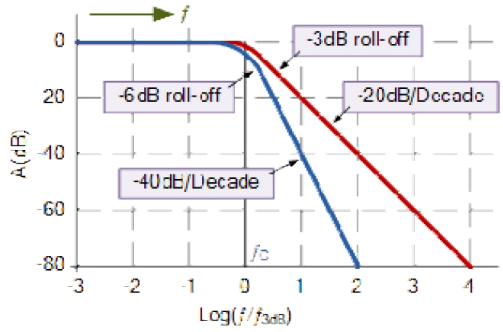

Figure 4-19. Attenuation rate of first order versus second order low pass filter

For the second order low pass filter, the Equation 4-33 then becomes:

$$T(s) = \frac{\omega_0^2}{s^2 + (\omega_0 / Q)s + \omega_0^2} \qquad \textbf{Eq. 4-34}$$

Applying $f_0 = 235Hz$ as the cut-off frequency ω_c and quality factor $Q = .707$ complying with the Butterworth second order low pass filter table, the expression for the transfer function can be given as:

$$T(s) = \frac{(2.\pi.235)^2}{s^2 + 2.\pi.235/.707 + (2.\pi.235)^2}$$

$$T(s) = \frac{2{,}177{,}928}{s^2 + 2{,}081.9s + 2{,}177{,}928}$$

Figure 4-19 shows the results of the filtering process. 4-20(a) shows the results of the filtered currents compared to its original signal, while Figure 4-20(b) shows the case for the voltages signals.

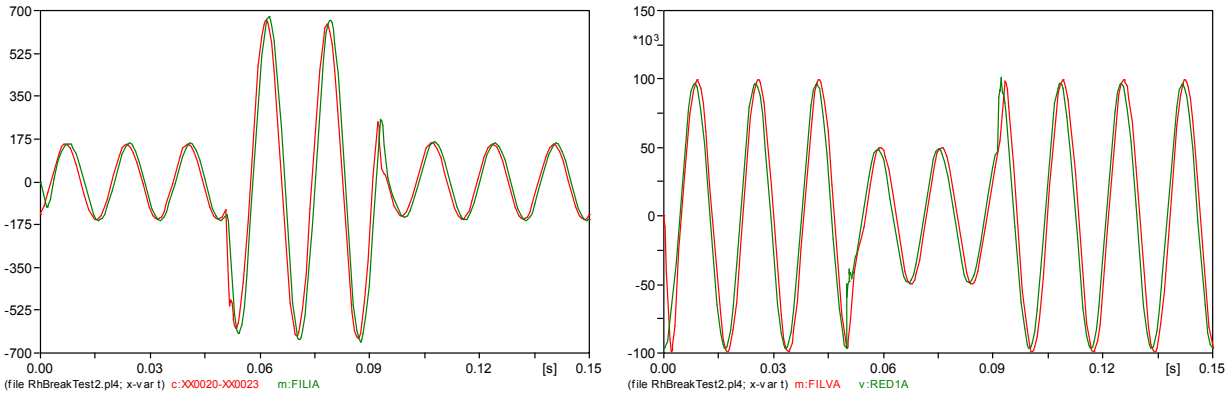

(a) (b)

Figure 4-20. Butterworth second order Filtered signal versus original signal
(a) currents (b) voltages

The filtered signals can be noticed to have some delays which are due to the computational filtering process. For the purpose of comparing the efficiency of the filter, third order Butterworth with the transfer as stated below will be tested to see the result compared to the second order version.

$$T(s) = \frac{3{,}219{,}164{,}663.78}{s^3 + 2{,}953.1s^2 + 4{,}355{,}856s + 3{,}219{,}164{,}663.78}$$

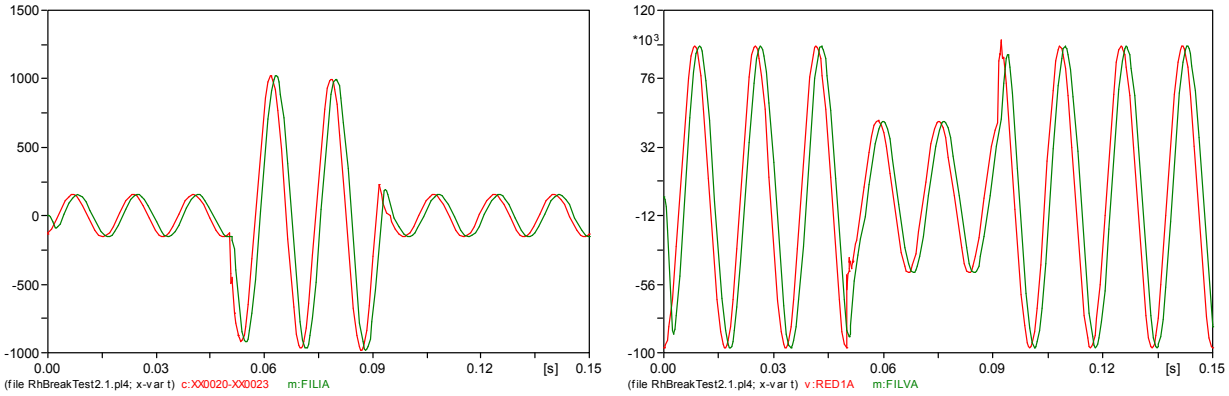

(a) (b)

Figure 4-21. Third ordered Filtered signal versus original signal
(a) currents (b) voltages

It can clearly be seen that now the delay has increased considerably compared to the second order filter. The performance of the second order is already sufficient and does not need further improvement especially with the computational delay as trade off.

4.2.2. Sampling

After filtering the signals, the next essential process for the operation of microprocessor-based distance relay is sampling. This is a process of converting the currents and voltages analog signal to an appropriate form so the digital hardware can perform calculations properly before reaching the relaying decision. The most common practice of the relay application involves sampling at a fixed rated that is a multiple of the nominal power system frequency [27].

The system timing and software design is based on the power line frequency. In this study, the analog inputs are continuously sampled 8 times per power line cycle or equal to 480 Hz. This means that the time-step used in the project is chosen at 2.083ms. The previously mentioned cut-off frequency is chosen at 235Hz to comply with the Nyquist criterion which states that the sampling frequency should be at least twice the highest frequency contained in the signal [28].

The flow of the sampling process delivers eight states per cycle, which corresponds to the aforementioned eight samples per cycle sampling rate. Movement from state to state is controlled by a timer. The timer is loaded with a state time at the beginning of the state. The code executed within a state should be completed before the timer expires. The software then waits for the timer to time out. The instantaneous voltage and current sampling values are converted to RMS and phasor values using Fourier algorithm in the next process.

Figure 4-21 shows the results of the sampling process from the filtered signals. 4-22(a) shows the results of the currents sampling compared to the filtered signals, while 4-22(b) shows the case for the voltages signals.

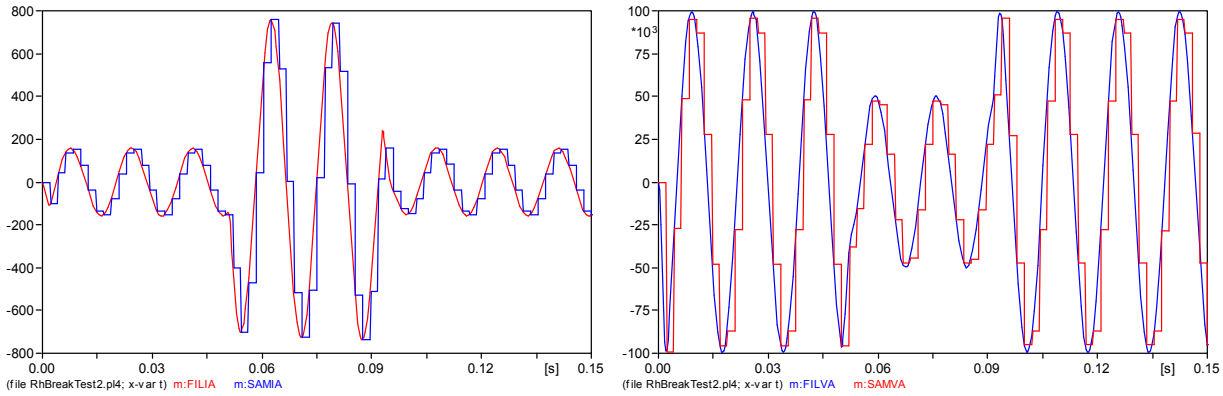

(a) (b)

Figure 4-22. Output signal from the sampling process versus filtered signals
(a) currents (b) voltages

4.2.3. Fourier Detector

The last part of the signal conditioning block is a detector block, which is responsible for estimating the fundamental frequency's value from the samples to the phasor terms consisting cosine and sine values, which the modeled detector used a recursive Fourier algorithm developed by Phadke and Thorp [24].

Fourier transform decomposes a function of time $f(t)$ into frequency domain $f(j\omega)$, where all the frequency components of the original input present. Using this transformation, the fundamental frequency can be extracted while undesired harmonics can be excluded.

The fundamental frequency components are given by:

$$\hat{Y}_c = \frac{2}{K}\sum_{k=1}^{k} y_k.\cos(k\theta) \qquad \textbf{Eq. 4-35}$$

$$\hat{Y}_s = \frac{2}{K}\sum_{k=1}^{k} y_k.\sin(k\theta) \qquad \textbf{Eq. 4-36}$$

While for p-th harmonics:

$$\hat{Y}_c^p = \frac{2}{K}\sum_{k=1}^{k} y_k.\cos(pk\theta) \qquad \textbf{Eq. 4-37}$$

$$\hat{Y}_s^p = \frac{2}{K}\sum_{k=1}^{k} y_k.\sin(pk\theta) \qquad \textbf{Eq. 4-38}$$

Where:

θ : $2K/\pi$

K : Samples per cycle

$\hat{Y}_s$: Sine coefficient

$\hat{Y}_c$: Cosine coefficient

4.2.3.1. Recursive Fourier Transformation

The complex form of the fundamental frequency components for the samples computation involving samples ending at L is given by the equation:

$$Y(L) = \frac{2}{K}\sum_{k=L-K+1}^{L} y_k.e^{-j(k+K-L)\theta} \qquad \textbf{Eq. 4-39}$$

Rotating by the angle of $(K-L)\theta$ to keep the result stationary:

$$\widetilde{Y}^{(L)} = Y^{(L)}.e^{j(K-L)\theta} = \frac{2}{K}\sum_{k=L-K+1}^{L} y_k.e^{-jk\theta}$$

Thus

$$\widetilde{Y}^{(L-1)} = \frac{2}{K}\sum_{k=L-K}^{L} y_k.e^{-jk\theta}$$

$$\widetilde{Y}^{(L)} - \widetilde{Y}^{(L-1)} = \frac{2}{K}\left[y_L - y_{L-K}.e^{jK\theta}\right]e^{-jL\theta}$$

$$\widetilde{Y}^{(L)} = \widetilde{Y}^{(L-1)} + \frac{2}{K}\left[y_L - y_{L-K}.e^{jK\theta}\right]e^{-jL\theta} \qquad \textbf{Eq. 4-40}$$

For the full cycle window $K\theta = 2\pi$, the recursive form of the full cycle algorithm becomes:

$$\hat{Y}_c^{(new)} = \hat{Y}_c^{(old)} + \frac{2}{K}[y_{new} - y_{old}]\cos(L\theta) \qquad \textbf{Eq. 4-41}$$

$$\hat{Y}_s^{(new)} = \hat{Y}_s^{(old)} - \frac{2}{K}[y_{new} - y_{old}]\sin(L\theta) \qquad \textbf{Eq. 4-42}$$

The phasor form consisting of magnitude and angle of the represented sine and cosine values can be calculated as:

$$Magnitude = \sqrt{\left(\hat{Y}_c\right)^2 + \left(\hat{Y}_s\right)^2} \qquad \textbf{Eq. 4-43}$$

$$angle = \tan^{-1}\left(\frac{\hat{Y}_s}{\hat{Y}_c}\right) \qquad \textbf{Eq. 4-44}$$

Figure 4-23 shows the results of the recursive Fourier transformation from the sampled signals. Figure 4-23(a) and 4-23(b) show the magnitude and angle from the sampled currents signals respectively. While Figure 4-23(c) and 4-23(d) show the cases for the sampled voltage signals. The magnitudes presented are already in RMS values.

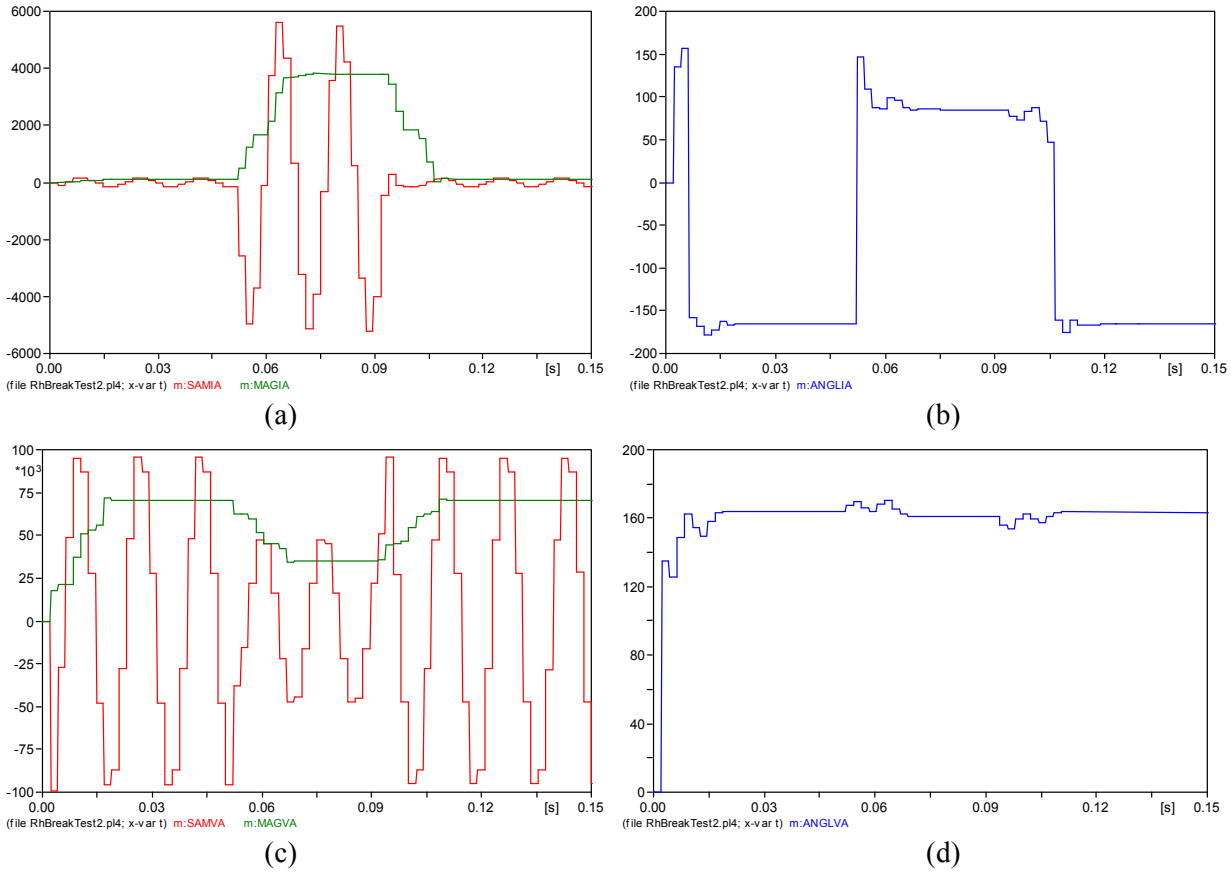

Figure 4-23. Output from the recursive Fourier transformation process
(a) currents magnitude (b) currents angle (c) voltages magnitude (d) voltages angle

The final output in this phasor form can then be used directly as the input for the single line to ground fault model block to produce the tripping decision.

4.3. Microprocessor-based Mho Relay Model

4.3.1. Single Line-A to Ground Fault

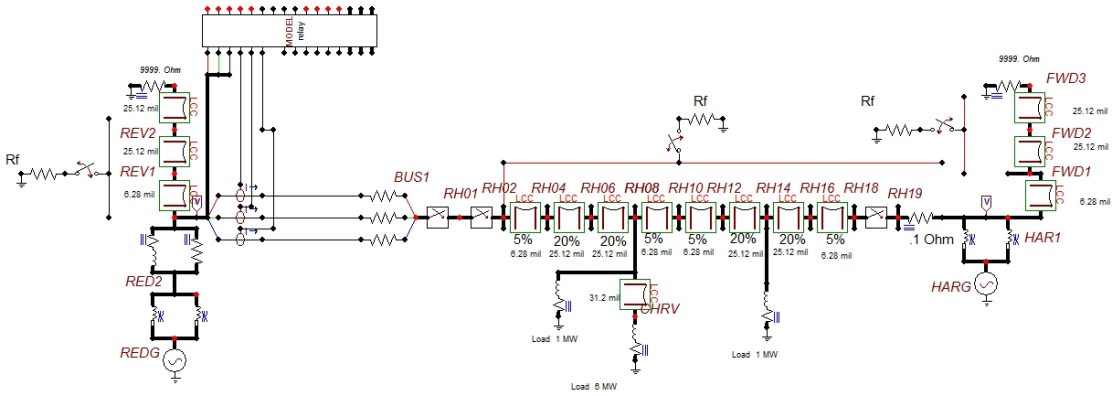

Figure 4-24. EMTP-ATPDraw model for single line to ground fault simulation

Figure 4-24 showcases the model used for single line to ground fault simulation. The transmission line is divided into several sections based on its impedance. Reverse line is also provided to test the proper operation of the relay algorithm. To produce single line to ground fault, phase-A is connected to a fault resistance R_F via time controlled switch TSWITCH. The parameters used for the inputs of the calculation are taken from three phase voltages and currents measured in the relay location. Zero sequence impedance current is calculated inside the model by adding the three phase currents.

$$I_0 = \frac{I_a + I_b + I_c}{3} \qquad \textbf{Eq. 4-45}$$

Modeling structure of the microprocessor-based mho distance relay as a whole is given in the Figure 4-18 below. As explained in the chapter 4.2, the signals need to be conditioned before entering the trip decision block which using the angle comparator algorithm. The signal conditioning steps have been explained thoroughly in the chapter.

Inputs for the angle comparator model are taken from the output of the Fourier detector in the complex form of voltage and current consisting real and imaginary value. Based on the equation that has been derived previously in chapter 4.1.5 for the single line to ground fault model, the equation for the operating and polarizing signals is written in the complex form. Where:

$\mathrm{Re}(x) = real \quad part$

$\mathrm{Im}(x) = imaginary \quad part$

Zero sequence current:

$I_3 0 = I_a + I_b + I_c$

$I_3 0$= Three times zero sequence current I_0

Z_1 = positive sequence impedance of the line

With:

$R_1 = Z_1.\cos\theta_1$

$X_1 = Z_1.\sin\theta_1$

Z_0 = Zero sequence impedance of the line

With:

$R_0 = Z_0.\cos\theta_0$

$X_0 = Z_0.\sin\theta_0$

- Zero compensation factor: $k_0 = \dfrac{Z_0 - Z_1}{3Z_1}$

  The real value is given by:

$$\mathrm{Re}(k_0) = \frac{\sqrt{(R_0 - R_1)^2 + (X_0 - X_1)^2}\,\cos\dfrac{(X_0 - X_1)}{(R_0 - R_1)}}{3\cdot\sqrt{R_1^2 + X_1^2}}$$

  While the imaginary value is given by:

$$\mathrm{Im}(k_0) = \frac{\sqrt{(R_0 - R_1)^2 + (X_0 - X_1)^2}\,\sin\dfrac{(X_0 - X_1)}{(R_0 - R_1)}}{3\cdot\sqrt{R_1^2 + X_1^2}}$$

For fault at phase A:

Operating signal is given by:

$$\mathrm{Re}(operate\_signal) = \mathrm{Re}(i_a)\cdot R_1 - \mathrm{Im}(i_a)\cdot X_1 + \big(\mathrm{Re}(I_3 0)\cdot\mathrm{Re}(k_0) - \mathrm{Im}(I_3 0)\cdot\mathrm{Im}(k_0)\big)\cdot R_1 - \big(\mathrm{Re}(I_3 0)\cdot\mathrm{Im}(k_0) + \mathrm{Im}(I_3 0)\cdot\mathrm{Re}(k_0)\big)\cdot X_1 - \mathrm{Re}(V_a)$$

$$\mathrm{Im}(operate\_signal) = \mathrm{Im}(i_a)\cdot R_1 + \mathrm{Re}(i_a)\cdot X_1 + \big(\mathrm{Re}(I_3 0)\cdot\mathrm{Im}(k_0) + \mathrm{Im}(I_3 0)\cdot\mathrm{Re}(k_0)\big)\cdot R_1 + \big(\mathrm{Re}(I_3 0)\cdot\mathrm{Re}(k_0) - \mathrm{Im}(I_3 0)\cdot\mathrm{Im}(k_0)\big)\cdot X_1 - \mathrm{Im}(V_a)$$

$$operating\_angle = ATAN\,2\big(\mathrm{Im}(operate\_signal),\ \mathrm{Re}(operate\_signal)\big)$$

ATAN2 function is used to return the angle with appropriate quadrant of the computed angle. The angle value is returned in Radian.

Polarization angle is developed based on the type of chosen polarization angle. In this case self polarization and cross polarization are simulated.

1. Self polarization

   For the fault at phase-A, the phase-A voltage can be directly used as the polarization angle in the angle comparator model. The drawback of this selection is that during a close-in fault, the relay may not be able to work properly because the voltage drops to zero.

$$Polarizati\ \ on\_angle\ = ATAN\ 2\left(\mathrm{Im}(V_a),\ \ \mathrm{Re}(V_a)\right)$$

2. Cross polarization (quadrature signals)

   Using Vbc shifted by 90 degrees:

$$Polarizati\ \ on\_angle\ = ATAN\ 2\left(\left(\mathrm{Im}(V_b)-\mathrm{Im}(V_c)\right),\ \ \left(\mathrm{Re}(V_b)-\mathrm{Re}(V_c)\right)\right)+1.5708$$

4.3.2. Line-A to Line-B Fault

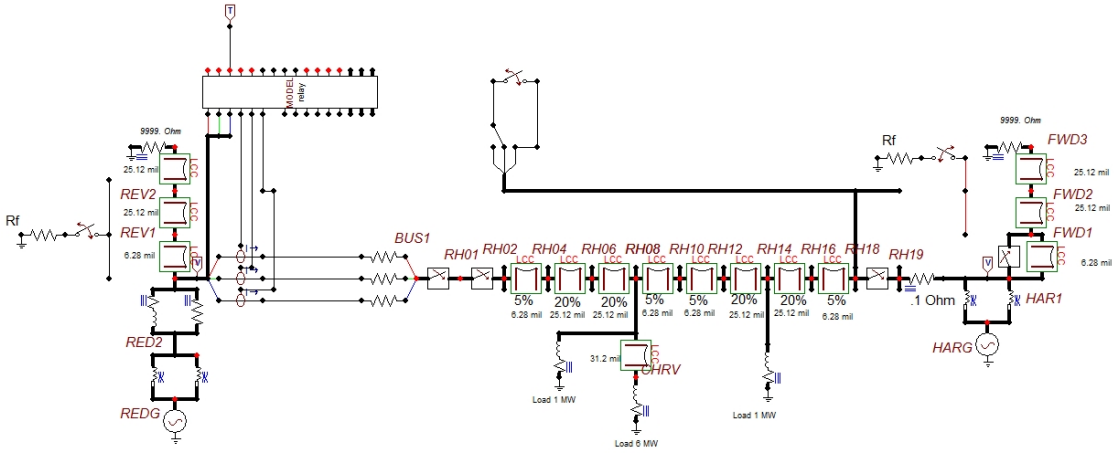

Figure 4-25. EMTP-ATP Draw model for line-to-line fault simulation

Line to line fault model used in the simulation is depicted in the Figure 4.25 shown above. To apply line to line fault, the line is connected to a SPLITTER which transforms a 3-phase node to three 1-phase nodes or vice versa. Phase-A and B is then connected via TSWITCH. This connection may involved a fault resistance or not (bolted fault).

For line-A to line-B fault, the operating signal is given by:

$$\mathrm{Re}(operate\_signal)=\left(\mathrm{Re}(i_a)-\mathrm{Re}(i_b)\right)\cdot R_1-\left(\mathrm{Im}(i_a)-\mathrm{Im}(i_b)\right)\cdot X_1-\left(\mathrm{Re}(V_a)-\mathrm{Re}(V_b)\right)$$

$$\mathrm{Im}(operate\_signal)=\left(\mathrm{Im}(i_a)-\mathrm{Im}(i_b)\right)\cdot R_1-\left(\mathrm{Re}(i_a)-\mathrm{Re}(i_b)\right)\cdot X_1-\left(\mathrm{Im}(V_a)-\mathrm{Im}(V_b)\right)$$

Angle of operating signal is then given by:

$$operating\ \ \_angle\ = ATAN\ 2\left(\mathrm{Im}(operate\ \ \_signal\ ),\ \ \mathrm{Re}(operate\ \ \_signal\ )\right)$$

Polarization angle is developed as single line to ground fault using self polarization and cross polarization:

1. Self polarization

$$Polarizati\ \ on\ \_\ angle\ = ATAN\ 2\left(\left(\mathrm{Im}(V_a) - \mathrm{Im}(V_b)\right),\ \ \left(\mathrm{Re}(V_a) - \mathrm{Re}(V_b)\right)\right)$$

2. Cross polarization (quadrature signals)

$$Polarizati\ \ on\ \_\ angle\ = ATAN\ 2\left(\mathrm{Im}(V_c), \mathrm{Re}(V_c)\right) - 1.5708$$

4.4. Electromechanical Mho Relay Model

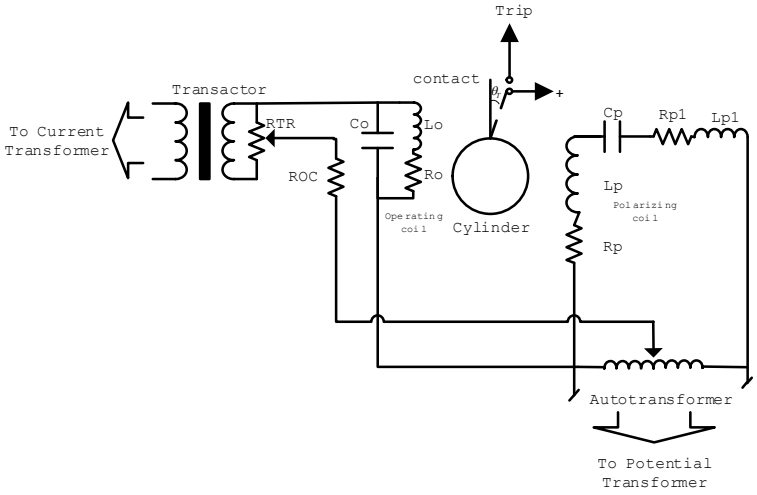

Figure 4-26. Schematic connection of typical mho distance relay

Relay shown in Figure 4-26 is single phase mho distance relay with two coils: polarizing coil and operating coil. The polarizing coil is connected to a potential transformer through a memory circuit consisting of a variable inductor L_{p1} and a capacitor C_p. The operating coil is connected to a current transformer through a transactor TR (a special transformer for impedance setting). The transactor is represented by a typical transformer equivalent circuit. The potentiometer RTR is split into two parts with their sum equal to RTR. There is also an autotransformer, from which comes a restraint, component exerted on the operating coil. The electromagnetic torque is developed by the interaction of currents through the two coils. If the torque is of the correct direction, magnitudes and duration, the relay will trip.

Mathematical model has been derived by [5] in order to construct a state space model of the relay. The ninth order state space model is given by:

$$\begin{bmatrix} X' \\ (9x1) \end{bmatrix} = \begin{bmatrix} A \\ (9x9) \end{bmatrix} \cdot \begin{bmatrix} \overline{X} \\ (9x1) \end{bmatrix} + \begin{bmatrix} B \\ (9x3) \end{bmatrix} \cdot \begin{bmatrix} U \\ (3x1) \end{bmatrix} \qquad \textbf{Eq. 4-46}$$

- x_1: current through the secondary of the transactor
- x_2: current through the operating coil
- x_3: voltage across the operating coil
- x_4: voltage across the capacitor in the memory circuit

- x_5: current through the polarizing coil
- x_6: maximum density of induced current by the polarizing coil
- x_7: maximum density of induced current by the operating coil
- x_8: angular displacement of the cylinder (X_8>0)
- x_9: angular velocity of the cylinder

It can be observed that the ninth order relay model only has one output x_8 (angular displacement) that controls the operation of the relay. The relay in this case is tripped if the displacement angle of the relay cylinder reaches maximum angular displacement θ_T.

$$Y = \begin{cases} 1 \ \ (trip), & X_8 \geq \theta_T \\ 0 \ \ (no \ \ trip), & otherwise \end{cases} \qquad \textbf{Eq. 4-47}$$

Details of the matrices are provided in the appendix-1. The model has been verified by [29] performing steady state, reverse and forward fault study. The simulation for electromechanical mho relay model will discuss the critical operation of the relay which includes single line fault test with and without DC offset with the fault location very close to the relay location, which is very critical for the transformer operation. Maximum DC offset occurs when the single line fault occurs at zero voltage. While single line fault test without DC offset is set at peak voltage.

The mechanical parameters of the relay are given as follow:

μ_0 permeability of air, $4\pi x10^{-7}$h/m
Np number of turns of the polarizing coil, 9000
No number of turns of the operating coil, 4000
h total length of the air gaps, 2mm
l length of the cylinder, 35mm
r radius of the cylinder, 14mm
T thickness of the cylinder wall, 1mm
Ks elastic coefficient of the spring, $2.829x10^{-5}$kgm
J moment of inertia of the cylinder, $4.226x10^{-6}$kgm^2

While the electrical properties of the relay are:

Lp inductance of the polarizing coil, 6h
Rp resistance of the polarizing coil, 665.4Ω
Cp capacitor in the polarizing circuit, 0.75μf
Lp1 variable inductor in the polarizing circuit, 4h
Rp1 resistance of the variable induCtor, 269.7Ω
Px tap of the autotransformer
Lo inductance of the operating coil, 2.5h
Ro resistance of the operating coil, 214.1 Ω
Co capacitor in the operating circuit, 2μf
Roc restraint resistor, 700 Ω
RTR potentiometer, 750 Ω
t ratio of the potentiometer (0.5)
ρ resistivity of the cylinder material, 10^{-7} Ω m

The simulation model of electromechanical mho relay model including the transmission line, CT and CVT model is presented in the Figure 4-27 below.

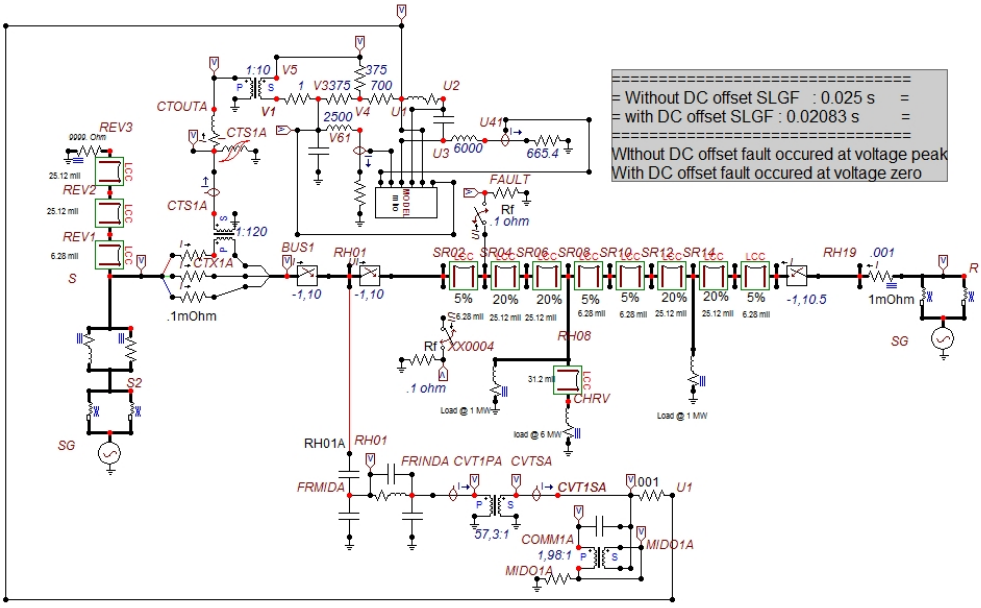

Figure 4-27. Simulation model for electromechanical mho relay

---This page is intentionally left blank---

5. Simulation Results

5.1. Microprocessor-based Relay

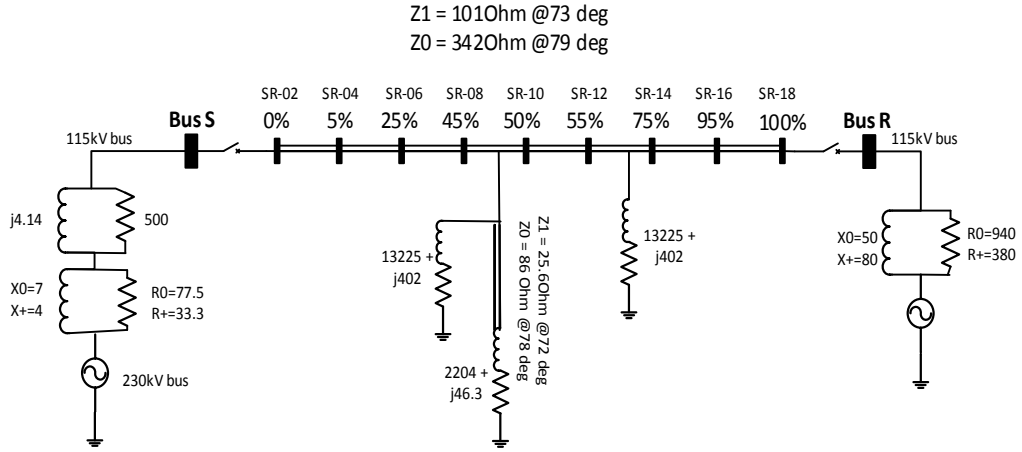

Figure 5-1. Transmission line model

Above single line transmission diagram is the model used for the simulation. The total impedance between bus-S and bus-R are given by:

$$Z_1 = 101{,}03\angle 73$$
$$Z_0 = 342\angle 79$$

The distance protection scheme can be set as the input of the model determining the characteristic of the relay protection scheme. In this application, zone-1 tripping zone is set to 80% of the total impedance with zone-2 set to 120%.

$$Zone-1_1 = 80\angle 73$$
$$Zone-1_0 = 274\angle 79$$
$$Zone-2_1 = 120\angle 73$$
$$Zone-2_0 = 410\angle 79$$

5.1.1. Simulation Setting

The modeling structure for the simulation can be seen as follows. Using the microprocessor based relay which is divided into four sections: The first part consists of the input analog anti-aliasing low-pass filter. The filter has a 3-db roll-off frequency of approximately 240Hz and is a second order Butterworth type. In the next section, a sample and hold block is modeled. This block samples 60Hz fundamental 8 times per cycle (480Hz). The third section is the detector where Fourier algorithm is applied to recover 60Hz phasor information. The final section is the relay measuring principle where angle comparator model is applied.

In this project, the performance of the relay is tested for the case of single line to ground fault. The test is performed in several positions of the transmission line. The fault is set to occur at 50ms after the simulation start as can be seen in the Figure 5-2 depicted below:

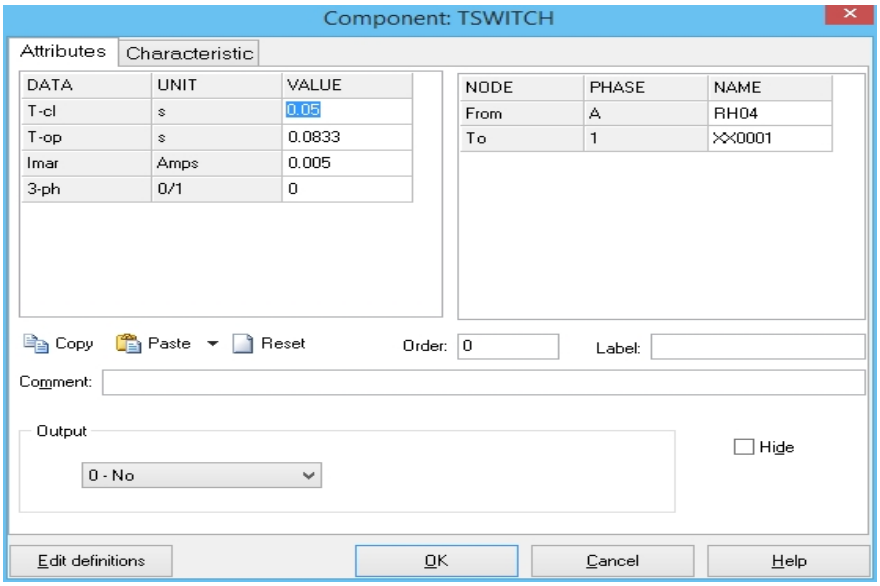

Figure 5-2. Setting for the fault occurrence

Setting for the mho protection as explained above (zone-1 at 80% and zone-2 at 120% of the total impedance between bus-S and bus-R) can be given in the Figure 5-3 below. Terms used for the setting input of the relay model are given as follows:

- Zpos11 : positive sequence impedance magnitude of zone-1
- Zpos12 : positive sequence impedance angle of zone-1
- Zzero11 : zero sequence impedance magnitude of zone-1
- Zzero12 : zero sequence impedance angle of zone-1
- Zpos21 : positive sequence impedance magnitude of zone-2
- Zpos22 : positive sequence impedance angle of zone-2
- Zzero21 : zero sequence impedance magnitude of zone-2
- Zzero22 : zero sequence impedance angle of zone-2

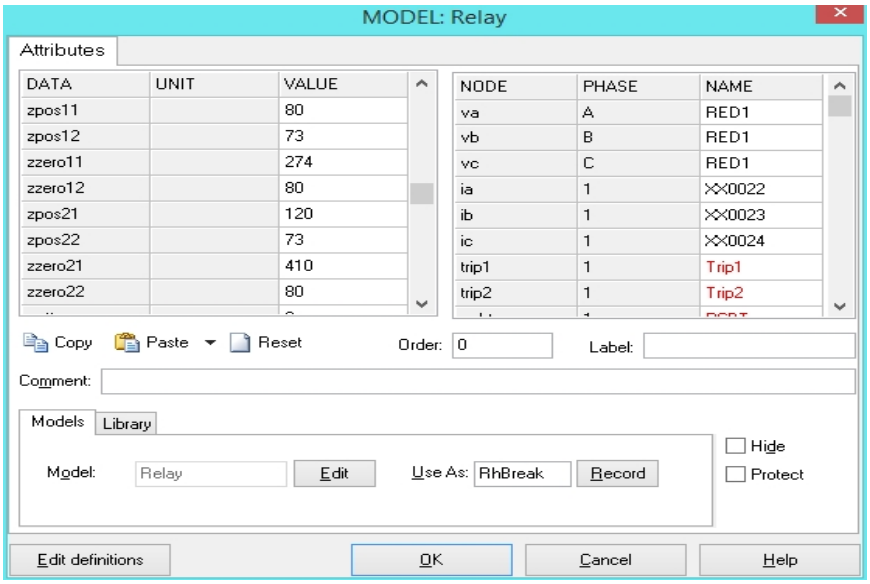

Figure 5-3. Setting for mho relay model

5.1.2. Single Line to Ground Fault Simulation Result

This study will evaluate the operation of relay protection due to single line to ground fault which is simulated in phase A of a high voltage cable transmission line. Phase A is connected to the ground through a fault resistance when the fault occurs. For the information, all the signals are measured from the relay location (bus S). Line location of the fault is also using bus S as the reference.

Fault at 0%

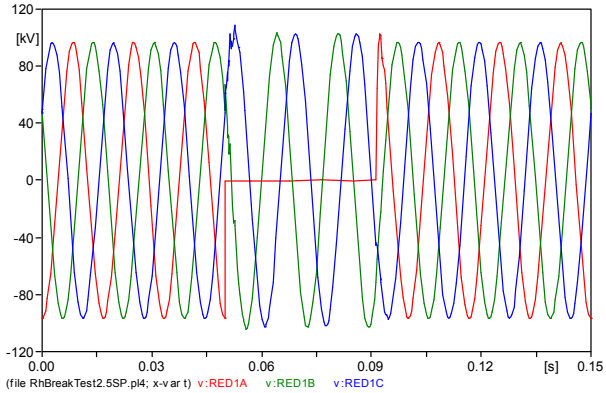

Figure 5-4. Voltage under SLGF at 0% with RF=0.01 Ohm

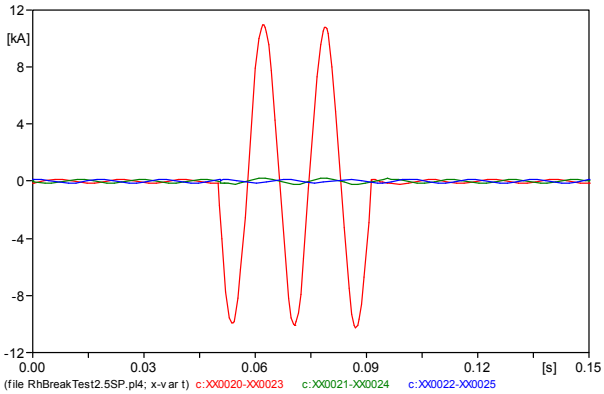

Figure 5-5. Current under SLGF at 0% with RF=0.01 Ohm

During the fault, the healthy phases (phase B and C) are not affected. The current in phase A jumps to a peak value of 11kA from the original value of 160A. While the voltage at phase-A drops significantly to almost zero.

The resulting trips from the fault are different based on the polarizing signals being used.

- Self polarization using Va:

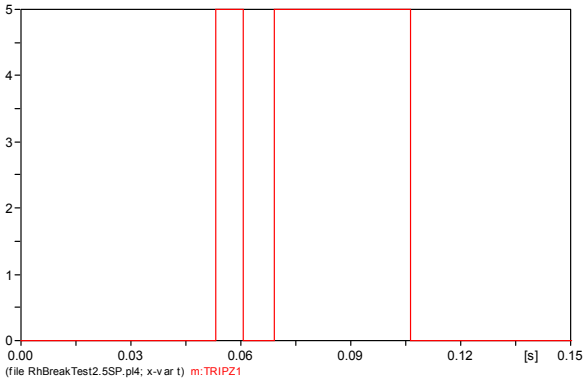

Figure 5-6. Self polarization Zone-1 trip output at 0% SLGF with RF= 0.01 ohm

Using the self polarization, the relay is still able to detect the fault after approximately 3ms after the fault occurs. However, the polarizing signals cannot maintain its stability. Thus after approximately ½ cycle, relay failed to operate. After another ½ cycle the relay is tripped again. This condition is even more severe by changing the fault resistance to a smaller value. For instance, changing the R_F to 1E-5 ohm will give the trip output as depicted in Figure 5-7 below.

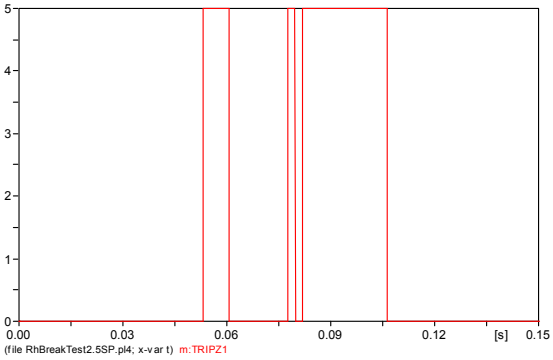

Figure 5-7. Self polarization Zone-1 trip output at 0% SLGF with RF= 1E-5 ohm

- Cross polarization using Vbc shifted by +90:

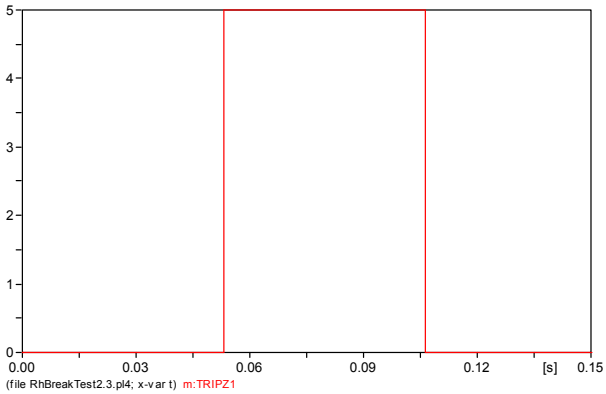

Figure 5-8. Cross polarization Vbc+90 Zone-1 trip output at 0% SLGF with RF= 0.01 ohm

Unlike using self polarization, cross polarization using cross polarization signal of Vbc+90 gives a good response to the fault at 0%. Changing the fault resistance to 1E-5 ohm also does not affect its performance.

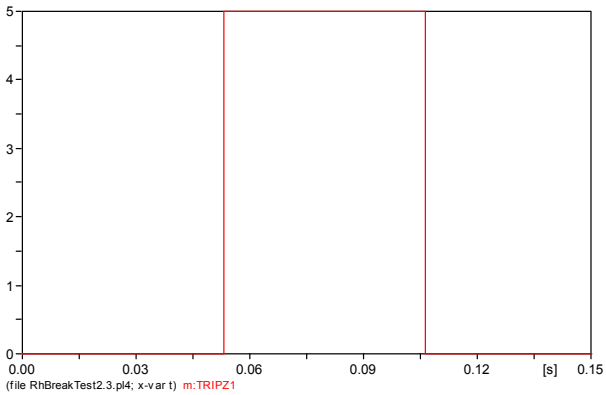

Figure 5-9. Cross polarization Vbc+90 Zone-1 trip output at 0% SLGF with RF= 0.01 ohm

The difference is as explained previously in chapter 4.1.3, the cross polarization is more reliable during a close-in fault, because during this type of fault, the faulted phase voltage is reduced significantly while the healthy phases are almost not affected. Thus the self polarized mho is less favorable to use, specifically when dealing with close-in fault.

Fault at 5%

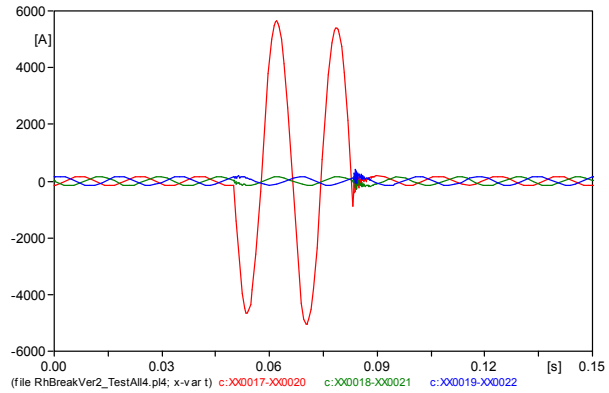

Figure 5-10. Current under SLGF at 5% with RF=0.01 Ohm

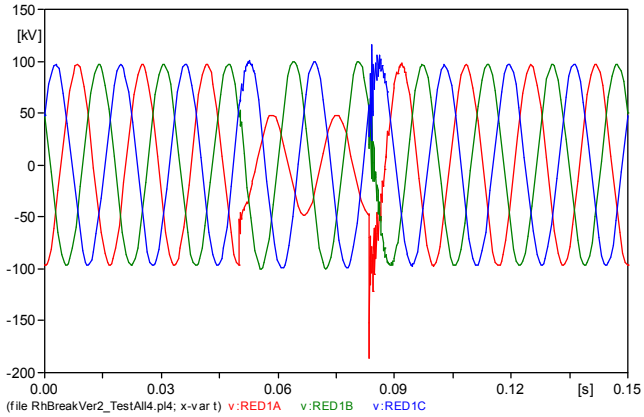

Figure 5-11. Voltage under SLGF at 5% with RF=0.01 Ohm

Figure 5-10 and 5-11 respectively show the phase currents and voltages under fault at 5%. Phase A current jumps to approximately 5.5kA while the voltage drops to approximately half the original value. The resulting trip is given by:

- Self polarization using Va:

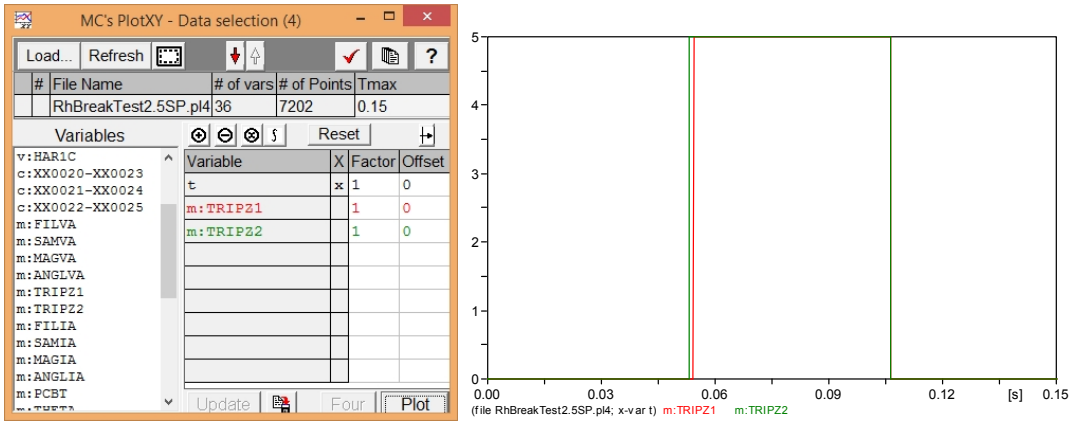

Figure 5-12. Self polarization zone-1 and zone-2 trip output at 5% SLGF with RF=0.01 Ohm

- Cross polarization using Vbc+90:

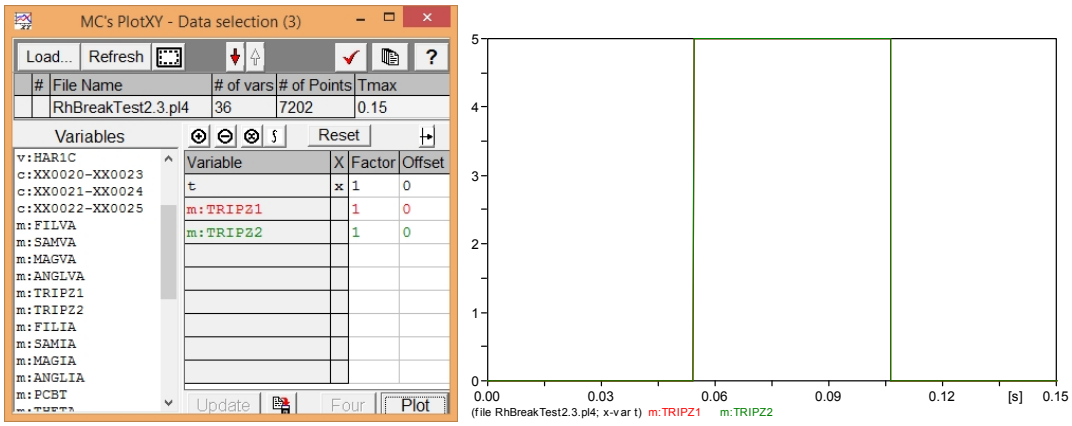

Figure 5-13. Cross polarization Vbc+90 zone-1 and zone-2 trip output at 5% SLGF with RF=0.01 Ohm

There is already not much differences can be seen for this fault from both the polarization quantity as the faulted phase voltage already has considerable value to be used as the polarizing signal. The responses from both the polarization method are understandably almost the same for the rests of the line location's fault bar the fault resistance. For instance, Figure 5-14 and 5-15 below shows the tripping responses of self polarization and cross polarization mho relay respectively for zone-1 with RF=50 Ohm.

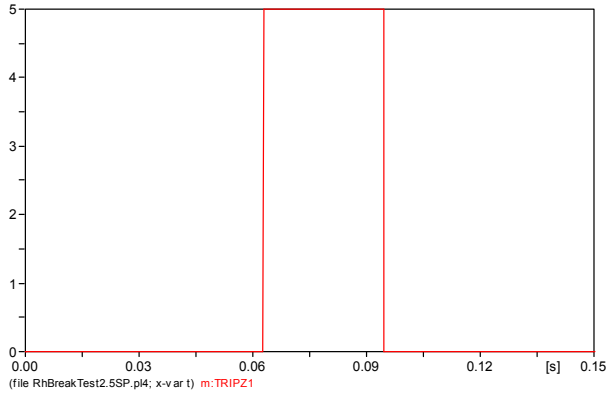

Figure 5-14. Self polarization zone-1 trip output at 5% SLGF with RF=50 Ohm

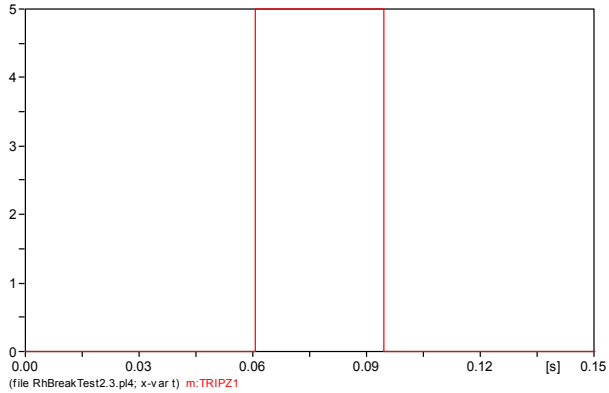

Figure 5-15. Cross polarization zone-1 trip output at 5% SLGF with RF=50 Ohm

Fault at 45%

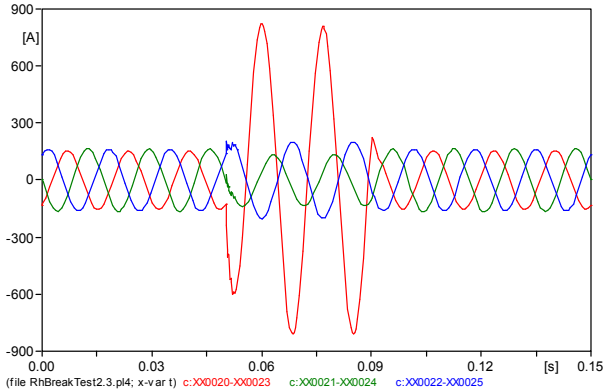

Figure 5-16. Current under SLGF at 45% with RF=0.01 Ohm

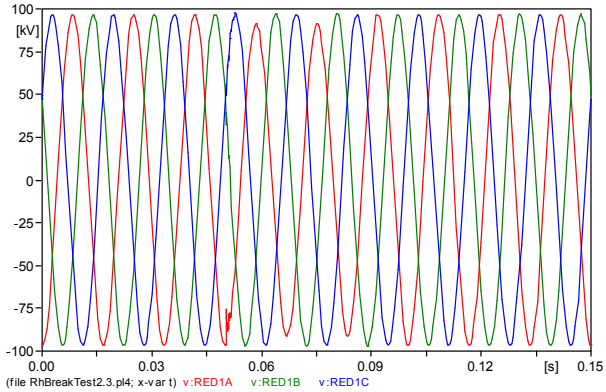

Figure 5-17. Voltage under SLGF at 45% with RF=0.01 Ohm

The resulting trip:

- Self polarization using Va:

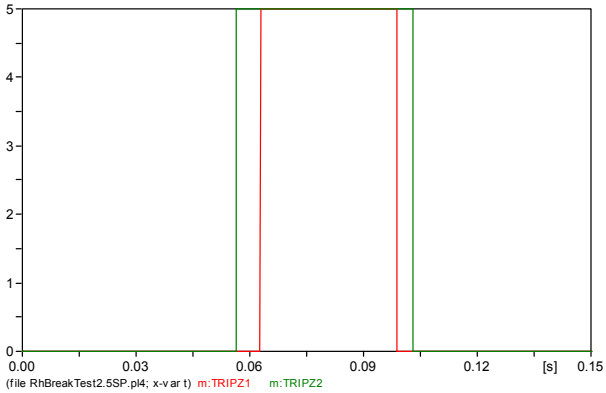

Figure 5-18. Self polarization zone-1 and zone-2 trip output at 45% SLGF with RF=0.01 Ohm

- Cross polarization using Vbc+90:

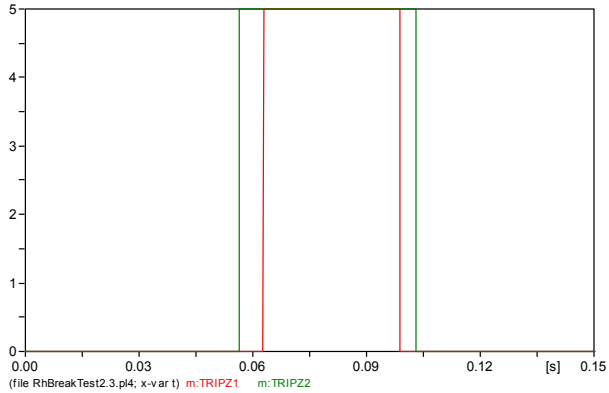

Figure 5-19. Cross polarization zone-1 and zone-2 trip output at 45% SLGF with RF=0.01 Ohm

Both polarization methods give the same tripping output with the zone-2 relay responds approximately 3/8 cycle (6.25ms) faster than zone-1. Replacing the fault resistance R_F with $50\,\Omega$, the tripping output can be shown at the following figure:

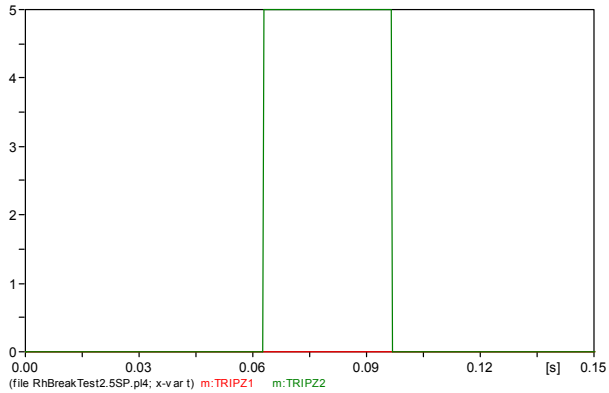

Figure 5-20. Self polarization zone-1 and zone-2 trip output at 45% SLGF with RF=50 Ohm

Zone-1 relay (shown with the red line) does not respond to the fault and only zone-2 relay (green line) trips to the fault.
The positive sequence impedance at 45% line can be calculated as:

$$Z^1_{45\%} = 45\% \cdot (101\Omega \angle 73)$$
$$Z^1_{45\%} = 45\%(29.53 + j96.59)$$
$$Z^1_{45\%} = 13.3 + j43.46$$

Adding with RF 50 Ohm:

$$Z^1_{total} = Z^1_{45\%} + 50$$
$$Z^1_{total} = 63.3 + j34.425$$
$$Z^1_{total} = 76.8 \angle 34.5$$

The magnitude of the positive sequence impedance is actually less than the positive sequence setting for zone-1 mho relay. However, the mho characteristic gives closer reach point when the angle is different

from the setting angle, which in this case is smaller than the setting (more resistive). Thus the failure of zone-1 mho relay to trip during this condition is understandable.

Fault at 75%

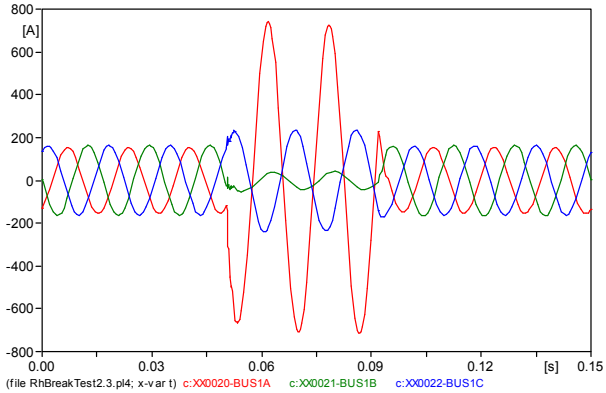

Figure 5-21. Current under SLGF at 75% with RF=0.01 Ohm

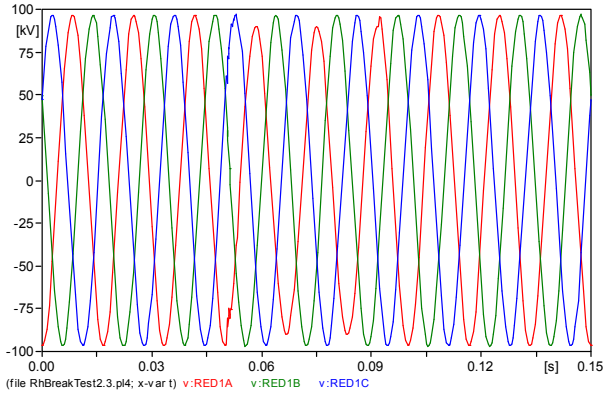

Figure 5-22. Voltage under SLGF at 75% with RF=0.01 Ohm

The resulting trip can be shown in the Figure 5-23 below:

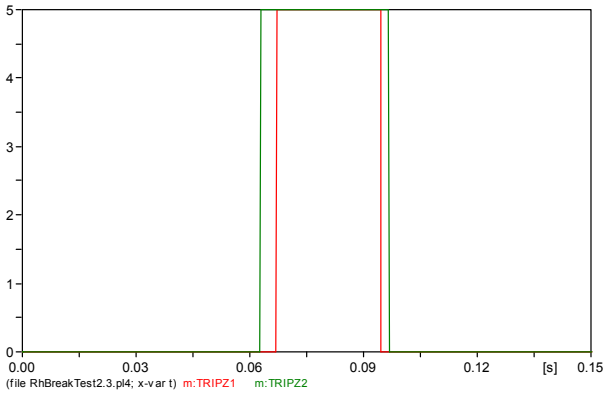

Figure 5-23. Cross polarization zone-1 and zone-2 trip output at 75% SLGF with RF=0.01 Ohm

Trip output from the self polarization is exactly the same with the one given by the cross polarization angle comparator mho. One thing to be underlined from the figure is that zone-1 mho relay (red line) needs a full 1 cycle to realize a fault and trips. In other words, zone-1 is waiting for the recursive Fourier to transform a full cycle of fault current and fault voltage to be able to realize that the fault is within its protection zone.

Replacing the fault resistance as previously done with RF=50 Ohm.

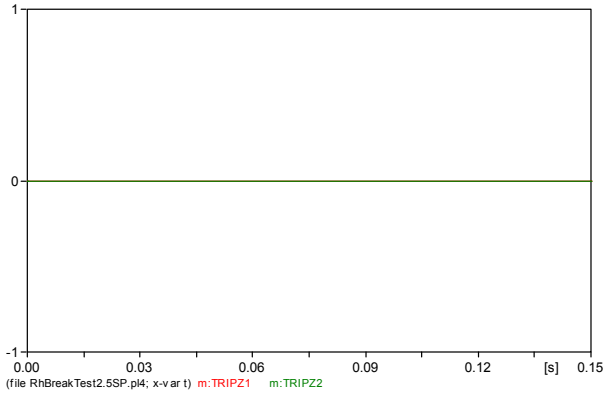

Figure 5-24. Cross polarization zone-1 and zone-2 trip output at 75% SLGF with RF=50 Ohm

Zone-2 relay is already failed to operate during the fault.
Doing the same calculation as previously done with the fault at 45% to find the positive sequence impedance:

$$Z^1_{75\%} = 75\% \cdot (101\Omega \angle 73)$$
$$Z^1_{75\%} = 75\%(29.53 + j96.59)$$
$$Z^1_{75\%} = 22.15 + j72.44$$

Adding with RF 50 Ohm:

$$Z^1_{total} = Z^1_{45\%} + 50$$
$$Z^1_{total} = 72.15 + j72.44$$
$$Z^1_{total} = 102 \angle 45$$

The same phenomenon as explained in the fault at 45% for zone-1 with RF=50 Ohm also occurs in this situation.

Summary of the simulation being done for the single line to ground fault can be presented in the tables below, where Table 5-1 presenting the simulation for mho relay using cross polarization Vbc shifted by 90 degrees. While Table 5-2 summarizes the result for the self polarization mho relays.

Location of fault(from relay location)	*Fault Impedance*	*Response time*	
		Zone 1	*Zone 2*
0%	0.01 Ω	3.1ms	3.1ms
	50 Ω	12.5ms	10.5ms
5%	0.01 Ω	4ms	4ms
	50 Ω	12.5ms	10.5ms
25%	0.01 Ω	6ms	4ms
	50 Ω	15ms	12.5ms
45%	0.01 Ω	12ms	6ms
	50 Ω	NT	12.5ms
50%	0.01 Ω	12ms	10ms
	50 Ω	NT	15ms
55%	0.01 Ω	12ms	10ms
	50 Ω	NT	15ms
75%	0.01 Ω	17ms	12ms
	50 Ω	NT	NT
95%	0.01 Ω	NT	14ms
	50 Ω	NT	NT
100%	0.01 Ω	NT	14ms
	50 Ω	NT	NT

Table 5-1.SLGF simulation results of cross polarized mho

Location of fault(from relay location)	*Fault Impedance*	*Response time*	
		Zone 1	*Zone 2*
0%	0.01 Ω	Incorrect trip	Incorrect trip
	50 Ω	Incorrect trip	Incorrect trip
5%	0.01 Ω	4ms	3ms
	50 Ω	12.5ms	10.5ms
25%	0.01 Ω	6ms	4ms
	50 Ω	15ms	12.5ms
45%	0.01 Ω	12ms	6ms
	50 Ω	NT	12.5ms
50%	0.01 Ω	12ms	10ms
	50 Ω	NT	15ms
55%	0.01 Ω	12ms	10ms
	50 Ω	NT	15ms

75%	0.01 Ω	17ms	12ms
	50 Ω	NT	NT
95%	0.01 Ω	NT	15ms
	50 Ω	NT	NT
100%	0.01 Ω	NT	15ms
	50 Ω	NT	NT

Table 5-2. SLGF simulation results of self polarized mho

From the table, it can be seen that the more sensitive longer reaching zone 2 model relay responds faster than zone 1. To ensure the correct operation, single line to ground fault is also tested in reverse line. The result is listed in table 5-3 below:

Location of fault	*Fault Impedance*	*Response time*	
		Zone 1	*Zone 2*
-5%	0.01 Ω	NT	NT
	50 Ω	NT	NT
-25%	0.01 Ω	NT	NT
	50 Ω	NT	NT
-45%	0.01 Ω	NT	NT
	50 Ω	NT	NT

Table 5-3. Reverse SLGF simulation results

5.1.3. Double Line Fault Simulation Result

This section discusses about the simulation results for the line to line fault. As the depicted simulation configuration in Figure 4-24, only bolted line will be simulated (R_F=0). Both self polarized and cross polarized mho relay simulation will be presented.

Fault at 0%

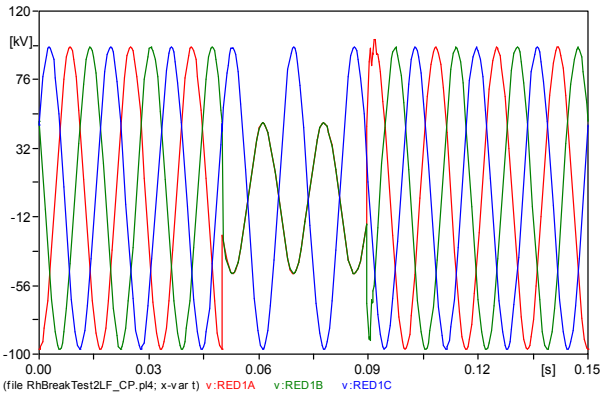

Figure 5-25. Voltages under line-A to line-B fault at relay location

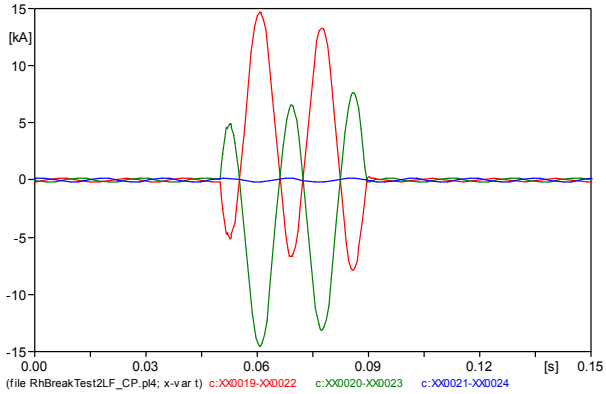

Figure 5-26. Currents under line-A to line-B fault at relay location

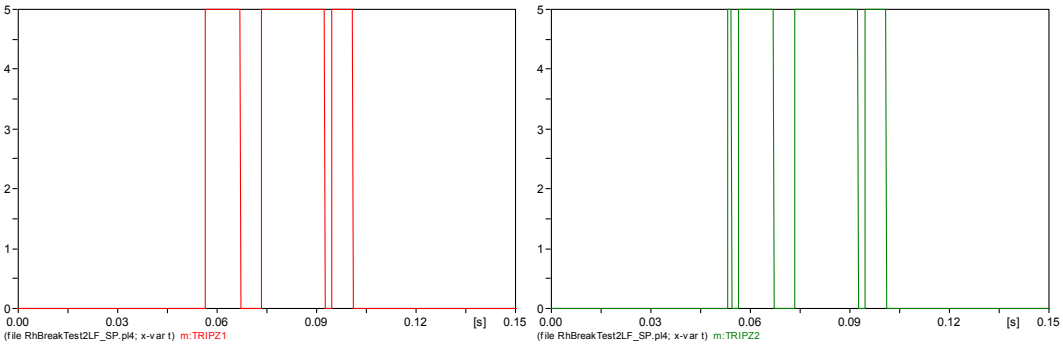

(a) Zone-1 (b) Zone-2

Figure 5-27. Self polarized mho trip output during close-in line to line fault

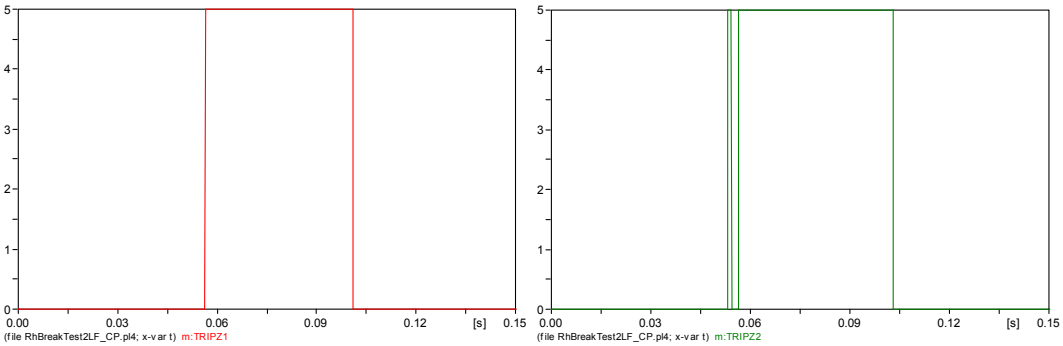

(a) Zone-1 (b) Zone-2

Figure 5-28. Cross polarized mho trip output during close-in line to line fault

Fault at 5%

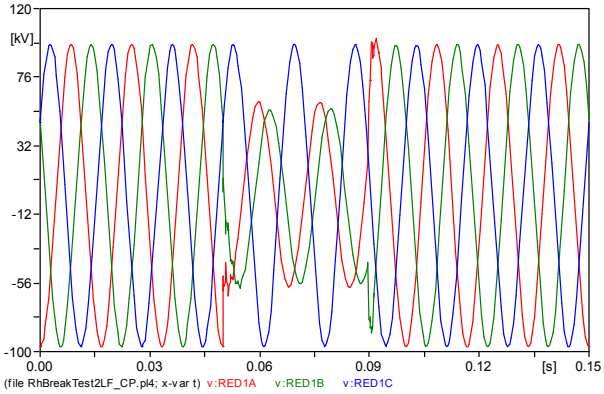

Figure 5-29 Voltages under line-A to line-B fault at 5% location

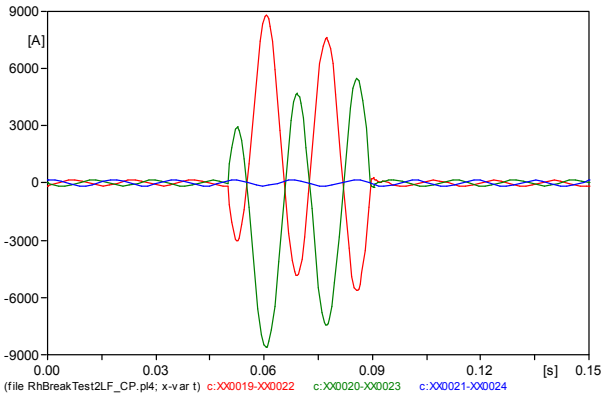

Figure 5-30. Currents under line-A to line-B fault at 5% location

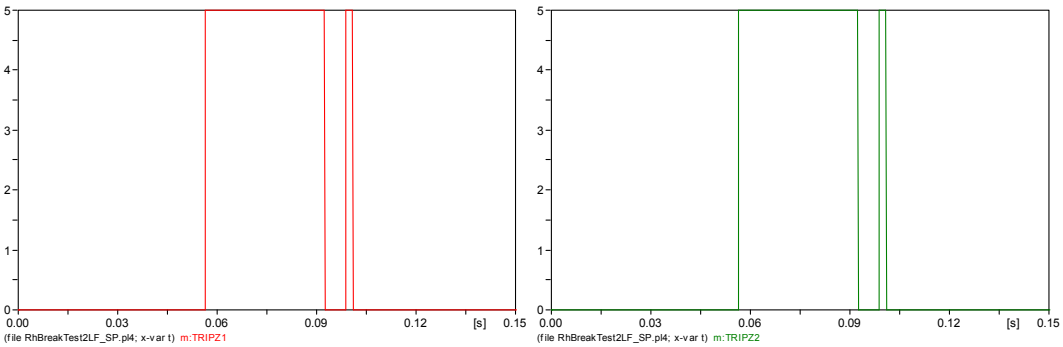

(a) Zone-1 (b) Zone-2

Figure 5-31. Self polarized mho trip output during line to line fault at 5%

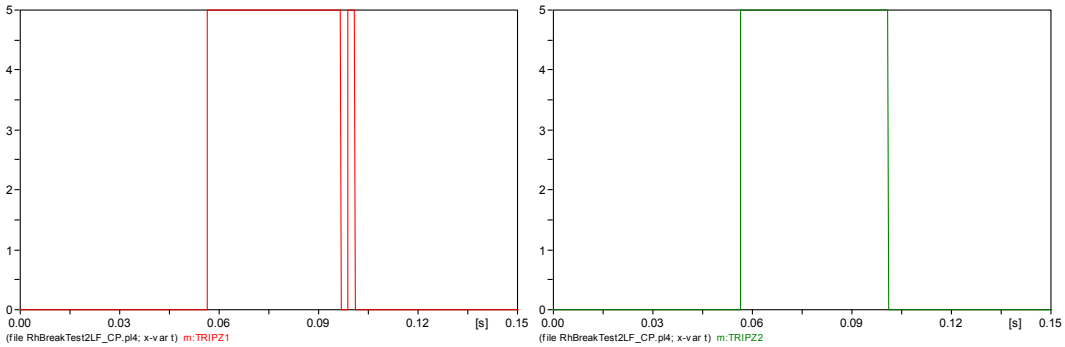

(a) Zone-1 (b) Zone-2

Figure 5-32. Cross polarized mho trip output during line to line fault at 5%

Fault at 45%

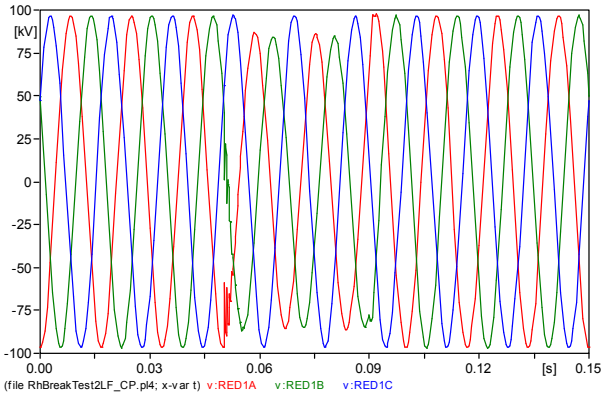

Figure 5-33. Voltages under line-A to line-B fault at 45% location

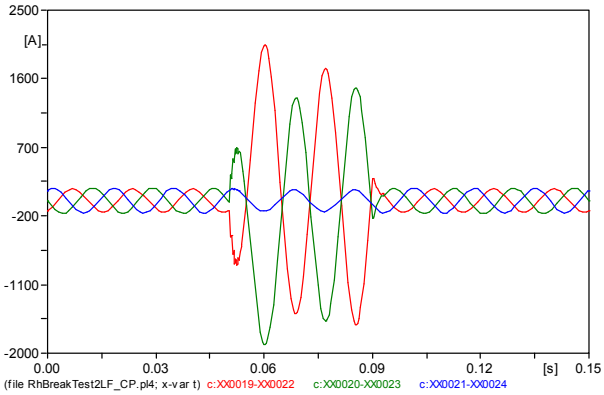

Figure 5-34. Currents under line-A to line-B fault at 45% location

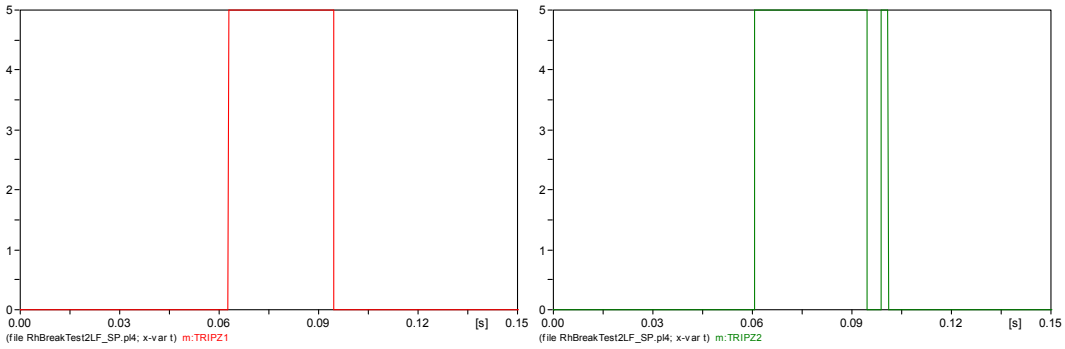

(a) Zone-1 (b) Zone-2

Figure 5-35. Self polarized mho trip output during line to line fault at 45%

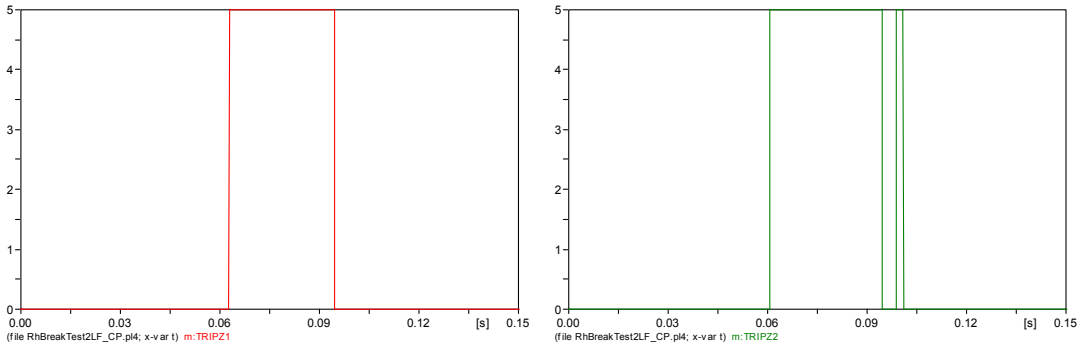

(a) Zone-1 (b) Zone-2

Figure 5-36. Cross polarized mho trip output during line to line fault at 45%

Fault at 55%

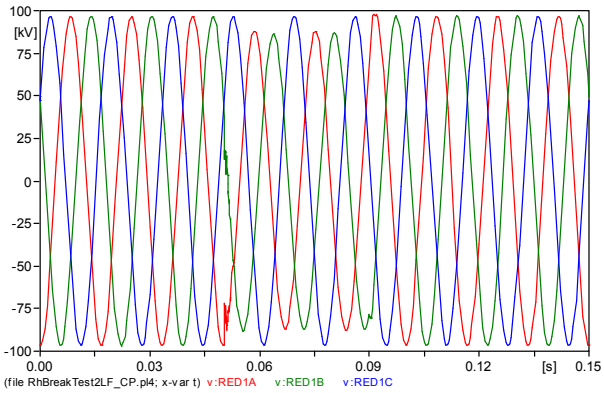

Figure 5-37. Voltages under line-A to line-B fault at 55% location

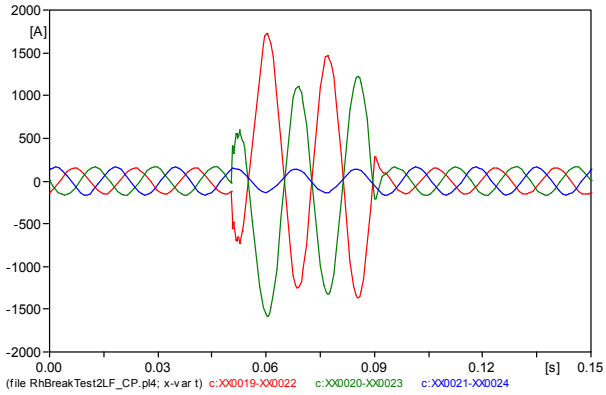

Figure 5-38. Currents under line-A to line-B fault at 55% location

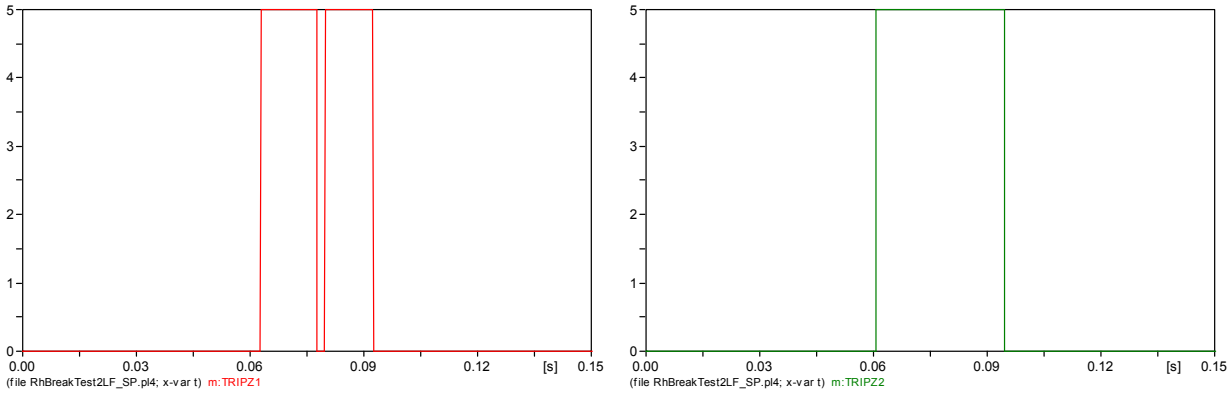

(a) Zone-1 (b) Zone-2

Figure 5-39. Self polarized mho trip output during line to line fault at 55%

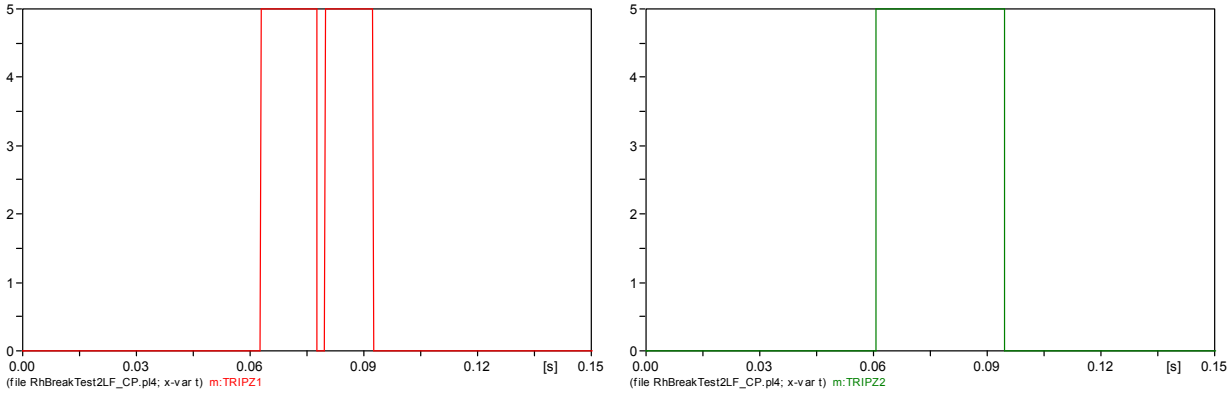

(a) Zone-1 (b) Zone-2

Figure 5-40. Cross polarized mho trip output during line to line fault at 55%

Fault at 75%

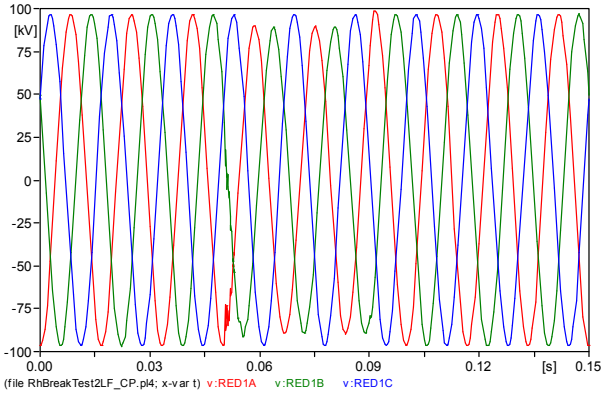

Figure 5-41. Voltages under line-A to line-B fault at 75% location

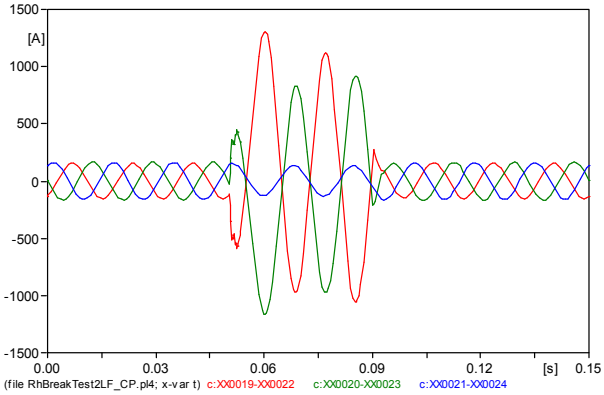

Figure 5-42. Currents under line-A to line-B fault at 75% location

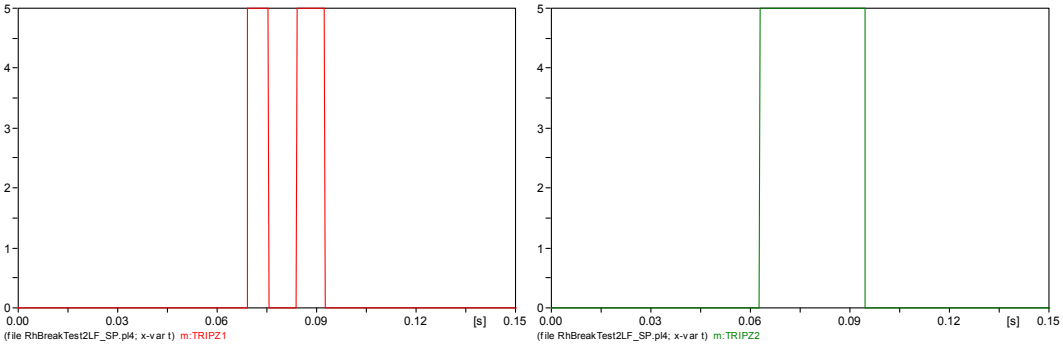

(a) Zone-1 (b) Zone-2

Figure 5-43. Self polarized mho trip output during line to line fault at 75%

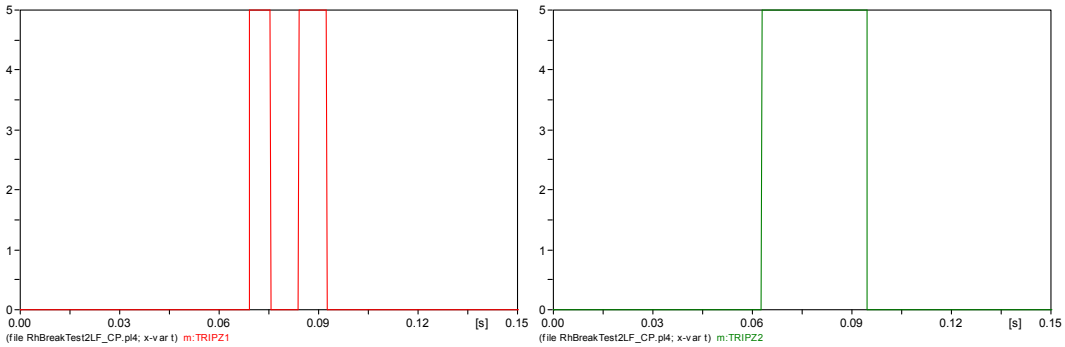

(a) Zone-1 (b) Zone-2

Figure 5-44. Cross polarized mho trip output during line to line fault at 75%

Fault at 100%

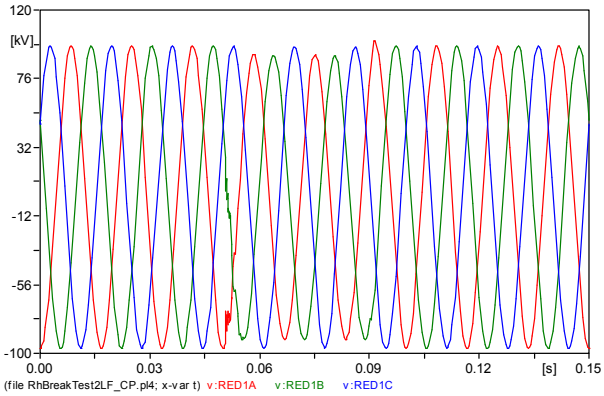

Figure 5-45. Voltages under line-A to line-B fault at 100% location

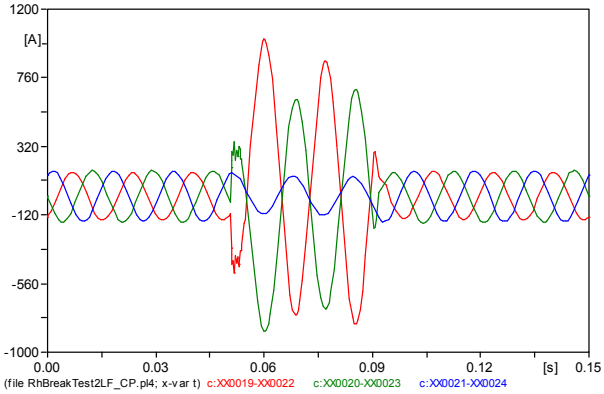

Figure 5-46. Currents under line-A to line-B fault at 100% location

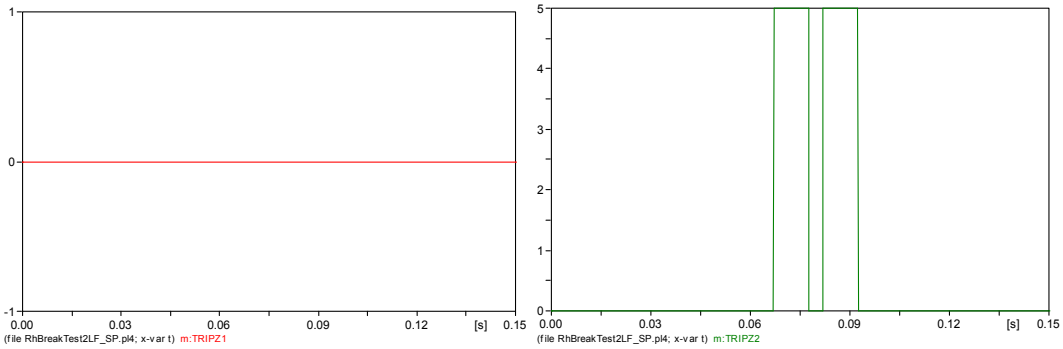

(a) Zone-1 (b) Zone-2

Figure 5-47. Self polarized mho trip output during line to line fault at 100%

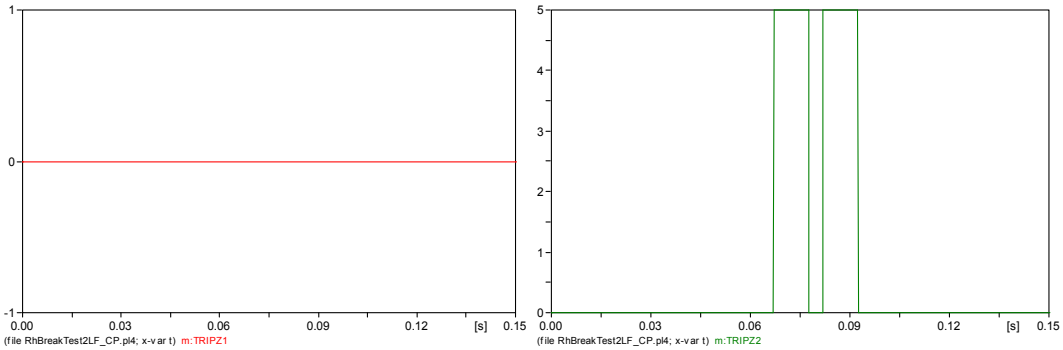

(a) Zone-1 (b) Zone-2

Figure 5-48. Cross polarized mho trip output during line to line fault at 100%

Responses of both the polarized mho relay are almost the same without much difference except for the close-in fault where it can be clearly seen that the cross polarization mho works better for this type of fault. It is the same phenomenon as explained in the single line to ground fault simulation, where during the close-in fault, Vab is equal to zero. Further observation into the tripping output, it can be seen that the reach point in this case is shorter than that of single line to ground fault. Zone-1 relay is no longer able to trip properly during fault at 55%, while Zone-2 is not able to properly operate at 100% location fault.

The Summary for line to line fault simulation results is presented in the tables below. Table 5-3 listed the simulation results for mho relay with cross polarized Vc – 90 degree. While table 5-4 present the results for the self polarized mho relay.

Location of fault(from relay location)	*Response time*	
	Zone 1	*Zone 2*
0%	Incorrect trip	Incorrect trip
5%	6.3ms	6.3ms
25%	6.3ms	6.3ms
45%	10.5ms	8.4ms
50%	12.6ms	10.5ms
55%	12.6ms	10.5ms
75%	Incorrect trip	12.6ms
95%	NT	Incorrect trip
100%	NT	Incorrect trip

Table 5-4. Line to line simulation results of self polarized mho

Location of fault(from relay location)	*Response time*	
	Zone 1	*Zone 2*
0%	6.3ms	6.3ms
5%	6.3ms	6.3ms
25%	10.5ms	8.4ms
45%	12.6ms	10.5ms
50%	12.6ms	10.5ms
55%	Incorrect trip	10.5ms
75%	Incorrect trip	12.6ms
95%	NT	Incorrect trip
100%	NT	Incorrect trip

Table 5-5. Line to line simulation results of cross polarized mho

Location of fault	*Response time*	
	Zone 1	*Zone 2*
-5%	NT	NT
-25%	NT	NT
-45%	NT	NT

Table 5-6. Reverse line to line fault simulation results

5.2. Electromechanical Relay

5.2.1. Model Input Parameters

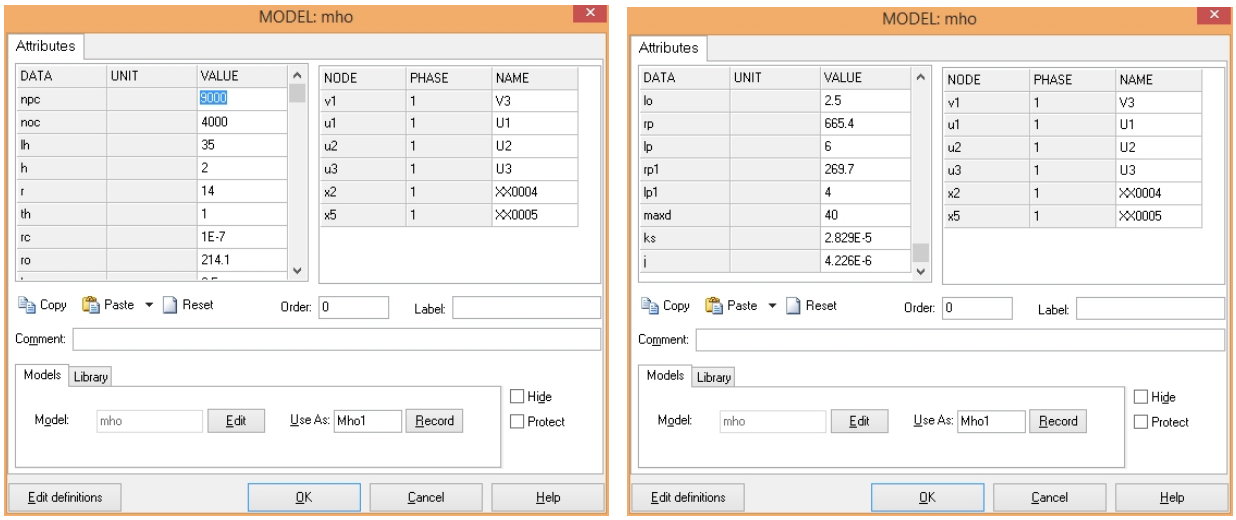

Figure 5-49. State space relay model input

Inputs for the model consists of electrical and mechanical parameters of the relay as explained in chapter 4.4. The value are taken from the work done by [5] and [29] with certain modification. This relay model will process the input from CT and CVT to give the output of relay torque and displacement angle.

5.2.2. Fault Simulation Results

To understand the distance relay performance under CVT transient and CT saturation, single line to ground fault (SLGF) will be simulated with the fault is very close to the relay location. Two types of SLGF in this case will be tested: SLGF with DC offset and SLGF without DC offset. SLGF with DC offset is the SLGF where the fault occurs at voltage zero, while SLGF without DC offset occurs at voltage peak. The SLGF is tested in phase A by connecting the phase to the ground through a resistance of 0.1Ω.

SLGF without DC offset at SR-04 (6.28 miles from relay location)

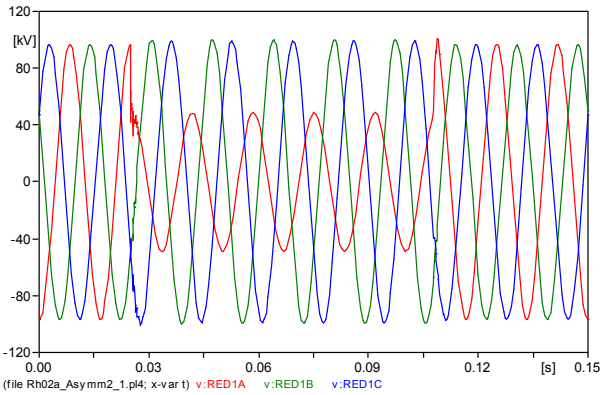

Figure 5-50. Phase voltages under SLGF without DC offset at SR-04

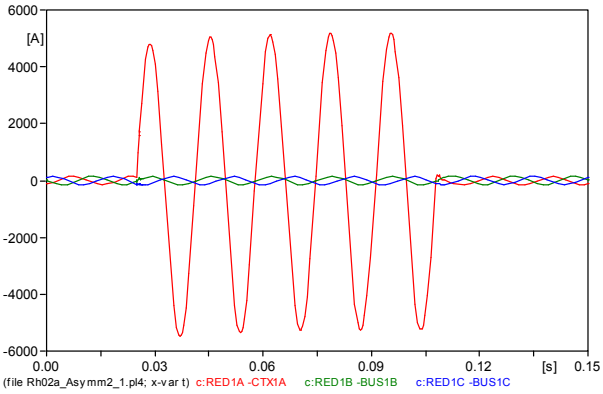

Figure 5-51. Phase currents under SLGF without DC offset at SR-04

Figures 5-50 and 5-51 are respectively the phase voltage and current when the symmetrical SLGF is tested at a distance of 6.28 miles from the relay location.

It can be seen from Figure 5-50 that voltage in phase-A drops to half the initial value while the other healthy phases are not affected. In figure 5-51, the current in phase-A jumps to around 5kA from its initial value of 160A while the other 2 healthy phases are also not affected.

The current in the secondary side of the CT can be seen in figure 5-52. The waveform is quite healthy without saturation and DC offsets. Figure 5-53 shows the voltage output from CVT compared to the output from regular PT. It can be seen that the waveforms are almost identical which means that the transient problem in CVT does not have to be addressed in this situation.

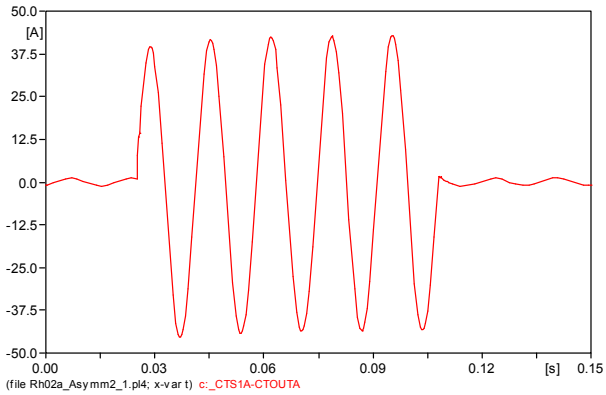

Figure 5-52. CT secondary output under SLGF without DC offset at SR-04

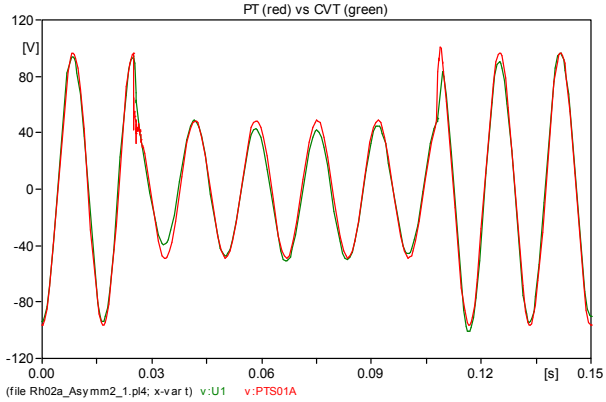

Figure 5-53. CVT versus PT secondary output under SLGF without DC offset at SR-04

The torque developed by the relay and the angle displacement can be seen in Figure 5-54(a) and 5-54(b) respectively.

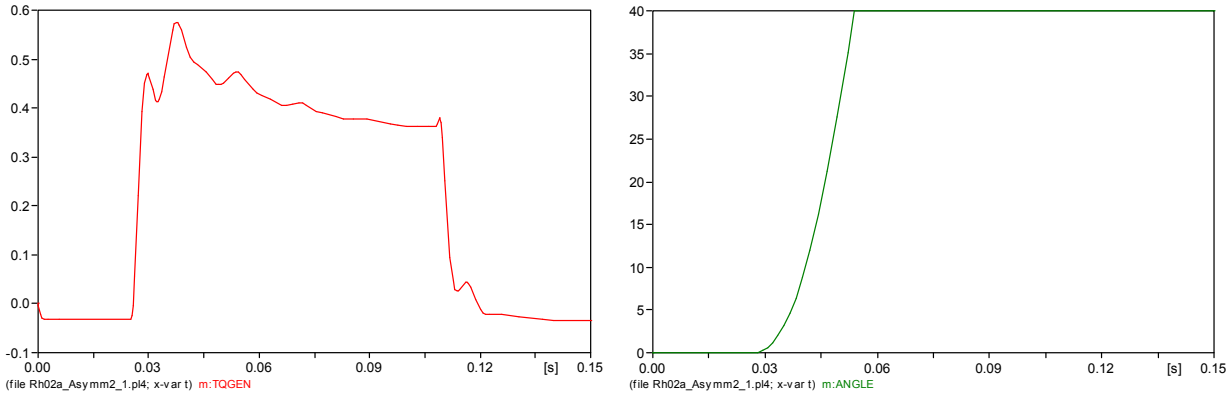

(a) (b)

Figure 5-54. Relay output under SLGF without DC offset at SR-04
(a) Developed torque (Nm) (b) Angle displacement (degree)

SLGF with DC offset at SR-04 (6.28 miles from relay location)

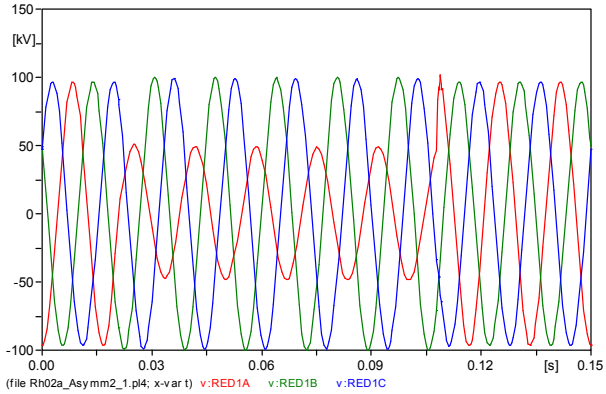

Figure 5-55. Phase voltage under SLGF with DC offset at SR-04

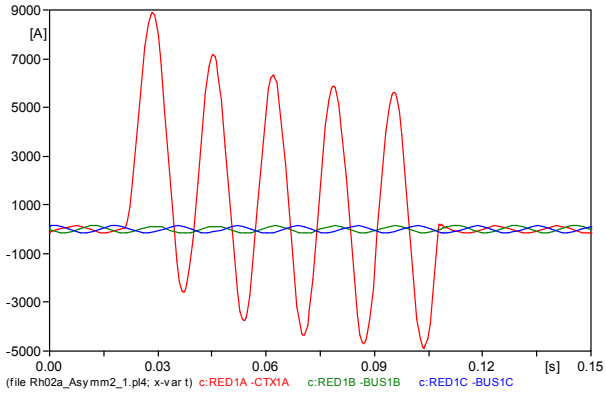

Figure 5-56. Phase currents under SLGF with DC offset at SR-04

Figures 5-55 and 5-56 show phase voltage and phase currents under asymmetrical fault at SR-04. Unlike the previous case, faulted phase-A current consist DC offset. This DC offset will introduce the rise of the flux which will cause saturation in the magnetic core of the CT. The output in the secondary side of the CT is depicted in the Figure 5-57.

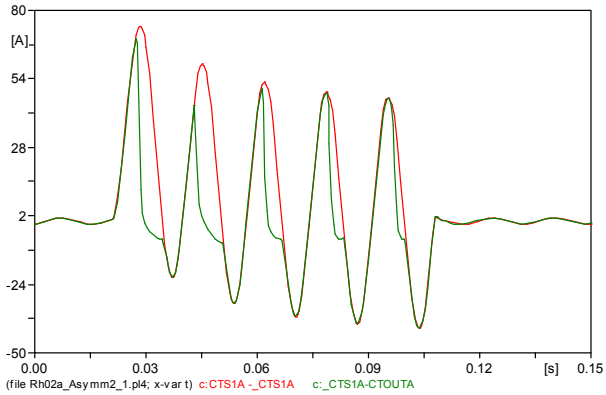

Figure 5-57. CT secondary output under SLGF with DC offset at SR-04

The output of CVT however is not much affected. As can be seen in the Figure 5-58 depicted below, the CVT performance is not much different from the PT.

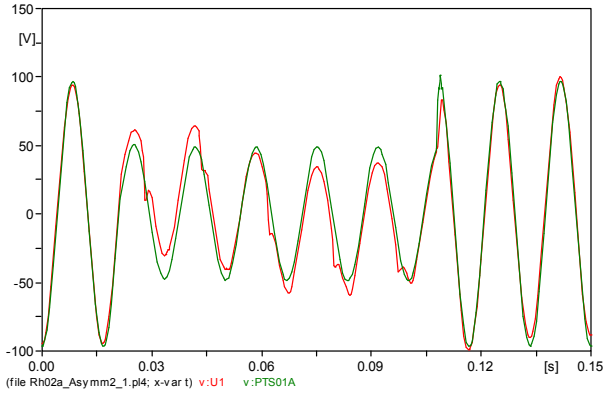

Figure 5-58. CVT versus PT secondary output under SLGF with DC offset at SR-04

Figure 5-59(a) and 5-59(b) show the torque and angle displacement under asymmetrical SLGF at SR-04. It can be seen that the maximum torque is much higher compared to symmetrical SLGF at the same location. This results in the faster operation of the relay. The angle displacement under this condition is faster compared to SLGF without DC offset by approximately 3-4ms.

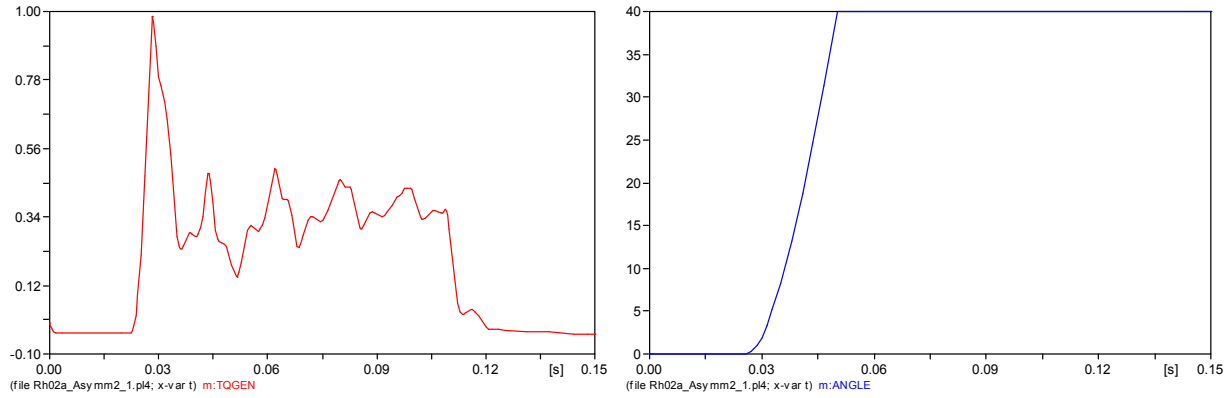

(a) (b)

Figure 5-59. Relay output under SLGF with DC offset at SR-04
(a) Developed torque (Nm) (b) Angle displacement (degree)

SLGF without DC offset at SR-02 (at the relay location)

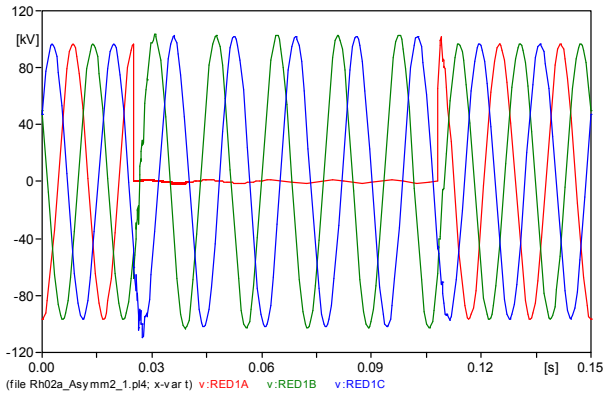

Figure 5-60. Phase voltage under SLGF without DC offset at SR-02

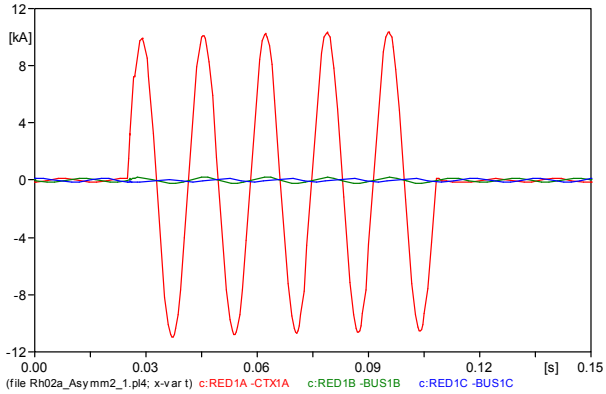

Figure 5-61. Phase currents under SLGF without DC offset at SR-02

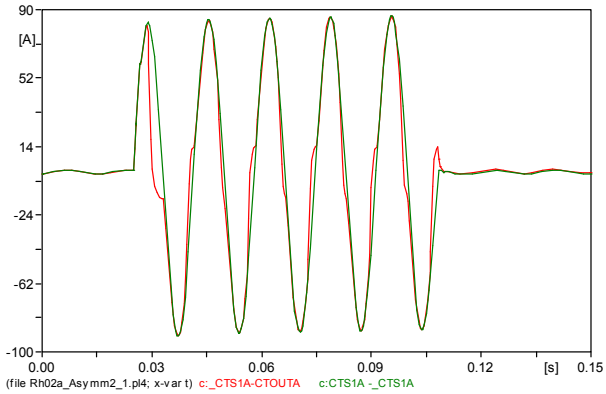

Figure 5-62. CT secondary output under SLGF without DC offset at SR-02

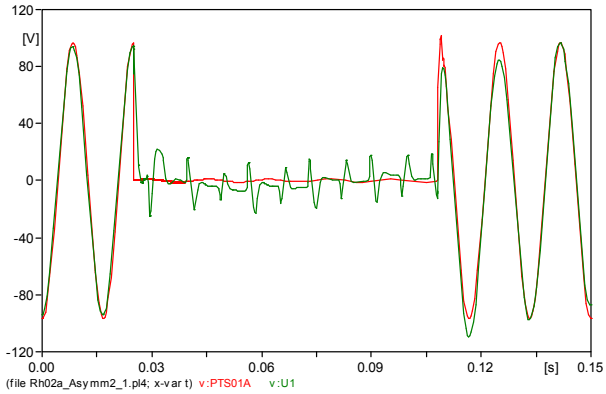

Figure 5-63. CVT versus PT secondary output under SLGF without DC offset at SR-02

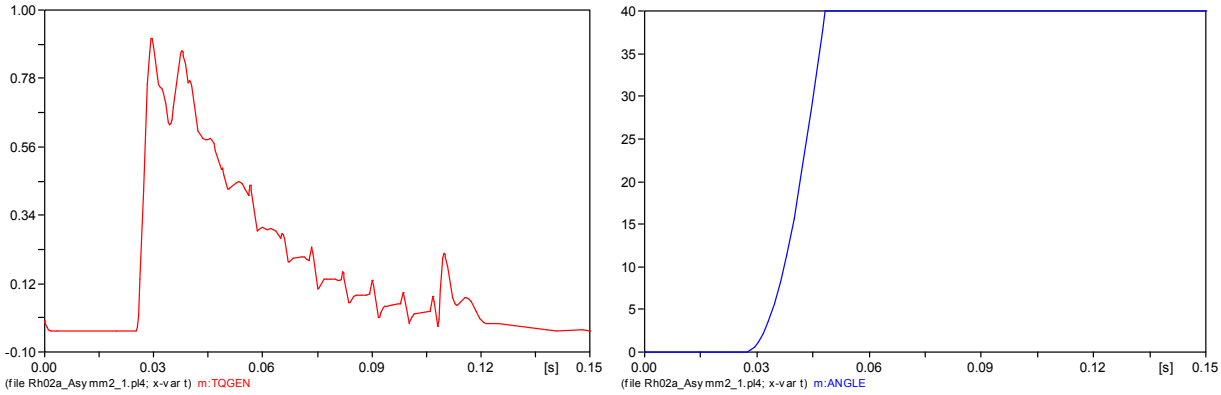

(a) (b)

Figure 5-64. Relay output under SLGF without DC offset at SR-02
(a) Developed torque (Nm) (b) Angle displacement (degree)

SLGF with DC offset at SR-02 (at the relay location)

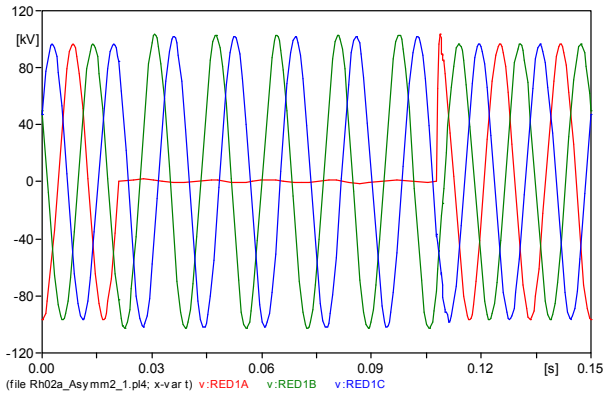

Figure 5-65. Phase voltage under SLGF with DC offset at SR-02

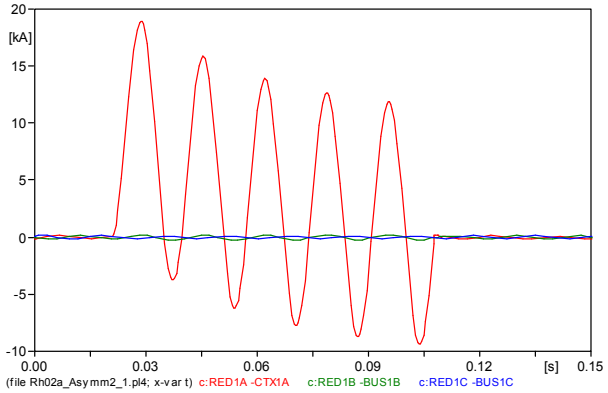

Figure 5-66. Phase voltage under SLGF with DC offset at SR-02

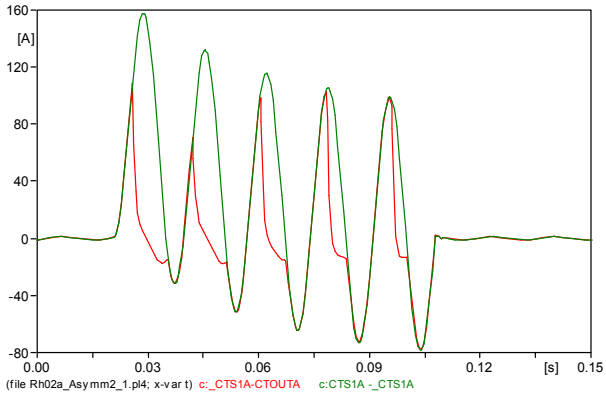

Figure 5-67. CT secondary output under SLGF with DC offset at SR-02

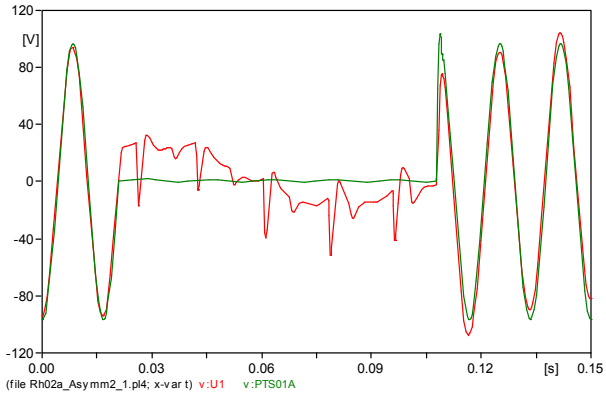

Figure 5-68. CVT versus PT secondary output under SLGF with DC offset at SR-02

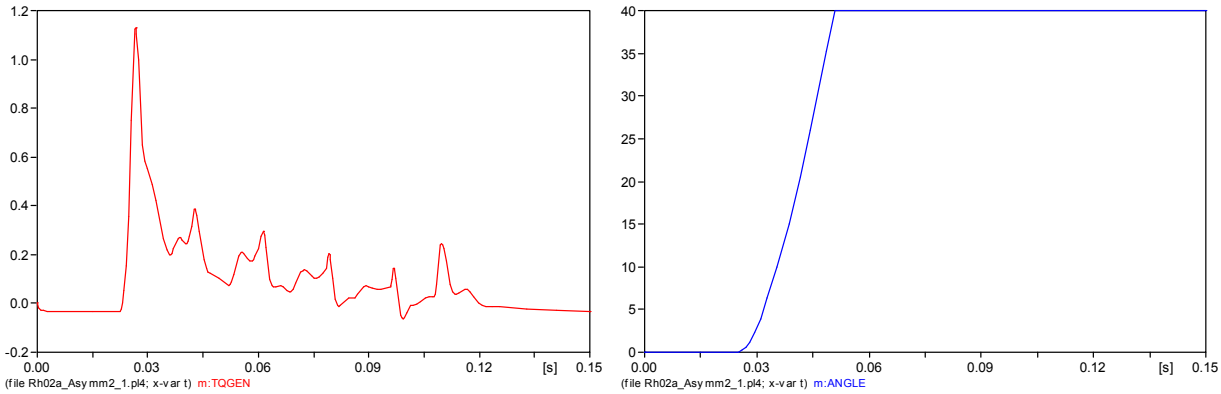

(a) (b)

Figure 5-69. Relay output under SLGF with DC offset at SR-02
(a) Developed torque (Nm) (b) Angle displacement (degree)

The situation is very severe during the SLGF with DC offset at the relay location. With the maximum DC offset contributing to considerable distortions on the CT secondary output accompanied by transient output of CVT. The peak torque developed during the fault with DC offset is much higher (approximately 20% higher) than the fault without DC offset. The relay operation, based on the displacement angle, however does not show much different between the two types of fault.

6. Conclusions and Recommendations

6.1. Conclusions

This thesis presents the application of a microprocessor based and an electromechanical mho relay model in the transmission lines. The first part of the study is related to the microprocessor based relay model. The model is developed using four main blocks: Filter, sampling, Fourier detector and a trip decision block. The tripping decision block is built based on the phase angle comparator model. From the simulation for single line to ground fault, it can be concluded that:

- Model works properly based on the characteristic of mho distance relay and the protection scheme for the fault with small fault resistance.
- Larger fault resistance tends to under-reach the protected line.
- Zero sequence compensation plays an important role in the operating signal for the single line to ground fault detection.
- Cross polarized mho model works better in the case of close-in fault. For fault at other locations, the operation is the same with the self polarized.

The Simulation results with the line to line fault show the reach point of the relay being closer than the protection scheme. As in the single line to ground fault, cross polarized mho relay shows better performance for close-in fault. It can also be noticed from both single line to ground fault and line to line fault that more sensitive longer reaching zone-2 relay responds faster to the fault than that of zone-1 with an inverse relationship of the response time to a fault distance. The maximum realization time from the simulations is in the figure of 17ms, which is approximately equal to 1 cycle of 60 Hz.

The developed model of the microprocessor based relay in this study does not include the model of a CT and a VT. The signals used as input are rather taken directly from the line, which is not representing the practical case. Thus the distorted signals due to saturation and transient effects of the transformer in this case are neglected. This is because the purpose of the study is to test the accuracy of the method implemented. However, the second part of the study which is related to the electromechanical model of a mho distance relay will discuss about the effects of the transformer distorted output signals to the relay operation.

The second part of the thesis is related with the modeling of electromechanical mho distance relay model which is built to simulate the fault in critical location (the location which is very close to relay). The purpose of the simulation is to analyze the relay performance under transient. The model consists of a CT model, a CVT model, a relay model and the ninth order state space model of relay. The state space model is developed as a tool that can replace the traditional “dynamic characteristic” of a relay, which is based on a phasor diagram and a memory action. The simulation results show that closer fault locations produce more distorted output transformer signals. In addition, at the same fault location, single line faults with a DC offset cause more distortion to the signals. The developed torque of the relay is also higher at closer fault locations and at faults with a DC offset.

6.2. Recommendations

The models block developed and used for the microprocessor based relay are basically independent block which can be used separately. It makes the blocks available to be used for other applications. Other types of relay measuring elements such as three phases fault can also be added easily into the model. The additions of other blocks such as DC offset correction may also be inserted into the model for a better application of relay model.

The electromechanical mho relay is developed by using only published information with some approximations which may limit the accuracy of the model. Reconstructing the model by using the exact value given by the manufacturer will obviously increase its accuracy.

Bibliography

[1] IEEE Working Group. (2001). Guide for Improving Lightning Performance of Electric Power Overhead Distribution Lines. *Approved as IEEE Standard P , 1410*, 2001.

[2] IEEE PES Power System Relaying Committee. (1984). Sine-wave distortions in power systems and the impact on protective relaying. *Rep. No. 84 TH 0115-6 PWR*.

[3] Chaudhary, A. K. S., Wilson, R. E., Glinkowski, M. T., Kezunovic, M., Kojovic, L., & Martinez, J. A. (1998). Modeling and analysis of transient performance of protection systems using digital programs. *A IEEE Working Group on Modeling and Analysis of System Transients Using Digital Programs DRAFT July*.

[4] Wilson, R. E., & Nordstrom, J. M. (1993). EMTP transient modeling of a distance relay and a comparison with EMTP laboratory testing. *Power Delivery, IEEE Transactions on*, *8*(3), 984-992.

[5] Peng, Z., Li, M. S., Wu, C. Y., Cheng, T. C., &Ning, T. S. (1985). A dynamic state space model of a MHO distance relay. *Power Apparatus and Systems, IEEE Transactions on*, (12), 3558-3564.

[6] Dommel, H. W. (1986). *Electromagnetic Transients Program: Reference Manual:(EMTP theory book)*. Bonneville Power Administration.

[7] Carson, J. R. (1926). Wave propagation in overhead wires with ground return.*Bell system technical journal*, *5*(4), 539-554.

[8] Greenwood, A. (1991). Electrical transients in power systems.

[9] PES ¨Tutorial on electromagnetic transient program applications to power system protection¨, IEEE 01TP150, 2000.

[10] Marti, J. R. (1982). Accurate modelling of frequency-dependent transmission lines in electromagnetic transient simulations. *Power Apparatus and Systems, IEEE Transactions on*, (1), 147-157.

[11] Fekete, K., Nikolovski, S., Knezević, G., Stojkov, M., & Kovač, Z. (2010, April). Simulation of Lightning Transients on 110 kV overhead-cable transmission line using ATP-EMTP. In *MELECON 2010-2010 15th IEEE Mediterranean Electrotechnical Conference* (pp. 856-861). IEEE.

[12] Makwana, V. H., & Bhalja, B. R. (2012). A new digital distance relaying scheme for compensation of high-resistance faults on transmission line. *Power Delivery, IEEE Transactions on*, *27*(4), 2133-2140.

[13] Orlhac, M. (1995). *Current Transformer for HV Protection*. Schneider Electric, Cahier Technique Merlin Gerin No. 164, Grenoble, France.

[14] Fonti, P. (2000). *Current Transformers: How to specify them.* Schneider Electric, Cahier TechniqueMerlin Gerin No. 194, Grenoble, France.

[15] "Requirements for Instrument Transformers," *ANSI/IEEE Standard C57.13-1978*.

[16] Ziegler, G. (2012). *Numerical differential protection: principles and applications*. John Wiley & Sons.

[17] Folkers, R. (1999). Determine current transformer suitability using EMTP models. *Schweitzer Engineering Laboratories, Pullman, WA EUA*.

[18] Chaudhary, A. K., Tam, K. S., &Phadke, A. G. (1994). Protection system representation in the electromagnetic transients program. *Power Delivery, IEEE Transactions on*, *9*(2), 700-711

[19] Kezunović, M., Kojović, L. J., Abur, A., Fromen, C. W., Sevcik, D. R., & Phillips, F. (1994). Experimental evaluation of EMTP-based current transformer models for protective relay transient study. *Power Delivery, IEEE Transactions on*, *9*(1), 405-413.

[20] Billig, E. (1949). The design of a capacitor voltage transformer. *Proceedings of the IEE-Part II: Power Engineering*, *96*(54), 793-802.

[21] Hou, D., & Roberts, J. (1996, May). Capacitive voltage transformer: transient overreach concerns and solutions for distance relaying. In *Electrical and Computer Engineering, 1996. Canadian Conference on* (Vol. 1, pp. 119-125). IEEE.

[22] Sweetana, A. (1971). Transient response characteristics of capacitive potential devices. *IEEE Transactions on Power Apparatus and Systems*, *5*(PAS-90), 1989-2001.

[23] Ziegler, G. (2011). *Numerical distance protection: principles and applications*. John Wiley & Sons.

[24] Phadke, A. G., & Thorp, J. S. (2009). *Computer relaying for power systems*. John Wiley & Sons

[25] Andrichak, J. G., & Alexander, G. E. (1998). Distance Relay Fundamentals.*General Electric Co Technical Papers*.

[26] Van Valkenburg, M. E. (1982). *Analog filter design*. Holt, Rinehart, and Winston

[27]Sachdev, M. S. (1997). Advancements in microprocessor based protection and communication. *IEEE tutorial course text, Publication*, (97TP120-0).

[28] Kester, W. (2009). What the Nyquist criterion means to your sampled data system design. *Analog Devices*, 1-12.

[29] Domijan Jr, A., &Emami, M. V. (1990). State space relay modeling and simulation using the ElectroMagnetic Transients Program and its transient analysis of control systems capability. *Energy Conversion, IEEE Transactions on*, *5*(4), 697-702.

Appendix-1: State space model of electromechanical mho relay

$$\begin{bmatrix} X' \\ (9x1) \end{bmatrix} = \begin{bmatrix} A \\ (9x9) \end{bmatrix} . \begin{bmatrix} \overline{X} \\ (9x1) \end{bmatrix} + \begin{bmatrix} B \\ (9x3) \end{bmatrix} . \begin{bmatrix} U \\ (3x1) \end{bmatrix}$$

Details of the matrices of state space model of electromechanical mho distance relay are listed as follows:

- x_1: current through the secondary of the transactor
- x_2: current through the operating coil
- x_3: voltage across the operating coil
- x_4: voltage across the capacitor in the memory circuit
- x_5: current through the polarizing coil
- x_6: maximum density of induced current by the polarizing coil
- x_7: maximum density of induced current by the operating coil
- x_8: angular displacement of the cylinder ($X_8>0$)
- x_9: angular velocity of the cylinder
- u_1: input voltage from PT
- u_2: $\frac{di}{dt}$, where i is the input current from CT
- u_3: $8.\mu_0.r^2.T.l(N_o.x_2.x_6 - N_p.x_5.x_7)/3h$, the electromagnetic torque

Where:

- μ_0 permeability of air, $4\pi.10^{-7}\,h/m$
- N_p number of turns of the polarizing coil
- N_o number of turns of the operating coil
- h total length of the air gaps
- l length of the cylinder
- r radius of the cylinder
- T thickness of the cylinder wall

[A] and [B] are stationary systems where the entries depend on the relay itself. The matrices consist of geometrical, mechanical and electrical parameters of the relay. The non-zero entries of the matrices are listed as follows:

- $a_{11} = -k_2\left[R_{TR2} + (1-t).R_{TR} + k_1.t.R_{OC}.R_{TR}\right]$
  $k_1 = [R_{OC} + (1-t).R_{TR}]^{-1}$
  $k_2 = [L_{TR} + L_{TR2}]^{-1}$
- $a_{13} = k_2[1 - k_1.R_{OC}]$

- $a_{22} = -R_O / L_O$
- $a_{23} = 1 / L_O$
- $a_{31} = -k_1.t.R_{TR} / C_O$
- $a_{32} = -1 / C_O$
- $a_{33} = -k_1 / C_O$
- $a_{45} = 1 / C_P$
- $a_{54} = -1/(L_P + L_{P1})$
- $a_{55} = (R_P + R_{P1}).a_{54}$
- $a_{64} = -4.N_P /(\pi.r.T.(L_P + L_{P1}))$
- $a_{65} = (R_P + R_{P1}).a_{64}$
- $a_{66} = -4.\rho.h.(l + 2r) / \mu_0.\pi.r^2.T.l$
- $a_{72} = -4.N_O.R_O / \pi.r.T.L_O$
- $a_{73} = -a_{72} / R_O$
- $a_{77} = a_{66}$
- $a_{89} = 1$
- $a_{98} = -K_s / J$
- $b_{11} = -P_X.a_{13}$
- $b_{12} = k_2.L_{TR}$
- $b_{31} = k_1.P_X / C_O$
- $b_{51} = -a_{54}$
- $a_{61} = -a_{64}$
- $b_{93} = 1 / J$

The meaning and value of each parameter are given as follows:

- L_p inductance of the polarizing coil
- R_p resistance of the polarizing coil
- C_p capacitor in the polarizing circuit
- L_{p1} variable inductor in the polarizing circuit
- R_{p1} resistance of the variable inductor
- P_x tap of the autotransformer
- L_O inductance of the operating coil
- R_O resistance of the operating coil
- C_O capacitor in the operating circuit
- R_{OC} restraint resistor
- R_{TR} potentiometer
- t ratio of the potentiometer
- R_{TR2} secondary resistance of the transactor
- L_{TR2} secondary leakage inductance of the transactor

- L_{TR} excitation inductance of the transactor
- K_S elastic coefficient of the spring
- J moment of inertia of the cylinder
- ρ resistivity of the cylinder material

---This page is intentionally left blank---

Appendix-2: Electromechanical mho relay model

```
MODEL mho
  CONST  mu {VAL:12.566371E-7}  -- Permeability of the air
  DATA   npc  -- Number of turns of the polarizing circuit
         noc  -- Number of turns of the operating coil
         lh   -- Length of the cylinder                                    (mm)
         h    -- Total length of the air gaps                              (mm)
         r    -- Radius of the cylinder                                    (mm)
         th   -- Thickness of the cylinder wall                            (mm)
         rc   -- Resistivity of the cylinder material                      (ohm.m)
         ro   -- Resistance of the operating coil                          (ohm)
         lo   -- Inductance of the operating coil                          (H)
         rp   -- Resistance of the polarizing coil                         (ohm)
         lp   -- Inductance of the polarizing coil                         (H)
         rp1  -- Resistance of the variable inductor                       (ohm)
         lp1  -- Inductance of the variable inductor-Polarizing circuit    (H)
         maxd -- Maximum angular displacement                              (rad)
         ks   -- Elastic coefficient of the spring                         (kg.m)
         j    -- Moment of inertia of the cylinder                         (kg.m2)
  VAR    a64  a65 -- Coefficients of the state-equations
         a66  a72 -- Coefficients of the state-equations
         a73  a77 -- Coefficients of the state-equations
         a89  a98 -- Coefficients of the state-equations
         b61  b93 -- Coefficients of the state-equations
         x6   y6  -- Maximum density of induced current by the polarizing coil
         x7   y7  -- Maximum density of induced current by the operating coil
         x8   y8  -- Angular displacement of the cylinder
         x9   y9  -- Angular velocity of the cylinder
         tor      -- Auxiliary variable
         torque   -- Electromagnetic torque
  INPUT   v1  -- Voltage across the operating coil
          u1  -- Voltage from the potential transformer
          u2  -- First node voltage of capacitor in polarizing circuit
          u3  -- Second node voltage of capacitor in polarizing circuit
          x2  -- Current trough the operating coil
          x5  -- Current trough the polarizing coil
  HISTORY  x6{dflt:0}     x7{dflt:0}     INTEGRAL(y8){dflt:0}  INTEGRAL(y9){dflt:0}
  INIT
      a64:=-4.E6*npc/(lp+lp1)/pi/r/th
      a65:=a64*(rp+rp1)
      a66:=-4.E6*rc*h*(lh+2*r)/mu/pi/(r*r)/th/lh
      a72:=-4.E6*noc*ro/pi/r/th/lo
      a73:=-a72/ro
      a77:=a66
      a89:=1
      a98:=-ks/j
      b61:=-a64
      b93:=1/j
      tor:=8*mu*r*r*th*lh/3/h/1.E9
      x6:=0
      x7:=0
      x8:=0
      x9:=0
  ENDINIT
```

```
EXEC
    y6:=a64*(u2 - u3) + a65*x5 + b61*u1
    LAPLACE(x6/y6):=1.0| / (-a66| + 1|s)
    y7:=a72*x2 + a73*v1
    LAPLACE(x7/y7):=1.0| / (-a77| + 1|s)
    torque:=tor*(noc*x2*x6 - npc*x5*x7)
    y8:= a89*x9
    x8:= INTEGRAL(y8) {DMIN:0  DMAX:maxd}
    y9:= a98*x8 + b93*torque
    x9:= INTEGRAL(y9) {DMIN:0}
  ENDEXEC
ENDMODEL
```

Appendix-3: Filter MODEL

```
MODEL Filter240
COMMENT
  S-domain Model of a second order 235 Hz Butterworth low-pass filter
  with gain,inputs sigA,B,C,0, and output array sig2[1..4].
ENDCOMMENT

  INPUT
   sigA, sigB, sigC, sig0

  VAR
   sig1[1..4], sig2[1..4], gain

  OUTPUT
   sig2[1..4]

  INIT
   gain:=2177928.0
 ---gain:=3219164663.8
  ENDINIT

  HISTORY
   sig1[1..4] {DFLT:0.0}

  EXEC
 --- The filtered signals are stored in phase A-B-C-0 sequence.
 --- 2nd Order
  LAPLACE(sig1[1]/sigA):=1.0|S0/(2177928|S0+1476.5|S1+1.0|S2)
  LAPLACE(sig1[2]/sigB):=1.0|S0/(2177928|S0+1476.5|S1+1.0|S2)
  LAPLACE(sig1[3]/sigC):=1.0|S0/(2177928|S0+1476.5|S1+1.0|S2)
  LAPLACE(sig1[4]/sig0):=1.0|S0/(2177928|S0+1476.5|S1+1.0|S2)
 --- 3rd Order
  ---LAPLACE(sig1[1]/sigA):=1.0|S0/(3219164663.8|S0+4355856|S1+2953.1|S2+1.0|S3)
  ---LAPLACE(sig1[2]/sigB):=1.0|S0/(3219164663.8|S0+4355856|S1+2953.1|S2+1.0|S3)
  ---LAPLACE(sig1[3]/sigC):=1.0|S0/(3219164663.8|S0+4355856|S1+2953.1|S2+1.0|S3)
  ---LAPLACE(sig1[4]/sig0):=1.0|S0/(3219164663.8|S0+4355856|S1+2953.1|S2+1.0|S3)

 --- Add gain term.

  sig2[1]:= gain * sig1[1]
  sig2[2]:= gain * sig1[2]
  sig2[3]:= gain * sig1[3]
  sig2[4]:= gain * sig1[4]

  ENDEXEC
ENDMODEL --- End Model Filter240 ========================================
```

---This page is intentionally left blank---

Appendix-4: Sample MODEL

```
MODEL Sample83

 COMMENT
 A model for sampling and storing three phase plus zero sequence current
 signals and storing the samples in arrays called store9A, store9B, store9C
 and store90.  The newest value is store9X[9].  Store9X[1] would be from the
 previous cycle.
 ENDCOMMENT

 TIMESTEP MIN: 0.002083  --- 1/8 cycle at 60 hz.
  INPUT
   sig2[1..4]

  VAR
   store9a[1..9] --- storage of sampled values for phase A
   store9b[1..9] --- phase B
   store9c[1..9] --- phase C
   store90[1..9] --- zero sequence

  OUTPUT
   store9A[1..9], store9B[1..9], store9C[1..9], store90[1..9]

  INIT
   store9A[1..9]:=0.0, store9B[1..9]:=0.0
   store9C[1..9]:=0.0, store90[1..9]:=0.0
  ENDINIT

  EXEC

  FOR i:=1 TO 8 DO
   store9A[i]:=store9A[i+1],  store9B[i]:=store9B[i+1]
   store9C[i]:=store9C[i+1],  store90[i]:=store90[i+1]
  ENDFOR

   store9A[9]:=SIG2[1],     store9B[9]:=SIG2[2]
   store9C[9]:=SIG2[3],     store90[9]:=SIG2[4]

  IF ( printcontrol = 4.0 ) THEN
   WRITE('In Sample-8-3 store9A[8]= ',store9A[8],' store9A[9]= ',store9A[9])
   WRITE('Store9B[8]= ',store9B[8],' store9B[9]= ',store9B[9])
   WRITE('Store9C[8]= ',store9C[8],' store9C[9]= ',store9C[9])
   WRITE('Store90[8]= ',store90[8],' store90[9]= ',store90[9])
  ENDIF

  ENDEXEC
 ENDMODEL  --- End Model Sample 83 ========================================
```

---This page is intentionally left blank---

Appendix-5: Fourier MODEL

```
MODEL fourier83
 TIMESTEP MIN: 0.002083 --- 1/8 of a cycle @ 60 Hz.

  INPUT
   temp9A[1..9], temp9B[1..9]
   temp9C[1..9], temp90[1..9]

  VAR
   ychat[1..4] --- ychat reads as y-sub-c-hat.  This is the same notation
               --- as in the reference and is the "cosine" coeficient of the
               --- Fourier fundamental frequency detector.
   yshat[1..4]
   l           --- A counting index
   mag, angle --- Mag is the magnitude, angle is the angle of the phasor.
   dummy1, dummy2 --- Dummy variables.
   f --- Factor for scaling.

  CONST
   mysin[1..8] {VAL:[0.0,0.707,1.0,0.707,0.0,-0.707,-1.0,-0.707]},
   mycos[1..8] {VAL:[1.0,0.707,0.0,-0.707,-1.0,-0.707,0.0,0.707]}

  OUTPUT
   mag, angle
   ychat[1..4], yshat[1..4]

  INIT
   ychat[1..4]:= 0.0001, yshat[1..4]:= 0.0, l:= 1.0
   f:= 0.1768 --- =0.25/1.414, factor for 2/ # of samples and peak to RMS.
  ENDINIT

  EXEC

   IF (l>8.0) THEN l:=1.0 ELSE l:=l
   ENDIF

   ychat[1]:= ychat[1] + ( temp9A[9] - temp9A[1] ) * f * mycos[l]
   yshat[1]:= yshat[1] + ( temp9A[9] - temp9A[1] ) * -1.0*f * mysin[l]
   ychat[2]:= ychat[2] + ( temp9B[9] - temp9B[1] ) * f * mycos[l]
   yshat[2]:= yshat[2] + ( temp9B[9] - temp9B[1] ) * -1.0*f * mysin[l]
   ychat[3]:= ychat[3] + ( temp9C[9] - temp9C[1] ) * f * mycos[l]
   yshat[3]:= yshat[3] + ( temp9C[9] - temp9C[1] ) * -1.0*f * mysin[l]
   ychat[4]:= ychat[4] + ( temp90[9] - temp90[1] ) * f * mycos[l]
   yshat[4]:= yshat[4] + ( temp90[9] - temp90[1] ) * -1.0*f * mysin[l]

   l:=l+1.0

   mag:=NORM( ychat[1], yshat[1] )
   angle:=DEG( ATAN2( yshat[1], ychat[1]) )

  ENDEXEC
 ENDMODEL --- End Model Fourier8-3 ==================================
```

---This page is intentionally left blank---